A BATTERY-LESS MEMS DEVICE FOR
ON-DEMAND AND CONTROLLED DRUG DELIVERY

by

Fatemeh Pirmoradi

B.Sc., The University of Tehran, Iran, 2001
M.A.Sc., The University of British Columbia, Canada, 2006

A THESIS SUBMITTED IN PARTIAL FULFILLMENT OF
THE REQUIREMENTS FOR THE DEGREE OF

DOCTOR OF PHILOSOPHY

in

THE FACULTY OF GRADUATE STUDIES

(Mechanical Engineering)

THE UNIVERSITY OF BRITISH COLUMBIA
(Vancouver)

August 2011

ABSTRACT

Drug therapy efficacy depends on therapeutic concentrations of drugs at disease sites. An ideal controlled and localized drug delivery system would deliver drugs to a target tissue and would locally maintain the required drug concentration. Furthermore, for many diseases, the delivery of therapeutic concentrations on an "on-demand" basis would be of tremendous benefit.

In this thesis, a MEMS (Microelectromechanical Systems) based drug delivery device has been developed that provides on-demand release of defined drug quantities. The device consists of a drug-loaded microreservoir that is sealed with an elastic PDMS (polydimethylsiloxane) magnetic membrane with a laser-drilled aperture. The drug release is triggered in the presence of an external magnetic field by deforming the magnetic membrane and therefore discharging the drug solution. The use of magnetic actuation for on-demand and controlled dose sequencing eliminates the need for an on-board power source.

A new magnetic membrane material has been developed for the proposed drug delivery device. The polymeric magnetic composites were developed by incorporating coated iron oxide nanoparticles within a PDMS matrix. The new composites show improvement in reducing particle agglomeration compared to existing polymeric magnetic materials. Free-standing PDMS magnetic membranes with a thickness of 35 µm have been fabricated and have shown to deflect in applied magnetic fields.

The MEMS drug delivery device has been used to deliver an antiproliferative, taxane-based drug, docetaxel (DTX). On-demand and controlled release of DTX with a dosage suitable for treatment of diabetic retinopathy has been achieved for 35 days. Biological activity of the released DTX was investigated two months after the drug was packaged in the device. These studies confirmed that the antiproliferative effect of DTX can be maintained for 2 months, and the drug does not degrade within the device. This device is a proof-of-concept development for on-demand and controlled delivery of taxane-based agents for treatment of

proliferative retinopathy, which requires accurate delivery of nanomolar drug concentrations.

PREFACE

The research presented in this dissertation was carried out at the University of British Columbia under the supervision of Dr. Mu Chiao in the Department of Mechanical Engineering. Some aspects of the work were conducted in collaboration with other researchers, as follows.

Chapter 2 is a version of the following article:

- **F. N. Pirmoradi**, L. Cheng and M. Chiao, "Magnetic Poly(dimethylsiloxane) Composite Incorporated with Uniformly Dispersed Coated Iron Oxide Nanoparticles", *Journal of Micromechanics and Microengineering*, vol. 20, No. 1, p. 15032, 2010.

All aspects of this work comprising literature review, material development, microfabrication, material characterization and laboratory experiments, and data analysis were performed by the author of this dissertation. The author wrote the manuscript under the direction of Dr. Mu Chiao. Dr. Mu Chiao provided her with his expert advice and editorial suggestions in this article. Ms. L. Cheng, an undergraduate student from Dr. Chiao's group, helped the author with repetitive fabrication of the magnetic material and free-standing membranes, once those processes were developed by the author.

Chapter 3 is a version of the following article:

- **F. N. Pirmoradi**, J. K. Jackson, H. M. Burt, M. Chiao, "A Magnetically Controlled MEMS Device for Drug Delivery: Design, Fabrication, and Testing", *Lab on a Chip*, vol 11, pp. 3072-3080, 2011 (DOI: 10.1039/c1lc20438f).

This work was also presented at the following conference:

- **F. N. Pirmoradi**, J. K. Jackson, H. M. Burt, M. Chiao, "A Novel Magnetically Controlled Drug Delivery Device", presented at *The 8ᵗʰ*

International Conference on the Scientific and Clinical Applications of Magnetic Carriers, Rostock, Germany, May 25-29, 2010.

The author conducted the literature review and magnetic and mechanical analysis, performed experimental designs and measurements, and developed fabrication processes. The author wrote the manuscript under the direction of Dr. Mu Chiao. Dr. Mu Chiao provided her with his expert advice, guidance in data interpretation, and editorial suggestions. Mr. J. K. Jackson from Dr. H. M. Burt's group at the Faculty of Pharmaceutical Sciences provided the author with assistance with equipment, technical advice and editorial suggestions, and Dr. H. M. Burt provided the author with editorial suggestions. Ms. S. Moayedinia, an undergraduate student from Dr. Chiao's group, helped the author with repetitive contact angle measurements, once those measurement processes were developed by the author.

Chapter 4 is a version of the following article which was selected as a highlighted article:

- **F. N. Pirmoradi**, J. K. Jackson, H. M. Burt, M. Chiao, "On-demand Controlled Release of Docetaxel from a Battery-less MEMS Drug Delivery Device", *Lab on a Chip*, vol. 11, pp. 2744-2752, 2011 (DOI: 10.1039/c1lc20134d).

This work was also presented at the Transducers' 11 conference and published in the proceedings:

- **F. N. Pirmoradi**, J. K. Jackson, H. M. Burt, M. Chiao, "Delivery of an Anti-cancer Drug from a Magnetically Controlled MEMS Device Shows Cytotoxicity in PC3 and HUVEC Cells", *Proceedings of the 16th International Conference on Solid-State Sensors, Actuators and Microsystems*, Beijing, China, June 5-9, 2011.

The author conducted the literature review and device fabrication. Simulation, experimental design, and measurements were performed by the author, as well as all drug release studies. The cell viability experiments were conducted in

collaboration with Mr. Jackson in Dr. Burt's laboratory. The author wrote the manuscript under the direction of Dr. Mu Chiao. Dr. Mu Chiao provided her with his expert advice and editorial suggestions. Mr. J. Jackson and Dr. H. Burt provided the author with technical advice on the application of the device and suggestions of the drug as well as editorial suggestions on the submitted article. The magnetic setup was made with the help of an undergraduate student, A. Alagheband, from Dr. Chaio's group.

The author has made the following major contributions in the work presented in this dissertation:

1. Developed a new all polymer MEMS drug delivery device which operates without the need for an on-board battery and can provide on-demand and precisely controlled drug release.

2. Developed and characterized new magnetic composites for use in MEMS and bioMEMS applications. This material was used for the first time as a membrane material for the fabrication of the MEMS drug delivery device proposed in this dissertation.

3. Developed the fabrication process for this new MEMS device including:

   a. drug loadings,

   b. laser ablation of polymer, and

   c. surface modification of the magnetic membrane.

4. Demonstrated reproducible drug release profiles with constant release rates and identified experimental parameters.

5. Demonstrated long-term performance of the device with minimal background leakage through experimental testing.

6. Demonstrated biological activity of the drug *in vitro*, after it was packaged in the MEMS device.

TABLE OF CONTENTS

LIST OF TABLES

LIST OF FIGURES

LIST OF SYMBOLS AND ABBREVIATIONS

ε	strain
θ	contact angle
μ_0	permeability of free space
µl	microliter
µm	micrometer
µN	micronewton
π	Pi (3.1415926)
σ	surface tension
ω_0	membrane centre displacement
$\varnothing$	diameter
°	degree
°C	degree Celsius
a	radius of membrane
A_a	area of aperture
A_m	area of membrane
B	magnetic flux density
BSA	bovine serum albumin
c	concentration
Ci	curie
cm	centimeter
CoNiMnP	cobalt-nickel-manganese-phosphorus
d	diameter

D	diffusion coefficient
DCM	dichloromethane
DI	de-ionized
DPM	disintegration per minute
DTX	docetaxel
E	elastic modulus
EMG 1200	iron oxide nanoparticles with fatty acid coating
EMG 1400	iron oxide nanoparticles with hydrophobic coating
emu	electromagnetic unit
FBS	fetal bovine serum
h	hour
H	magnetic field strength
H_d	demagnetization field
H_{int}	internal magnetic field
^{3}H-DTX	tritium-labeled docetaxel
HUVEC	human umbilical vein endothelial cell
IPA	isopropanol
IR	infrared
kA	kiloampere
kPa	kilopascal
L	length
M	magnetization
MB	methylene blue
MEMS	microelectromechanical systems

mg	milligram
min	minute
ml	milliliter
mm	millimeter
MPa	megapascal
M_s	saturation magnetization
mT	militesla
M_w	molecular weight
N	demagnetization tensor
NdFeB	neodymium iron boron
ng	nanogram
nm	nanometer
nM	nanomolar
n_z	demagnetization factor in z direction
O_2	oxygen
Oe	oersted
p	pressure
Pa	pascal
PAA	poly(acrylic acid)
PBS	phosphate buffer solution
PC3	prostate cancer
PDMS	poly(dimethylsiloxane)
Pe	Péclet number
PECVD	plasma-enhanced chemical vapor deposition

pH	measure of acidity or basicity
PPI	pulse per inch
R	principal radius of curvature
R_a	arithmetic mean
rpm	revolutions per minute
R_q	root mean square
R_z	average maximum heights
s	second
SEM	scanning electron microscope
SQUID	superconducting quantum interface device
SU-8	negative photoresist
SiO_2	silicon dioxide
Si	silicon
t	thickness of membrane
T	tesla
TB	trypan blue
t_d	discharge time
t_w	mixing time
u	flow velocity
UV	ultraviolet
v	volume of magnet
v	flow velocity
V_d	displaced volume
w	width of aperture

wt%   weight percentage

% w/v   weight (grams) to volume (milliliter) percentage

% w/w   weight to weight percentage

ACKNOWLEDGEMENTS

My deepest gratitude goes to my family for their unconditional love and support throughout my life. This thesis would have not been possible without them. I am indebted to my parents (Maliheh and Yadollah) who have been always a source of endless inspiration, encouragement, and love for me. They have taught me to pursue big dreams and lead my life to achieve beyond what I imagine. They have always been there for me and have given me their prayers. I have no suitable words to describe their everlasting love, care, and support for me. I love you Maman joon and Baba joon.

I am immensely blessed and proud to have wonderful siblings, Vahid my brother and Maryam my sister, who have been always there for me whenever I needed a helping hand even from miles away. I am very grateful for their constant support, continuous love, and encouragement. Thank you Vahid. Thank you Maryam.

تقدیم به مادر وپدر عزیزم

To My Dear Parents

CHAPTER 1

Introduction

1.1   Controlled and Localized Drug Delivery

The field of drug delivery covers a broad range of technologies, all of which involve transporting therapeutic agents into human bodies, and has been an important area in medical practice. Efficient drug delivery and administration are needed to realize the full potential of molecular therapeutics, especially since the effectiveness of drug therapy is dependent on the availability of therapeutic concentrations of drugs at the disease site. In this regard, precise control over the delivery of drugs is an important and rapidly advancing field of study.

Conventional drug delivery routes such as oral or intravenous lead to a high initial drug concentration in the blood followed by an exponential decrease. This profile is shown schematically in Figure 1.1. It also highlights two limiting concentrations: (1) toxic concentrations above which the drug produces undesirable side effects; and (2) minimum drug efficacy levels below which the drug is not therapeutically effective and may induce a risk of creating drug resistance. In modern therapeutic techniques, effective drug delivery requires that the fluctuations of the drug concentration be maintained within the drug therapeutic window for extended periods of time [1]. Controlled release of drugs is especially important for

administering drugs with narrow therapeutic windows and for diseases requiring long-term treatments such as cancer [2].

It has been shown that systemic administration of anticancer drugs such as taxane-based drugs is effective and provides antitumor efficacy against a range of cancers such as breast, lung, and ovarian cancers. However, due to rapid clearance of these potent drugs from the blood [3], administering high systemic doses of them are required to produce any therapeutic effect at the site of disease. This indeed increases potential toxicities in other body organs and tissues [4, 5]. These adverse effects can be reduced by locally delivering the drugs at a specific site of disease. Furthermore, controlled drug delivery systems that can provide temporal control of drug release may offer significant advantages over conventional immediate release systems by decreasing fluctuations in drug concentrations and lowering the potential for toxicity [6].

1.2   Overview of Controlled Release Systems

1.2.1   Polymeric Drug Delivery Systems

To date, a large number of localized controlled release systems for drug delivery have been developed, most of which are based on polymers with different physical and chemical characteristics [7]. These characteristics include biodegradability [8] or drug release that is triggered by pH or temperature changes [9]. In these conventional polymeric systems, the drug is often released continuously and at a predetermined rate, irrespective of patient needs. These passively-controlled drug delivery systems rely on diffusion or osmotic pressure to deliver the drug payload slowly over a period of time and offer limited dosing flexibility. Furthermore, difficulties in achieving controlled release of drugs using biodegradable polymers has been reported, including uncontrolled burst release of drugs in the first days of implantation, followed by non-zero order release kinetics [10, 11]. A typical release profile from a polymeric implant is illustrated in Figure 1.2.
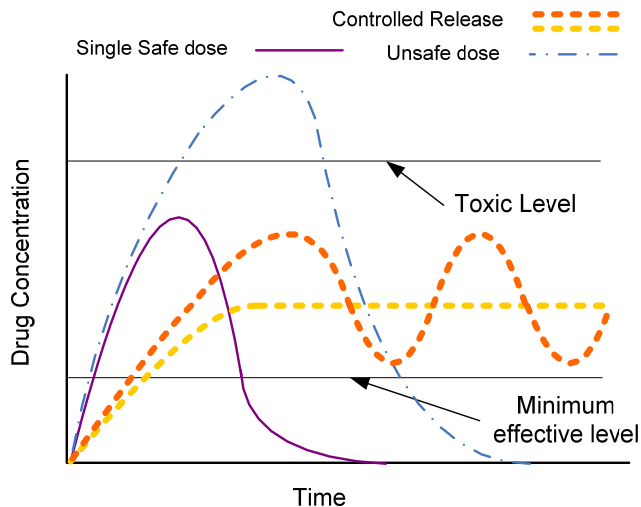
Figure 1.1 Drug concentration as a function of time.
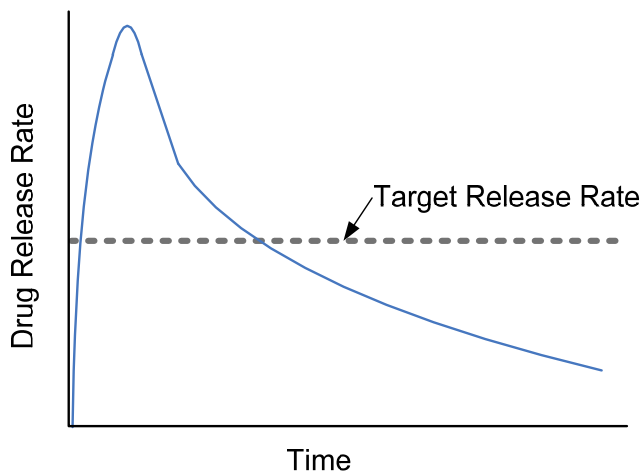
Figure 1.2 A typical release rate from a polymeric implant when a constant release rate is desired.

1.2.2   On-Demand Drug Delivery and MEMS Technology

For many disease applications, the delivery of therapeutic concentrations on an "on-demand" basis would be of tremendous benefit [6]. Ideally, on-demand drug delivery systems could determine the timing, duration, and dose of release and could allow remote, noninvasive, and repeatable switching of therapeutic agent release rate [12]. Furthermore, having an active control over the release of the drug is greatly advantageous in circumstances where the physiological conditions of the

patient change unexpectedly and therefore changes may be required in the administration of the drug.

Some studies show that polymeric drug delivery systems that are responsive to external stimuli such as electric fields [13] or magnetic fields [14] have the advantage of providing on-demand drug release compared to passive degradation-based polymeric delivery systems [15, 16]. Other triggerable materials that are sensitive to visible light, near-infrared light, and ultrasound have been proposed for drug delivery [12]. These drug delivery systems can actively control the time of release but the control of the delivery rate remains a major challenge.

Microelectromechanical Systems (MEMS) technology offers the potential to develop drug delivery devices with precise control of drug release, which are usually suitable for implantation [2, 17-19]. Developed MEMS devices could be categorized into systems with and without on-board power source.

1.2.2.1 Systems with an On-board Power Source

Miniature reservoirs loaded with drugs and sealed with thin film material have been introduced by Santini *et al.* [20]. In these devices, electrochemical [20] and electrothermal [21] methods have been used to break off the films and allow the release of stored doses of drug inside each reservoir. Using the microreservoir system, controlled pulsatile release of the polypeptide leuprolide was shown over a period of 6 months in dogs [22]. Furthermore, with this system, localized release of various compounds with defined temporal profiles was achieved *in vivo* [23, 24]. In another design [25], heat generated by microresistors located in a reservoir, increased the internal pressure and resulted in bursting of the sealant film and discharge of the contained solution. In these actively controlled devices, both drug release time and drug release rate could be controlled. Pulsatile release of individual doses enables a desirable release profile, 'generated' by repetitively releasing dose after dose. Several approaches to delivering drugs with micropumps have been developed using various diaphragm pumping mechanisms [19, 26].

All of aforementioned MEMS drug delivery devices need an on-chip battery for operation and therefore the overall size of the device is dominated by the battery size and its supporting electronics. This is a limiting factor in further miniaturization, and thus application, of these devices. Small battery fabrication is still challenging for drug delivery systems [17]. Wireless powering may be feasible using inductive coupling to shrink the device size [27]; however extra controlling circuitry may increase the system complexity.

1.2.2.2   Battery-less Systems

An alternative approach may use external magnetic actuation to circumvent the need for an integral power supply for MEMS devices. Magnetic micropumps with microchannels and valves have been proposed for drug delivery [19]. Most of these devices require relatively large pumping pressure (over 3 kPa) for operation due to the friction loss in microchannels and in some designs the large size may be a limiting factor for further implantation. Furthermore, valves with moving parts may also introduce reliability/sticking issues. Osmosis-based micropumping systems have been used for drug delivery [28]. They are, however, generally controlled by predetermined release rates based on the physical and chemical design of the device and share the same disadvantages as polymeric systems, as discussed previously.

Magnetic stimulus has also been used as a trigger for antiepileptic drug release from a flexible membrane, made by electrodeposition of drug-carrying core-shell magnetic nanoparticles, both *in vitro* and *in vivo* [29]. The membrane was made by electrodeposition of a layer of drug-carrying core-shell magnetic nanoparticles, coated with porous SiO_2. Switchable (i.e. on-off) release behavior was demonstrated. This device may not be suitable for treatment of chronic diseases, where long term drug release with highly controlled rates is desired. In another drug delivery device, a continuous directional magnetic field was used to control the rate of drug diffusion from a drug reservoir [30]. In this device, magnetic force was used to move free magnetic particles in a reservoir to block or unblock the porous membrane sealing the reservoir. However, the design requires continuous exposure to magnetic fields for both on and off states. This continuous magnetic field

requirement may be a limiting factor in application of such devices for chronic diseases.

A non magnetic, passive MEMS drug delivery device that requires no on-chip battery has been demonstrated [31]; however, the drug release that is activated by manually depressing the drug reservoir has unclear prospects for controllable and reproducible dosing.

In summary, developing battery-less drug delivery systems to treat chronic diseases that require on-demand and precise delivery of therapeutic agents over a long period of time is still a challenge. Such systems could provide an invaluable contribution to the therapy of diseases such as proliferative retinopathy.

1.3   Potential Applications

Late stage proliferative retinopathy is the leading cause of visual loss and marks the onset of blindness for diabetic patients [4]. Proliferative diabetic retinopathy involves unwanted proliferation of capillary cells in the retina (ocular angiogenesis), compromising retina function and causing vision loss [32, 33]. The conventional treatment for this disease is laser ablation therapy (panretinal laser photocoagulation), where unwanted capillary cells are ablated [34]. Although temporarily effective in reducing vision loss, this approach is inherently destructive and is associated with unavoidable side effects of diminished side and night vision and potential unwanted burns from the laser [35], whilst providing little or no improvement in visual acuity [36].

Current research efforts focus on less destructive methods to prevent the development of diabetes associated eye disease and inhibit disease progression [37]. Chemotherapeutic intervention to prevent the proliferation of retinal capillary cells has been proposed [38]. In vitro, antiproliferative drugs such as taxanes (paclitaxel or docetaxel) produce an antiangiogenic effect at low nanomolar concentrations [39]. However, following systemic administration, taxanes are rapidly cleared from the blood [3], so the need to administer high systemic doses of these drugs, to produce any localized antiangiogenic effect in the eye, would increase potential

toxicities to other tissues [5]. On the other hand, a localized, controlled release drug delivery system (Implanted in the periocular space at the posterior segment of the eye, enabling the release of drug molecules adjacent to the surface of the sclera) would provide the benefits of controlled release of an antiangiogenic drug delivered directly to the retinal tissues, with decreased systemic exposure and fewer side effects.

Various novel ocular drug delivery methods such as intravitreal injections, biodegradable and non-degradable implants, polymeric systems, and microneedles have been reviewed and described [36, 40]. In most of these implant systems, drug release occurs via diffusion and release rates are seldom constant/zero order. Furthermore, the dosing cannot be stopped except by surgical removal of the implant. Having active control of drug release (i.e. switchable on-off modes) is especially important when the physiological conditions of the patient change unexpectedly and a corresponding change in the dosing is required. Therefore, ocular drug delivery systems that are capable of providing precisely controlled and targeted dosing would be optimal for treating diseases such as proliferative diabetic retinopathy [41].

Recently, taxane-cobalamin bioconjugates have been proposed for local ophthalmic delivery at doses of approximately 0.001 to 10 μg/day [42]. Polymeric delivery systems have been described that allow the controlled release of taxanes for treating proliferative diseases. These include paclitaxel loaded microspheres for the prevention of intra-peritoneal tumor seeding [43], pastes for prostate cancer [44], and polymeric flexible films for vascular stenosis [45]. However, similar to conventional polymeric drug delivery systems, these formulations usually deliver a sustained amount of drug over extended time periods but there is little control of the dose. In the treatment of proliferative retinopathy, the following would provide significant advantages: intra-ocular placement of a polymeric film-type delivery system, to allow for unrestricted eye movement; and a large surface area of the drug formulation close to the target tissue, delivering a small but defined dose of drug via an external on-demand actuation.

A MEMS drug delivery device would be a suitable candidate for ocular applications, if the following conditions were met: (1) controlled and on-demand dosing; (2) biocompatibility; (3) minimum drug degradation within the device over the period of implantation; and (4) localized drug delivery to minimize systemic toxicities.

1.4   Objectives and Design Concept of a MEMS Drug Delivery Device

The main objective of this thesis is to develop a new magnetically controlled drug delivery device that can offer on-demand and controlled delivery of chemical compounds such as antiproliferative drugs with a prospect of future implantation. Specifically, this work aims at providing controlled and on-demand delivery of docetaxel at the concentrations suitable for the treatment of proliferative diabetic retinopathy, which requires accurate delivery of nanomolar drug concentrations.

Docetaxel used in this study exemplifies a model drug with high potency and considerable adverse effects when administered intravenously, but which could be of clinical value if delivered locally with a controlled release rate through a MEMS device. On the other hand, development of alternative, less toxic solutions for delivery of taxanes would provide significant advantages and is of great interest [3].

It is further necessary that the antiproliferative effect of docetaxel be maintained after the drug is packaged inside the MEMS device and the drug does not degrade during the desired operation time of the device.

The device consists of a drug-loaded microreservoir that is sealed with an elastic magnetic membrane with a laser-drilled aperture (100×100 μm^2). The principle of operation is shown schematically in Figure 1.3. During actuation, the force generated by an applied magnetic field causes the membrane to deform and build up pressure inside the reservoir to discharge the drug solution out of the reservoir, analogous to squeezing water out of a flexible bottle. The desired release profile may be "synthesized" by adjusting the amount and timing of drug release using different parameters such as the number of actuations and the strength of the

applied magnetic field. On-demand actuation of the device by application of a magnetic field determines the time of drug release.
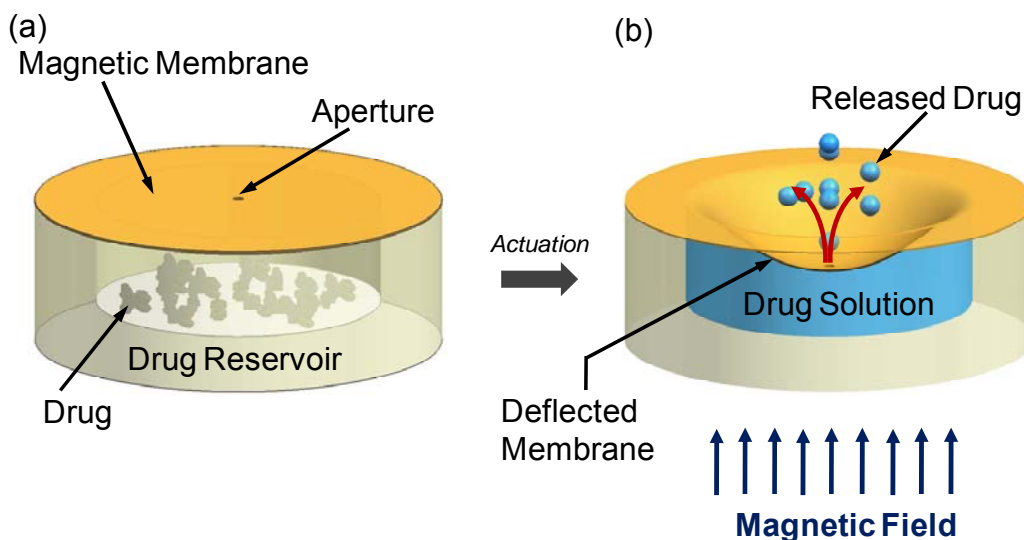
Figure 1.3 Principle of operation, (a) before actuation, (b) drug release after magnetic field application.

The design criteria for the membrane material are to:

1. Achieve large deflections to increase the displaced volume in each actuation; and

2. Have magnetic property and capability of being actuated under an applied magnetic field while not adversely affecting the deformability of the membrane.

1.5 Thesis Overview

This thesis is presented with an introductory chapter followed by three main chapters and concludes with a chapter summarizing the thesis and giving future directions. Each of the main chapters is a version of a published or a submitted article to a peer-reviewed journal.

Chapter 1 briefly reviews the advantages of controlled and localized drug delivery. It proceeds with an overview of current controlled drug delivery systems including

polymeric systems and MEMS technology. The existing limitations of current technologies are discussed followed by solutions proposed in this thesis, including potential use of them in the treatment of a particular disease.

Chapter 2 reports the development of a new magnetic composite membrane material for use in the proposed drug delivery device. This chapter reviews existing magnetic materials for MEMS applications, presents a fabrication process of the new magnetic composites using an elastomeric polymer and magnetic nanoparticles, and addresses particle agglomeration issues. It proceeds with the characterization of the mechanical and magnetic properties of the composites, surface roughness measurements, and finally free-standing membrane fabrication and actuation. This membrane is used in the fabrication of the MEMS drug delivery device in Chapter 3.

Chapter 3 presents the development of the MEMS drug delivery device proposed in this thesis. This chapter offers a magnetic and mechanical analysis for the device and provides a description of magnetic actuation forces and the resulting membrane deflections. It then proceeds to present the fabrication process of the MEMS device, model drug loading, and laser ablation of the aperture. Post-fabrication procedures including surface modification of the magnetic membrane and its characterization are described. Finally, on-demand delivery of a model drug is presented.

Chapter 4 reports the on-demand and controlled delivery of an antiproliferative drug, docetaxel, from the proposed MEMS drug delivery device. It reports on the drug release rate and effects of the controlling parameters, the long term release rate, and the leakage of drug from the device in 'off' state. It is followed by studying the biological activity of the released drug after two months, using cell viability assay. This chapter also describes the actuation setup and the time constants required for achieving constant release rates.

Chapter 5 summarizes the work presented and the conclusions reached in this thesis, followed by an assessment of potential future work.

CHAPTER 2

Development and Characterization
of Magnetic PDMS Composites[1]

2.1 Introduction

In this chapter, the development of a new magnetic membrane material for the proposed MEMS drug delivery device is presented. The fabrication processes of the material and the free-standing membranes are described. Furthermore, the mechanical and magnetic properties of the magnetic material are characterized as well as the surface roughness of the membranes. Finally, free-standing magnetic membrane actuations in magnetic fields are described. This chapter is organized as follows: in Section 2.2 an overview of the state-of-the-art magnetic material for MEMS applications is given. Section 2.3 presents the materials and methods including fabrication processes and measurement techniques. It proceeds with experimental results followed by discussions in Section 2.4.

---

[1] A version of this chapter has been published.

- **F. N. Pirmoradi**, L. Cheng and M. Chiao, "Magnetic Poly(dimethylsiloxane) Composite Incorporated with Uniformly Dispersed Coated Iron Oxide Nanoparticles", Journal of Micromechanics and Microengineering, vol. 20, No. 1, p. 15032, 2010.

2.2   Overview of Magnetic Materials in MEMS

Incorporating magnetic material in Microelectromechanical (MEMS) for sensing and actuation has attracted much attention during the past decade [46-49]. Among many different microscale actuation mechanisms, magnetic MEMS actuation has the advantage of producing large forces (hundreds of μN) and large displacements (tens to hundreds of μm) [50-52]. One of the unique characteristics of magnetic actuation compared to other actuation methods is that it can be performed without on-chip power sources.

Magnetic actuation mechanisms, such as magnetostatic, Lorentz force and magnetostriction, have been utilized to develop various magnetic MEMS devices and new magnetic materials [46, 53, 54]. Magnetic material can be integrated into MEMS through a variety of techniques such as electroplating, screen-printing, assembly and sputtering. Sputtering films thicker than 10 μm is a time consuming process and the films have been reported to have altered the magnetic property with an increase in thickness [55]. Microassembly requires extra post-fabrication steps and dimension concerns might limit their application in MEMS [56].

Electroplating of permalloy (19%Ni–81%Fe alloy) and nickel has been widely used in MEMS devices [57]. Electroplated thin-films of NiFe and nickel were attached to mechanical flexures (e.g. polysilicon cantilever) and actuated in a magnetic field [58, 59]. Electroplated permalloy actuators were used for fluid dynamics control [60]. Thick films (>50 μm) of CoNiMnP were electroplated to form arrays of permanent magnets that could be useful when integrated with MEMS components [61, 62].

Screen-printed polymer magnets have been demonstrated in MEMS devices. Commercial polyimide was used as an organic polymer matrix and strontium ferrite powder (1.5 μm average particle size, 55–80% by volume) as an embedded inorganic magnetic material [63]. The magnetic composite had the ability to be patterned by photolithography and wet etching processes (features greater than 200 μm) and required a 300°C curing step. A cantilever beam-type magnetic actuator

carrying a screen-printed disc magnet on the free end was also demonstrated [64]. Epoxy resin was used as a polymer matrix to reduce the maximum processing temperatures to 80°C that resulted in more flexibility in fabrication steps and the possibility of using photoresist as sacrificial layers. A screen-printed magnetic NdFeB film of 50 μm thick was reported that was made up of 80 wt% powder in a resin [65]. The commercial NdFeB powders were wet-milled for 20–50 h to achieve an average particle size of 50 μm and large particle sizes were removed by sieving. They have observed powder agglomerations used in high concentrations. A composite magnet with 40% volume fraction of powder in polymer has been fabricated (5 mm diameter × 2.2 mm thickness) by mixing polydimethylsiloxane (PDMS) and NdFeB magnetic powder (particle size of ∅200 μm) [66]. Subsequently, a polymeric micropump system was made by attaching the rough magnetic composite block to a pure PDMS membrane. The design avoids the contact of the magnetic composite to fluid in the channel and possible corrosion of the magnet. Finally, NdFeB and barium ferrite powders mixed with PDMS were used to screen-print a magnetic membrane of thickness 216 μm [67]. Recently, the possibility of local actuation of a magnetic micro-slab made from 25% w/w coated magnetic nanoparticles in PDMS has been investigated through simulation [68].

Another type of magnetic membrane fabrication was performed by precise positioning of magnetic blocks of electroplated permalloy (100 μm × 870 μm) inside a 40 μm thick PDMS membrane and optimized for maximum deflection [51]. However, precise placement of blocks in the thin film sophisticates the fabrication process and its application in MEMS.

There has been a growing interest in developing new membrane materials and fabrication methods for micro-total analysis systems since membrane-type actuators have found applications in MEMS. For instance, Sundararajan *et al.* showed the integration of a deformable polymer membrane as an active component into a single microfluidic chip to perform pumping, mixing and sorting [69]. Polymer membranes incorporated with magnetic particles combine the favourable properties of magnetic material with simple and economical processing sequences of polymers

with low Young's modulus to achieve large deflections. Therefore, magnetic flexible thin membranes have a great potential for integration in lab-on-a-chip and multilayer microfluidic systems for actuation and sensing purposes. Microvalves and micropumps, which are the critical components in such systems for handling and transportation of fluid or gas in microchannels, have been demonstrated to be promising applications of such magnetic membranes. For example, Yamahata *et al.* demonstrated the pumping of mammalian cells using electromagnetically actuated micropump [70].

One of the main challenges in incorporating magnetic particles into a polymer matrix is the aggregation of particles in the polymer matrix which leads to their non-uniform distributions [71]. The resulting surface roughness may cause difficulties in bonding of membranes to substrates and moreover, the light scattering surface will make optical characterization a challenge. Furthermore, the agglomeration of particles could affect mechanical properties of the membrane due to stress concentration.

2.3   Materials and Methods

PDMS (Sylgard 184 Silicone Elastomer, Dow Corning Corporation) was used as the polymeric matrix. PDMS was supplied in two compounds: a pre-polymer and a crosslinker (or hardener). Typical mixing ratio of pre-polymer and crosslinker is 10:1; however, we used a 5:1 ratio to achieve a greater link formation in the polymer. This led to a more rigid polymer with reduced liquid absorption [72]. Three types of magnetic PDMS composites were prepared by using two types of coated and one type of uncoated iron oxide particles as filler materials. The coated particles (Ferrotec, MA, USA) were (1) EMG 1200, proprietary fatty acid-coated iron oxide nanoparticles; and (2) EMG 1400, iron oxide nanoparticles with a proprietary hydrophobic surfactant. Both were obtained as dry particles. The weight percent of iron oxide in EMG 1200 and EMG 1400 were 67.2–72.6% and 77.0–83.0%, respectively. The particles were a 50/50 mixture of Fe_3O_4 / γ-Fe_2O_3 with an average particle size of 10 nm. The uncoated iron oxide particles with a diameter

range of 20–30 nm were purchased from Nanostructured & Amorphous Materials, Inc. (TX, USA) and used as received.

Colloid dispersions of EMG 1200 and EMG 1400 particles were made separately to form the ferrofluid by dissolving dry particles in toluene (Fisher Scientific, ON, Canada), a compatible solvent for the dry particles. Successive additions of particles into toluene were followed by stirring, heating at 35°C, and sonicating in an ultrasound bath (Kell-Strom, Branson Model 1510), that was necessary to achieve a stable colloid. The final ferrofluid was dispersed by sonication for 30 min. The PDMS pre-polymer was dissolved in toluene and stirred for 10 min to achieve a diluted polymer base. The ferrofluid was then mixed with the polymer base at a mass fraction of 40% w/w particles to the polymer. Considering iron-oxide weight content of the particles is ~72% to 80% and considering the surfactant has a density of 1 g/cm^3 and iron oxide has a density of 5.2 g/cm^3, the weight concentration of 40% particles in PDMS corresponds to volume percentage of 7.6% to 8.3% of magnetic content in composites. The ferrofluid and polymer base mixture was sonicated for 10 min using a high-power sonic tip (Misonix Inc., XL2020, NY, USA) and followed by sonication in a sonic bath at 35°C and stirring for 30 min. The composite solution was then stirred for 3 h under a fume hood to allow the toluene to evaporate and then degassed in a desiccator for another 60 min. The crosslinker of PDMS was then added and mixed fully for 15 min followed by degassing for 30 min. Use of different solvents and fabrication processes compared to the ones in [68] allows for higher loadings of particles in PDMS while maintaining spinnable liquid composites that could cure properly and form thin (~35 μm) free-standing membranes.

The magnetic PDMS composite with uncoated iron oxide particles was fabricated using the same method except that a longer time of 4–6 h of sonication by a high-power sonic tip was necessary before and after the addition of PDMS pre-polymer to minimize particle agglomerations.

Scanning electron microscope (SEM) images of the PDMS composites were taken both at a 55° angle and from above. Samples were sputter coated with platinum for

30 s prior to SEM experiments. Particle sizes were measured from the SEM images using the UTHSCSA ImageTool program v.3 (University of Texas Health Science Centre at San Antonios, Texas, maxrad6.uthscsa.edu). Surface roughness of the composites was measured while they were spin-coated on glass slides using a Wyko surface profiler (VEECO Metrology Group, AZ, USA).

Superconducting Quantum Interference Device (SQUID) (Quantum Design, CA, USA) was used to measure the magnetic moment (emu) as a function of applied magnetic field (Oe). Specimens for magnetic tests were fabricated by curing the polymer composites on a glass slide and peeling them off. Since the specimen in SQUID was considered as a point source, the size of the specimens did not exceed 4 mm in diameter. To minimize the background effect from the air gap in the quartz sample holder, the specimens were made of films with a thickness of about 0.5 mm.

The stress and strain behavior of the PDMS composites was measured by tensile testing using a thermo mechanical analyzer (TMA 2940-Q series, TA Instruments, DE, USA) with a films/fibres probe. The specimens were fabricated as films on glass slides and had a width and a thickness in the range of 0.4–0.5 mm and 0.6–0.9 mm, respectively. The films were peeled off from the glass slides after curing and were clamped at two ends on a sample holder for measurement. The temperature was held at 23°C during the test. The applied force was then ramped in three steps: (1) 0–0.01 N with a step size of 0.001 N/min, (2) 0.01–0.05 N with a step size of 0.01 N/min and (3) 0.05–0.8 N with a step size of 0.1 N/min. The unloading was performed uniformly at a rate of 0.1 N/min.

Free-standing magnetic PDMS membranes were fabricated using a combination of micro-molding, sacrificial etching and bonding techniques, and were tested in an external magnetic field. Figure 2.1 shows the fabrication steps of the free-standing membranes. Photoresist (AZ-P4110, Clariant Corporation, QC, Canada) was deposited on a silicon substrate to be used as a sacrificial layer.

The PDMS magnetic membrane was formed by spin-coating on the photoresist layer in three spinning steps (500 rpm for 15 s, 1000 rpm for 15 s and 2500 rpm for

30 s) and cured at 80°C. Fabrication of thin (down to ~3 μm) and ultra-thin (down to ~70 nm) PDMS membranes were demonstrated before [73, 74]. Arrays of SU-8 pillars with different sizes (4–7 mm diameter) were fabricated on a silicon wafer by photolithography and used as a mold. Subsequently, pure PDMS was poured onto the mold, cured at 80°C in convection oven and peeled off from the mold resulting in formation of cavities in PDMS. Next, this PDMS substrate was permanently bonded to the PDMS magnetic membrane by O_2 plasma treatment of both surfaces [75] using PECVD (Trion Technology Inc., FL, USA). The structure was then immersed in an acetone bath to release it from photoresist to form suspended membranes. Finally the samples were dried in the oven.
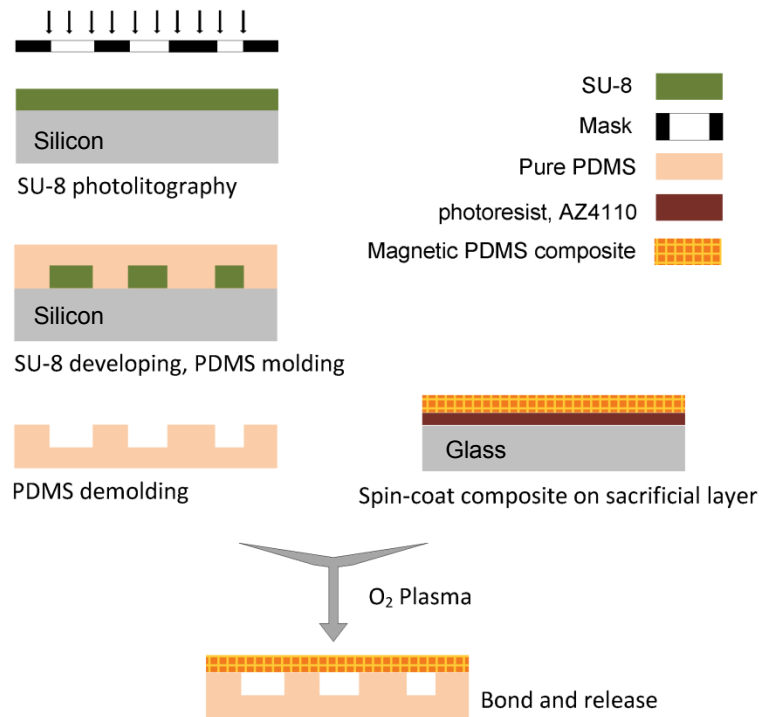
Figure 2.1 The fabrication process of a free-standing magnetic membrane

The membrane deflection was measured as a function of the magnetic field. An axially magnetized, neodymium cylinder permanent magnet with a diameter of $\frac{1}{2}$" and thickness of $\frac{3}{4}$" (D8C, K&J Magnetics, Inc., PA, USA) was used as the source of magnetic field. The magnetic field of the permanent magnet was characterized as a function of the distance from the magnet using an F. W. Bell Gaussmeter (Sypris

Test & Measurement, FL, USA). The permanent magnet was positioned to approach the free-standing membrane from the top and able to precisely travel vertically away or towards the membrane. A stereo microscope (Olympus SZ61, Olympus Imaging America Inc., PA, USA) was used to take series of images of the deflected membrane in different magnet positions (i.e. different external magnetic fields) followed by image processing (UTHSCSA Image Tool program v.3).
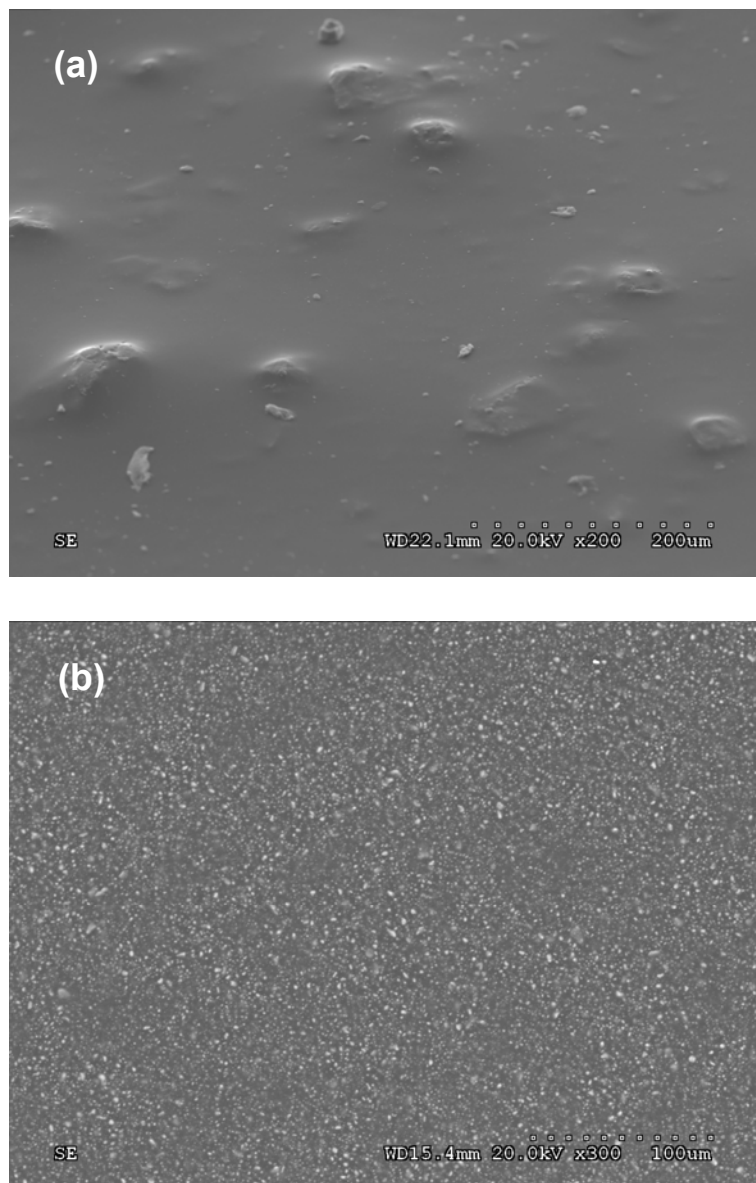
Figure 2.2 (a) PDMS loaded with 40% w/w uncoated iron oxide particles, (b) PDMS loaded with 40% w/w of EMG 1200 particles.

2.4   Results and Discussions

Figure 2.2-a shows an SEM image of a spin-coated composite film made of PDMS loaded with 40% w/w uncoated iron oxide particles. The surface has non-uniformly distributed aggregates of particles as large as 51 ± 24 μm. Figure 2.2-b shows an SEM image of a spun film that is made of PDMS loaded with 40% w/w of EMG 1200 particles (7.6% volume content). The surface does not show significant aggregates compared to the uncoated iron oxide composite surface. Furthermore, a reduction of agglomeration is observed with the largest particle size measured as 1.6 ± 0.25 μm. The largest particle size in the PDMS loaded with 40% w/w of EMG 1400 is measured as 2.68 ± 0.97 μm (SEM not shown).

The surface roughness profiles of the PDMS composite films with a sample size of 600 μm × 450 μm × 50 μm (length × width × thickness) are shown in Figure 2.3. A comparison of the surface roughness of the films made of EMG 1200, EMG 1400 and uncoated iron oxide particles loaded in PDMS is given in Table 2.1. The surface roughness values are the average of the values measured from three specimens for each material. Due to the very large random-shape aggregates of the particles in the uncoated iron oxide composite film that resulted in light scattering, it was challenging to measure the profile of the film. The roughness of the film was measured excluding the large aggregates (larger than 15 μm) and the results still show a 4.2 times increase in surface roughness (root mean square) compared to PDMS composite films loaded with EMG 1400 particles.
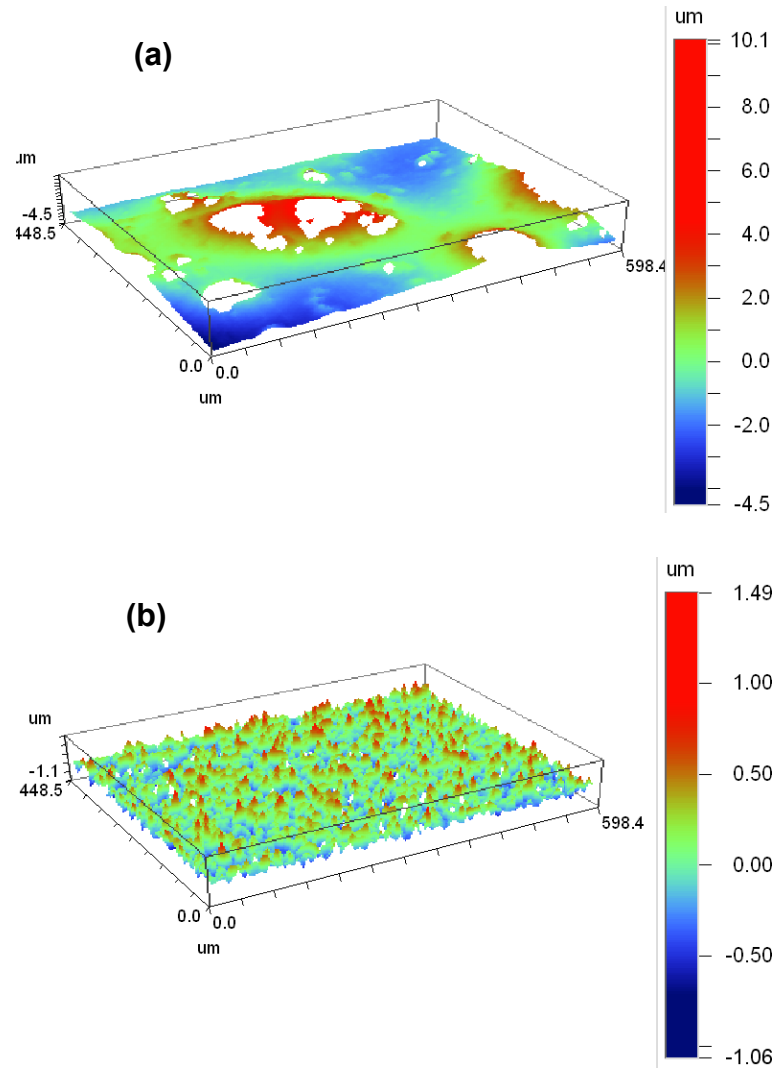
Figure 2.3 The surface roughness profile of the composites: (a) 40% w/w of uncoated iron oxide particles in PDMS (film thickness of ~30 µm), and (b) 40% w/w of EMG 1400 particles in PDMS (film thickness of 50 µm).

Table 2.1 Surface roughness measurements for 40% w/w of EMG 1200, EMG 1400, and uncoated iron oxide particles in PDMS.

Surface roughness	Root mean square (R_q)	Arithmetic mean (R_a)	Average Max. Heights (R_z)
EMG 1200 in PDMS	171.1 ± 2.58 nm	131.8 ± 0.94 nm	1.78 ± 0.09 µm
EMG 1400 in PDMS	300.9 ± 2.5 nm	240.9 ± 2 nm	2.34 ± 0.02 µm
Uncoated iron oxide in PDMS	1.27 ± 0.33 µm	1.76 ± 0.5 µm	23.6 ± 11.6 µm

Figure 2.4-a shows the magnetic moment per unit mass of the composite samples with respect to the magnetic field strength. Data for each condition is from one sample measurement. It is observed from Figure 2.4-b that both composites show remanent magnetization less than 0.43 emu/g which shows small deviation of the composites' magnetic property from its iron oxide nanoparticles superparamagnetic characteristics (data provided by the manufacturer). The non-zero remanent magnetization after removal of the field is due to small clusters of magnetic nanoparticles in the range of 0.5–5 μm [76]. In [68], for less particle loadings of 25% w/w, no rise to a measurable hysteresis in the magnetization curves and thereby no significant change in superparamagnetic property has been observed. Table 2.2 summarizes sample specifications and their measured magnetic properties. Both samples show less than 1% increase in the magnetization slope above 3000 Oe (238.7 kA/m) field, which corresponds to the magnetization of 20.85 emu/g and 21.9 emu/g for EMG 1200 and EMG1400 composites, respectively. The saturation magnetization (M_s) was calculated as the average of the magnetization values with a slope of less than 0.4%.
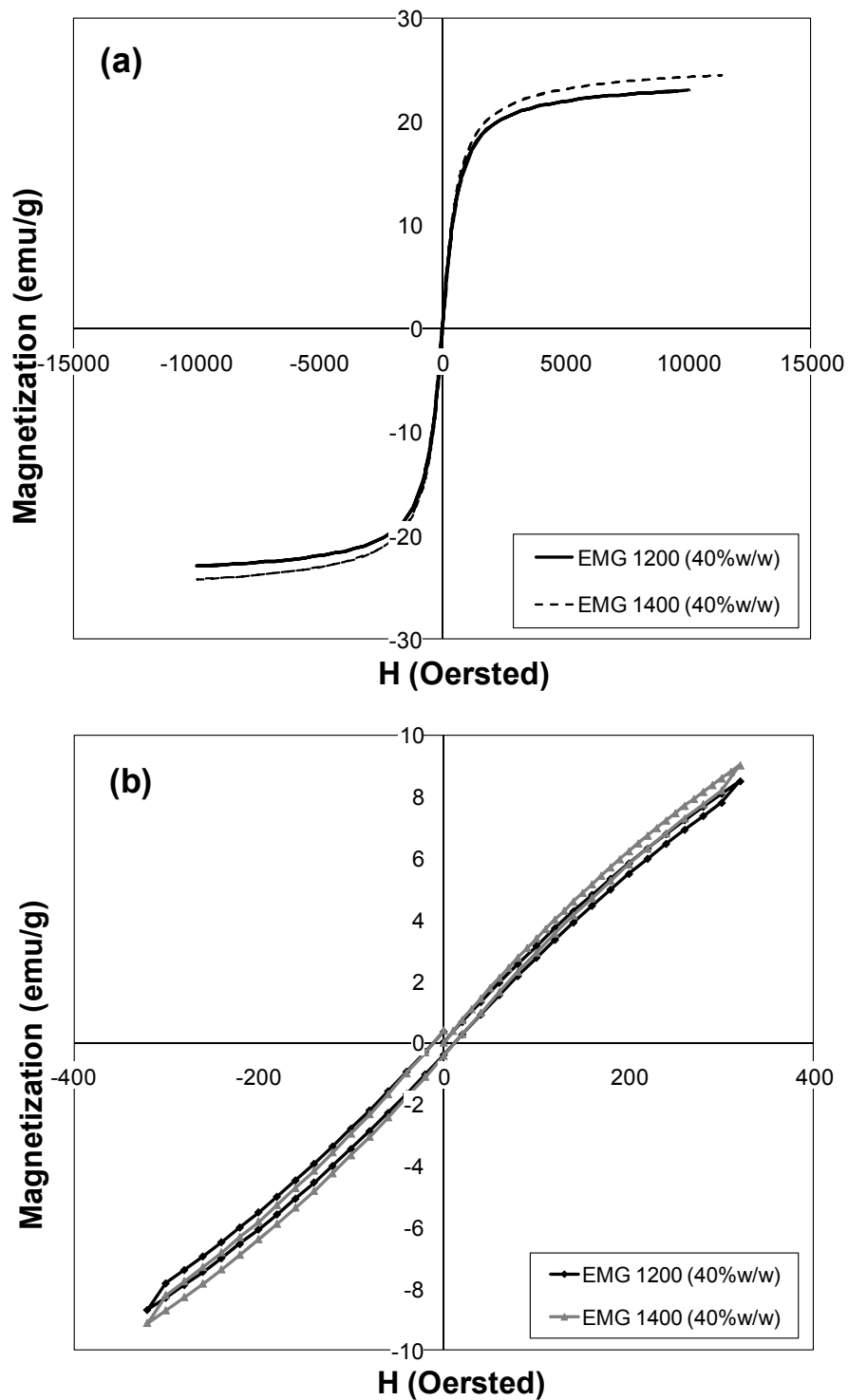
Figure 2.4 Magnetization curves versus field strength for the composites composed of (a) 40% w/w of EMG 1200 and EMG 1400 particles in PDMS measured at room temperature (23°C), and (b) magnetization curves at low magnetic field values at 23°C.

Table 2.2 The iron oxide percentage and magnetic properties of the composites.

Sample	Particle loading (wt%)	Iron-oxide content in composite (wt%)	M_s (emu/g), at 23°C	Field at saturation (Oe), at 23°C	M_s (emu/g), at 37°C	Field at saturation (Oe), at 37°C
EMG 1200 Composite	40	28	22.8	6970	22.2	7010
EMG 1400 Composite	40	32	23.94	4740	23.68	7620

To investigate the effect of temperature on the magnetic properties of the composites, specimens were additionally measured at 37°C. As a result, the saturation magnetization, M_s, has decreased less than 3% and 1% compared to the results for EMG 1200 and EMG 1400 composites at 23°C, respectively (Table 2.2).
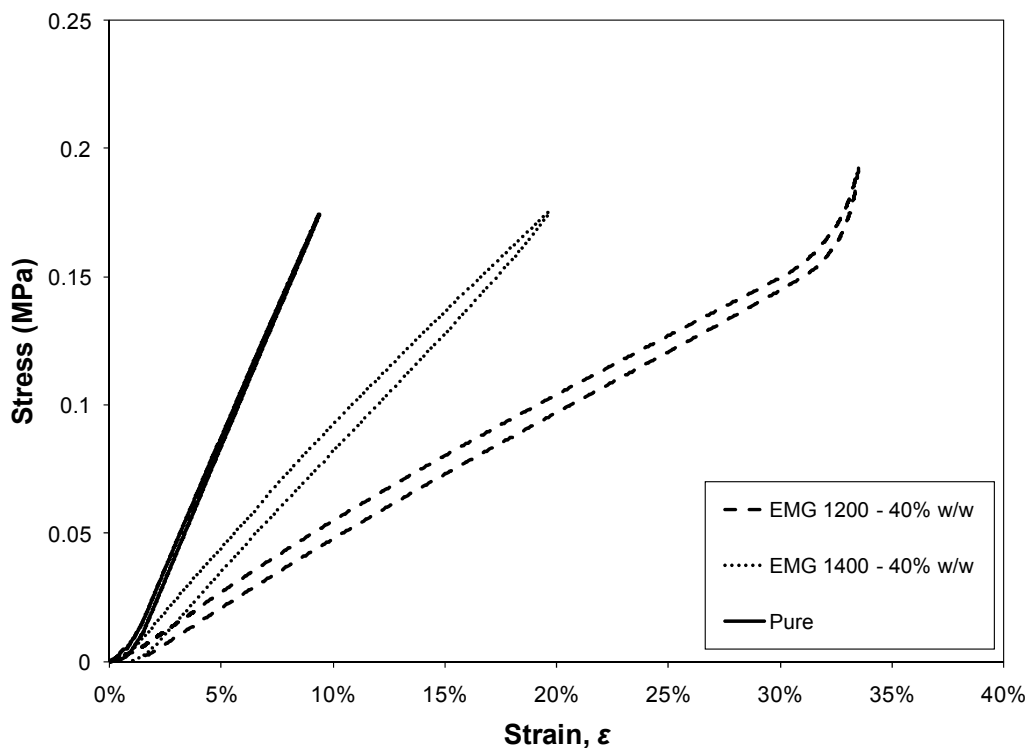
Figure 2.5 Stress-strain curves of the PDMS composites.

Figure 2.5 shows the stress–strain data of pure PDMS, PDMS loaded with 40% w/w EMG 1200 and PDMS loaded with 40% w/w EMG 1400 particles. In all cases, the

curves are linear at low strains. At strains above 30%, the EMG 1200 composite film starts to show strain hardening while other materials do not exhibit such behavior within the experimental window. The specimens for each material were tested and Young's moduli for each are summarized in Figure 2.6 (The Young's modulus of iron oxide was reported to range from 214 to 350 GPa). Both composites show a decrease in Young's modulus compared to that of the pure PDMS specimen. Low Young's modulus of the composites is advantageous since actuation of a magnetic structure is possible with lower magnetic fields. Previously, reduced moduli and tensile strengths have been observed when coupling agents were introduced to the polymer composite [77]. The reduction in Young's modulus of a polymer composite could be the result of poor interactions between the polymer network and the filler material. The surface characteristics of the filler material determine the chemical and physical interaction between the filler and the polymer chain network and have a great effect on the mechanical properties of the composites [78].

Poor adsorption of the polymer network chains onto the filler particle surfaces may reduce the possibility of entanglement and prevent the possibility of crosslinking [77, 79]. Similar results for decreased elastic modulus with the same order of magnitude were observed in [68] which has been attributed to pollution of catalyst that promotes crosslinking by magnetic particles. Aggregated particles in the composite may also contribute to the decrease in Young's modulus of the composites which require further investigation for validation.
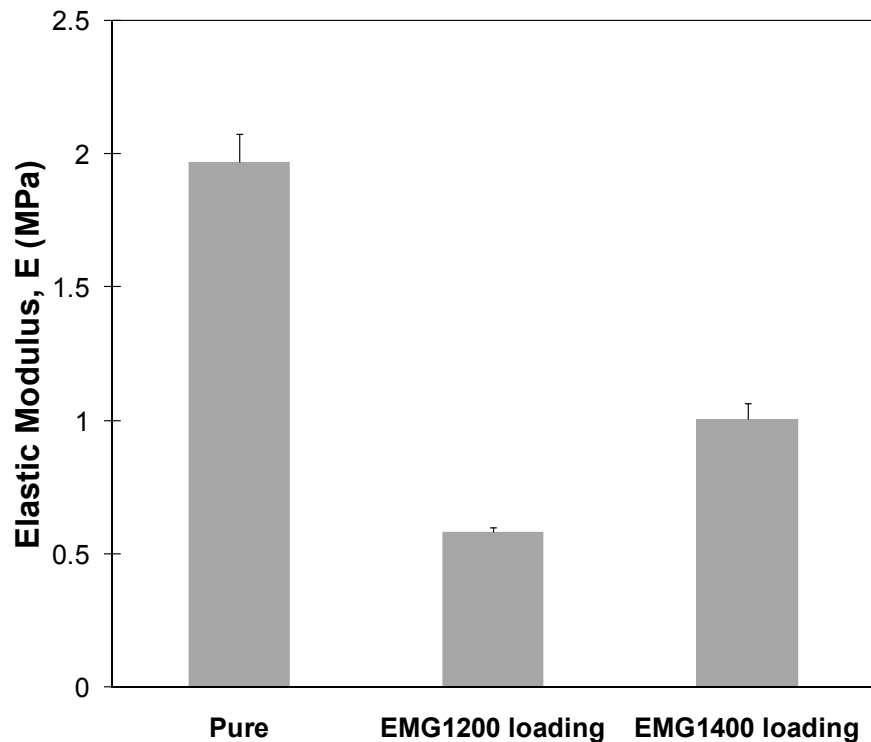
Figure 2.6 Elastic moduli of pure PDMS, and PDMS loaded with 40% w/w of EMG 1200 and EMG 1400 particles.

In Figure 2.7, a permanent magnet was positioned above the free-standing magnetic membrane with a diameter of 7 mm and a thickness of 37 μm. It shows three sample images that were taken while the permanent magnet was travelling away from the magnetic membrane and as a consequence the membrane deflection decreased. The centre of the membrane is not in the plane of the permanent magnet; thus, the membrane experiences a magnetic field gradient. Therefore, a magnetic force is created in the vertical direction, which is proportional to both the magnetic field gradient and the magnetization of the composite membrane in the vertical direction, causing the membrane to deflect. The magnetic field strength perpendicular to the membrane surface decreases with the increase in the distance from the permanent magnet to the magnetic membrane. Therefore, membrane deflection decreases as the magnet moves away. Suspended magnetic membranes with 35.5 ± 1.5 μm thickness were fabricated in different sizes (4–7 mm in diameter) and were actuated in an applied magnetic field. Figure 2.8 shows the

deflection of these membranes at their centre as a function of a magnetic field. The 7 mm diameter membrane achieved deflection of 625 μm in a 0.417 T field. The results show that it is possible to make membranes in different sizes to achieve sequential actuation of the membranes that can be used in different applications such as timed triggering for series of vales.
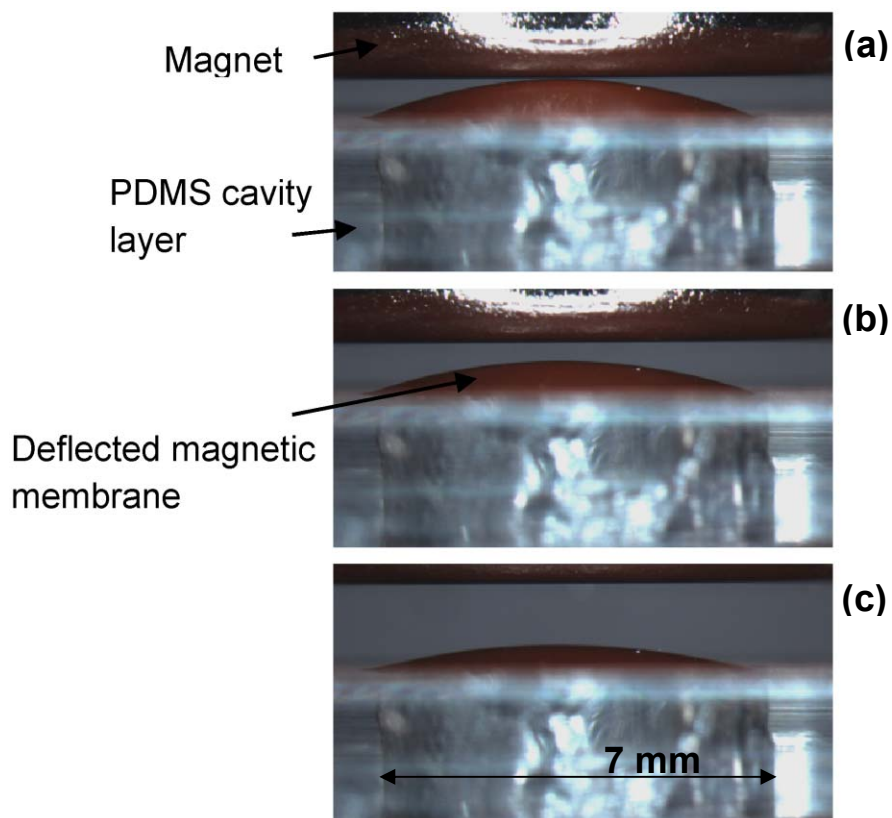
Figure 2.7 Membrane (7 mm in diameter and 37 μm in thickness, made of 40% w/w of EMG 1200 particles in PDMS) deflection as a function of magnet position. The membrane shows reduced deflection by increasing magnet distance, (a) through (c).
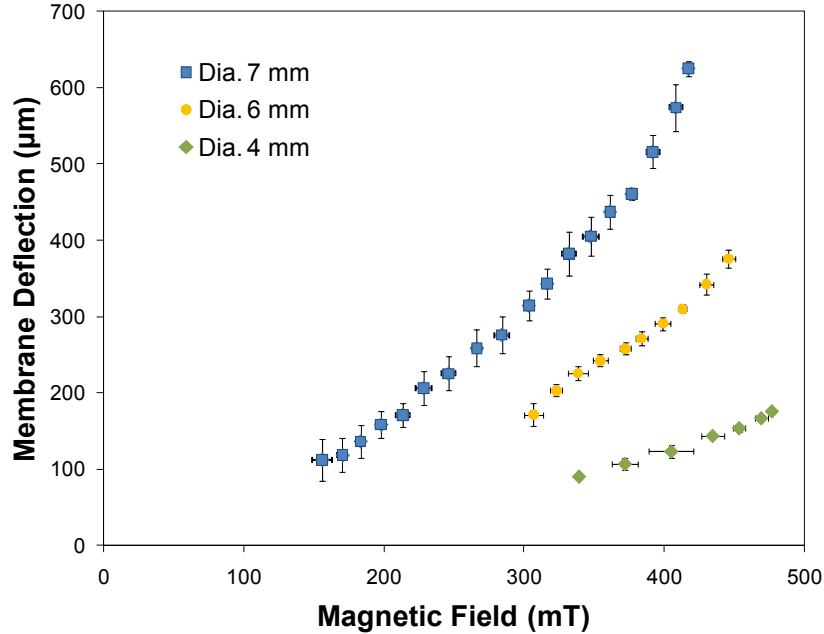
Figure 2.8 Center deflections of the membranes with different sizes as a function of the applied magnetic field. The membranes are made of 40% w/w of EMG 1200 particles in PDMS and have a thickness of 35.5 ± 1.5 μm. The vertical error bars represent the deviation in three sets of measurements using the same membrane. The data on x-axis were sorted into same length intervals (bins) and all the points belonging to the same bin were treated as readings at the middle of that bin. The horizontal bars represent these intervals.

The nonlinear deflection curve may be due to the nonlinearities in the system such as (1) the operating external magnetic field which corresponds to the nonlinear transition region from linear magnetization to saturation magnetization (Figure 2.4); (2) the nonlinear relationship between the pressure caused by the magnetic field on the membrane with its deflection, $p \sim (\omega_0, \omega_0^3)$ [80] where p is the uniform pressure and ω_0 is the centre deflection; (3) the nonlinear dependence of the magnetic field and gradient on the distance.

2.5 Concluding Remarks

In this chapter, a new magnetic material was developed by incorporating coated iron oxide nanoparticles with PDMS matrix. The developed material exhibited significant reduction in agglomerated particle size and membrane surface

roughness. Their favorable elastic properties make them suitable to be used as membrane materials. Free-standing membranes could be fabricated as thin as 35 µm and actuated as a function of applied magnetic field. This magnetic material is used to fabricate the actuating membrane for the drug delivery device that is presented in Chapters 3 and 4.

CHAPTER 3

Design, Fabrication, and Testing
of the MEMS Drug Delivery Device[2]

3.1 Introduction

In this chapter the development of the magnetically controlled drug delivery device for on-demand drug release is described. The device consists of a drug-loaded microreservoir that is sealed by a magnetic PDMS membrane with a laser-drilled aperture. It is actuated remotely by a magnetic field to trigger drug release. This device uses the magnetic PDMS material that was described in Chapter 2. The material in this chapter is organized as follows: in Section 3.1, a detailed analysis of the magnetic actuation forces is presented followed by an estimate of the resulting membrane deflections. In Section 3.2, the materials and the employed measurement techniques are explained. This section also outlines the fabrication steps including

---

[2] A version of this chapter has been presented at a conference and published.

- **F. N. Pirmoradi**, J. K. Jackson, H. M. Burt, M. Chiao, "A Novel Magnetically Controlled Drug Delivery Device", *The 8th International Conference on the Scientific and Clinical Applications of Magnetic Carriers*, Rostock, Germany, May 25-29, 2010.

- **F. N. Pirmoradi**, J. K. Jackson, H. M. Burt, M. Chiao, "A Magnetically Controlled MEMS Device for Drug Delivery: Design, Fabrication, and Testing", *Lab on a Chip,* vol 11, pp. 3072-3080, 2011 (DOI: 10.1039/c1lc20438f).

model drug loading and laser ablation processes. Section 3.3 presents necessary post-fabrication procedures including surface modification of the magnetic membrane and reservoir filling. Finally, on-demand delivery of a model drug is presented.

3.2 Magnetic and Mechanical Analysis

The overall design of the device may be described schematically as shown in Figure 3.1. A suspended magnetic membrane is bonded to a drug reservoir and placed in a magnetic field induced by a permanent magnet. The body coordinate frame is located at the surface of the permanent magnet and the z-axis is aligned with the axis of symmetry perpendicular to the surface of the permanent magnet. The center of the circular membrane is aligned with the *z*-axis. The membrane radius and thickness are *a* and *t*, respectively. The membrane is placed in an external magnetic field **H** which magnetizes the membrane to magnetization **M**. The applied magnetic field can also be expressed as an applied magnetic flux density **B** in Tesla: $\mathbf{B} = \mu_0 \mathbf{H}$ where μ_0 is the permeability of free space and equals to $4\pi \times 10^{-7}$ T.m/A.
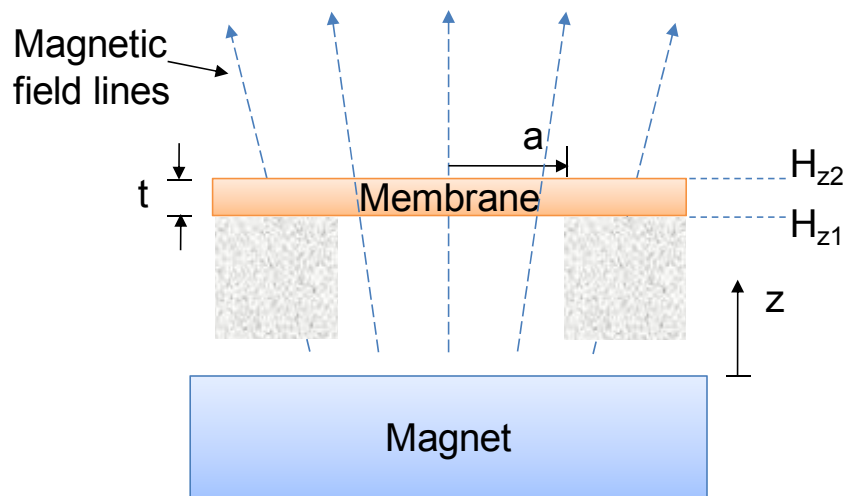
Figure 3.1 Schematic illustration of the actuation mechanism of the suspended magnetic membrane under an external magnetic field using a permanent magnet.

The magnetic membrane is a composite material made of iron oxide nanoparticles dispersed in a PDMS (polydimethylsiloxane) matrix and was previously described

in Chapter 2. The composite is a soft magnetic material with negligible hysteretic effect. Therefore, as opposed to permanent magnet analysis where the magnetization of the membrane can be assumed to be independent of the applied magnetic field and equal to M_s, the membrane's magnetization is a nonlinear function of the applied magnetic field. Although detailed modeling of the magnetic membrane is not the focus of this work, an analysis using the experimental data provides helpful estimations for some device parameters, such as drug reservoir volume change as a result of magnetic actuation and membrane deflection.

Figure 3.2 shows the magnetization curve for the magnetic composite (40% w/w EMG 1200) measured at both 23°C and 37°C. In low applied magnetic fields the magnetization grows linearly with the field strength and after a transient region where the magnetization dependence on the field is nonlinear, it reaches a constant magnitude saturation magnetization. The saturation magnetization of the material is approximately 37 mT at 23°C and 36.1 mT at 37°C in a 700 kA/m field.
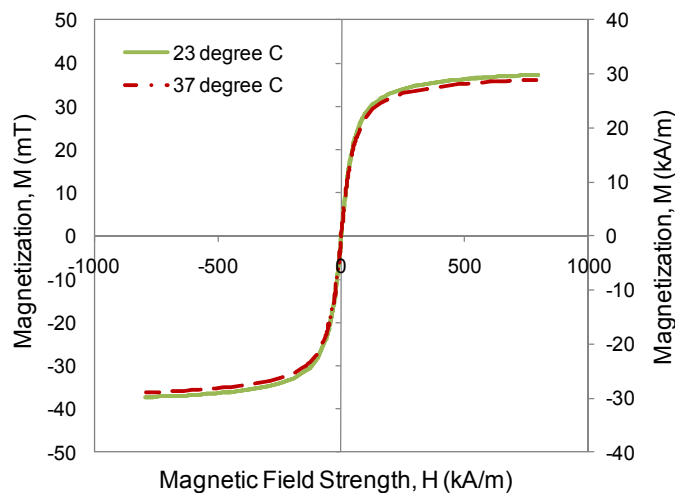
Figure 3.2 Magnetization of the magnetic composite material (40% w/w of EMG 1200) in 23°C and 37°C.

3.2.1   Magnetic Force

Once the magnetic PDMS membrane is placed in a magnetic field, the demagnetization field arises due to its shape anisotropy opposing the applied field. The magnetization in the magnetic membrane is related to the internal true

magnetic field ($\mathbf{H}_{int}$) acting on it. The internal magnetic field is a function of the applied magnetic field ($\mathbf{H}$) as well as the demagnetization field ($\mathbf{H}_d$). The following formula describes the above relation [81]:

$$\mathbf{H}_{int} = \mathbf{H} + \mathbf{H}_d \tag{3.1}$$

The demagnetization field is proportional to the magnetization by a tensor N of demagnetization factors

$$\mathbf{H}_d = -N\mathbf{M} \tag{3.2}$$

where the elements of N are between zero and 1 in SI units. In the analysis for z-direction, since the z-axis is the shortest axis of the membrane and thus the hard axis of magnetization, the demagnetization factor in z-direction (n_z) is higher compared to other axes. Consequently, the internal magnetic field in the sample cannot simply be taken as the applied magnetic field. To realize if the force exerted on the membrane is large enough to deflect the magnetic membrane, consider the force on a magnetic dipole [82]

$$\mathbf{F} = \mu_0 v \begin{bmatrix} \frac{\partial}{\partial x}\mathbf{H}^T \\ \frac{\partial}{\partial y}\mathbf{H}^T \\ \frac{\partial}{\partial z}\mathbf{H}^T \end{bmatrix} \mathbf{M} \tag{3.3}$$

where v is the volume of the magnetic membrane in cubic meters (m^3) and the force is in newton (N). The magnetic force in a given direction is the dot product of the derivative of the field in that direction and the magnetization vector [82]. Therefore, an increase in the directional derivatives in the applied field generates larger force on the magnetic membrane. We assume that local changes in the applied magnetic field along the radial direction of the membrane are negligible and therefore, the magnetic effects may be approximated as lumped effects at the centre of the membrane. Also, the field is assumed to change linearly across the membrane.

Since the membrane material is soft-magnetic, the magnetization vector rotates away from the easy axis to align with the external field direction [59]. To calculate

the magnetic force based on Eq. (3.3), the equilibrium angle of the magnetization vector with the field direction is desired which is an exhaustive modeling task due to the likely changes of this angle with applied field magnitude. For simplified calculations of the force, the direction of the magnetization vector **M** may be assumed in the direction of the applied field. This assumption may overestimate the applied force; however it can be a good estimation from the design perspective. Consequently, Eq. (3.3) is simplified as

$$F_z = \mu_0 v \frac{\Delta H_z}{\Delta z} M_z \tag{3.4}$$

where $\Delta H_z = H_{z2} - H_{z1}$ which H_{z1} and H_{z2} correspond to magnetic field strengths at z_1 and z_2 positions away from the surface of the magnet at $z=0$ and Δz corresponds to the thickness of the membrane (Figure 3.1). Therefore, the field gradient generated due to the distance creates a force on the membrane in z-direction. Equation (3.4) also indicates that using higher concentrations of magnetic particles, leading to higher magnetization, is a contributing factor in increasing the force; however, fabrication of membranes with such characteristics remains challenging due to particle agglomeration at higher particle concentrations in the polymer.
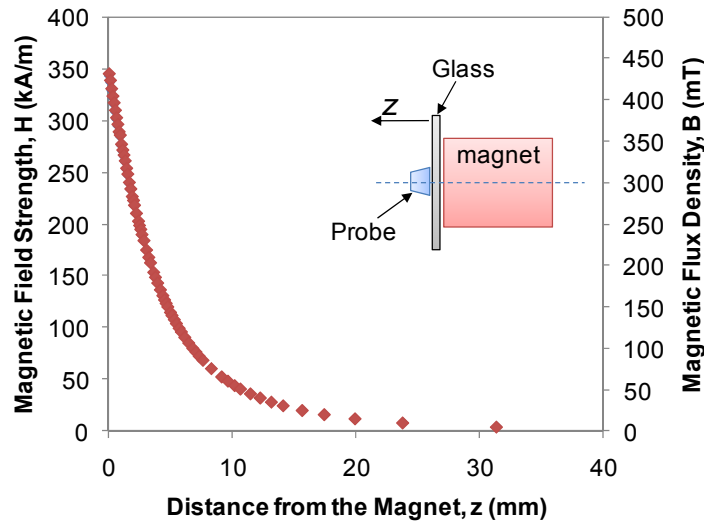
Figure 3.3 Magnetic field strength of the permanent magnet as a function of the distance from the surface of the magnet (neodymium, diameter $=\frac{1}{2}$", thickness $=\frac{3}{4}$").

33

Figure 3.3 shows the magnetic field strength and flux density as a function of distance from the surface of the permanent magnet. Since $z_1 < z_2$ $(z_2 = z_1 + t)$, $H_{z1} > H_{z2}$ and therefore, increasing the thickness of the membrane may increase the applied force on the membrane. However, from a mechanical design perspective, an increase in thickness of a membrane leads to a higher bending modulus and may result in the need for a greater force to deflect the membrane. Figure 3.4 shows the theoretical magnetic force on membranes of various sizes considering a typical thickness of 40 μm for all. The magnetic force is calculated based on Eq. (3.4) where M is the measurement data presented in Figure 3.2 considering the true internal magnetic field in the membrane according to Eq. (3.1) and $\frac{\Delta H_z}{\Delta z}$ is based on the measurement data shown in Figure 3.3. The demagnetization factor for thin disks when the field is perpendicular to the surface of the disk and the membrane is uniformly magnetized is 0.96 [81].
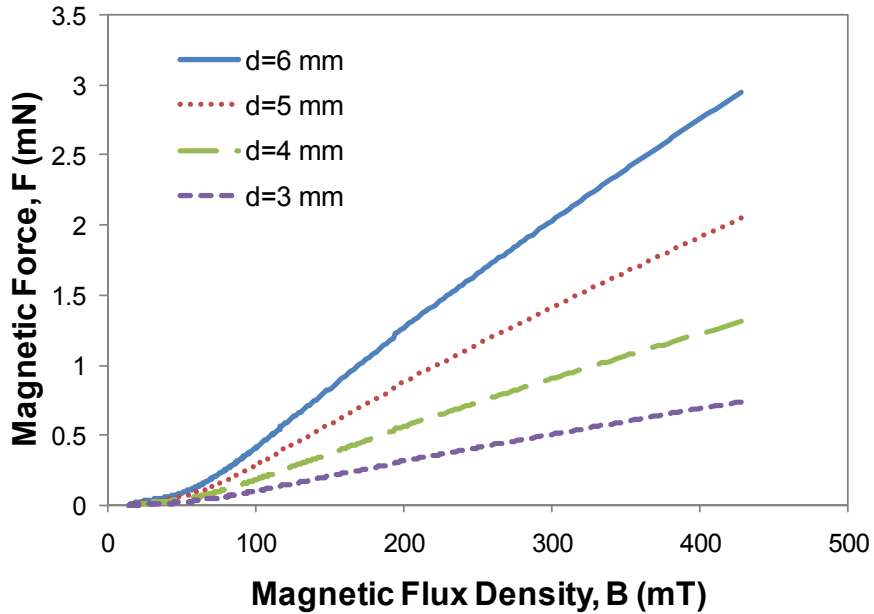
Figure 3.4 Theoretical force exerted on the various diameter membranes with a nominal thickness of 40 μm in the permanent magnet generated field.

3.2.2   Membrane Deflection Estimation

In cases of thin plates where the deflection may become large in comparison with the thickness of the plate, the resistance of the plate to bending may be neglected and the plate be treated as a flexible membrane [80]. The approximate solution for uniformly loaded circular membranes clamped at the edge, ignoring the liquid dynamic effects, is given by [80]

$$\omega_0 = 0.662 \, a \, \sqrt[3]{\frac{p \, a}{E \, t}} \qquad\qquad (3.5)$$

where ω_0 is the centre deflection of the membrane, a is the radius of the membrane, p is the intensity of uniformly distributed load, and E is the elastic modulus of the membrane material. The approximate solution suggests that the rigidity of the membrane increases with increased deflection. Based on Eq. (3.5), to achieve large deflections of the membrane at constant load, low elastic modulus membrane materials should be used. The required deflection may be tuned by changing the radius of the membrane.

The magnetic PDMS composites reported in Chapter 2 exhibit favorable elastic properties with elastic modulus ranging from 0.6 MPa to 1.1 MPa.   They can be fabricated as thin as 35 µm or less and exhibit superior sealing properties when they are non-reversibly bonded to PDMS surfaces by oxygen plasma treatment. Based on Eq. (3.5), a magnetic force of 0.5 mN which is exerted at ~6 mm distance from the permanent magnet (111.5 mT) can deflect a membrane with a diameter of 6 mm and a nominal thickness of 40 µm to approximately 219 µm. This deflection corresponds to a displaced volume of ~2 µl corresponding to ~13.3% of the reservoir volume, released in each actuation. Substituting the values from Eq. (3.4) in Eq. (3.5) as exerted pressures, the centre deflection of the membrane is derived and shown in Table 3.1 for elastic modulus of 1 MPa. A typical reservoir depth is 550 µm.

Table 3.1 Theoretical displacements of the centre of the membrane ($\varnothing$6 mm, *t*=40 μm) in the permanent magnet setting.

Force (mN)	Magnetic Field (mT)	Distance from Magnet (mm)	Estimated Deflection (μm)	Displaced Volume (μl)	% of Reservoir Volume
0.5	111.5	6	219	2.1	13.3
1	172	4.1	277	2.6	16.8
1.5	230	2.8	315	3	19.1
2	295	1.8	346	3.3	21

3.3   Materials and Methods

EMG 1200 (Ferrotec, MA, USA), iron oxide nanoparticles (~10 nm) coated with a proprietary fatty acid surfactant, was purchased as dry particles and dispersed in a PDMS matrix, and used for membrane material. The iron-oxide weight content of the particles is ~70% and considering the surfactant has a density of 1 g/cm^3 and iron oxide has a density of 5.2 g/cm^3, the density of composite is derived as 1.29 g/cm^3 for 40% w/w particle loading of EMG 1200. The measurement of magnetization (emu) versus applied field (Oersted) were taken using SQUID magnetometer (Quantum Design, CA, USA) [83] and were derived in SI units using composite density. An axially magnetized, neodymium cylinder permanent magnet with a diameter of $\frac{1}{2}$" and a thickness of $\frac{3}{4}$" (D8C, K&J Magnetics, Inc., PA, USA) was used as the source for magnetic field. The magnetic field of the permanent magnet was characterized as a function of the distance from the centre of the magnet using a F. W. Bell Gaussmeter (Sypris Test & Measurement, FL, USA). Scanning electron microscope (SEM) images were taken after the samples were sputter coated with gold for 30 s. The geometrical dimensions were measured using Image J, a general purpose open source image-processing package.

3.3.1   Fabrication

The fabrication process for the drug delivery device is summarized in Figure 3.5 and described in detail in various steps as follows:

Step 1: Drug reservoirs were made by molding PDMS from photoresist structures using standard photolithography. A layer of SU-8 2150 (MicroChem Corp., MA, USA) photoresist was spin-coated on a previously cleaned (piranha etch) silicon substrate in two spinning steps (500 rpm for 10 s and 1400 rpm for 50 s) and patterned as pillars in different sizes ($\varnothing$ 3-6 mm). The photolithography process was followed according to manufacturer's instructions. The height of the pillars was measured 480 to 580 μm using a Wyko surface profiler (VEECO Metrology Group, AZ, USA).

Step 2: PDMS (Sylgard 184 Silicone Elastomer, Dow Corning Corporation) was prepared with a mixing ratio of 5:1 (pre-polymer to crosslinker), poured on the SU-8 patterned silicon substrate, degassed for 30 min, cured at 80° C in a convection oven, and peeled away from the mold.

Step 3: The SU-8 transferred features into PDMS created cavities that were then ready for loading with the model drug. For example, a powder dye, Methylene Blue (MB) could be loaded in two ways: 1) as a powder using spatulas where the amount of drug in the reservoir was determined by weighing it before and after drug loading, 2) as a solution where MB was dissolved in a volatile solvent such as isopropanol in different concentrations and then the solution was deposited in the reservoirs using a pipette. In this study of drug release, we used MB because of its high solubility, high sensitivity of detection using UV-Vis absorbance spectroscopy, and clear observation (by eye) of drug release under actuation. Desired amounts of dye deposition could be achieved by evaporating the solvent and repeating the deposition. Leaving a thin layer of a water-soluble polymer as a coating to the content of the reservoir was optional.

Step 4: An aqueous solution of poly(acrylic acid) (PAA) was used as a water-soluble sacrificial layer material. PAA was purchased as powder (M_w=1800, Sigma-

Aldrich, Canada) and was mixed with distilled water to achieve a concentration of 20% w/v. It was heated for 10 min in a 90°C water bath to promote dissolution and was then filtered (4.5 μm pore size, Millipore Corp., MA, USA). After a glass substrate was cleaned with organic solvents (e.g. IPA and acetone), it was treated with air plasma for 2 min prior to coating to help improving the wettability of the glass substrate which was found an important step for achieving a uniform coating of PAA solution on the glass substrate. PAA solution was dispensed onto the glass substrate until about 90% of the surface was covered with the solution and then spin-coated in two spinning steps (500 rpm for 10 s and 1000 rpm for 20 s). It was cured at 150°C on a hotplate for 5 min. The resulting sacrificial layer has a typical thickness of ~8 μm.

The magnetic PDMS membrane was formed by spin-coating of the prepared composite on the sacrificial layer in three spinning steps (500 rpm for 15 s, 1000 rpm for 15 s and 2000 rpm for 30 s) and cured at 80°C. The fabricated membrane has a typical thickness of ~40-45 μm. Detailed description of the magnetic PDMS composite preparation was described in Chapter 2. Briefly, EMG 1200 was dissolved in toluene to form the ferrofluid and mixed with toluene-diluted PDMS pre-polymer at a mass fraction of 40% w/w particles to polymer. After intermittent sonication and stirring periods, toluene was allowed to evaporate and the PDMS crosslinker was mixed with the ratio of 5:1 pre-polymer to crosslinker and was degassed.

Step 5: Once the magnetic membrane was cured and the drug loading process finished, both surfaces were treated with oxygen plasma for 20 s [83] and brought together for irreversible bonding. There was no observed change in the UV-Vis absorbance spectrum of MB following O_2 plasma treatment, suggesting no plasma-induced changes in MB had occurred. Alternatively, to avoid plasma exposure, drug loading can be performed after the reservoir layer was exposed to plasma. (i.e. performing step 3 after step 5). It is optional to heat the sample to 65°C in a convection oven for 1 hour to enhance the bonding quality for the drug compounds that are not sensitive to higher temperatures.

Step 6: The device was released from the glass substrate by dissolving the PAA layer in DI water.

Step7: The aperture was created by a laser ablation process using both CO_2 and UV laser, for comparison purposes. The CO_2 laser, XL-9200 (Universal Laser Systems Inc., Scottsdale, AZ), have a characteristic wavelength of 10.6 μm, and the infrared laser operates with variable settings for power, speed, and pulses per inch (PPI). The assist gas utilized by this specific laser was air, supplied coaxially. Powers presented are relative to the maximum allowable input power of 60 watts (e.g. 50% power is equivalent to 30 watts). Speeds are fractions of the maximum speed of 254 cm/s (e.g. 50% speed is equivalent to 127 cm/s). The UV laser was a Nd:YAG laser system, Quicklaze (New Wave Research, Sunnyvale, CA), with 355 nm wavelength.
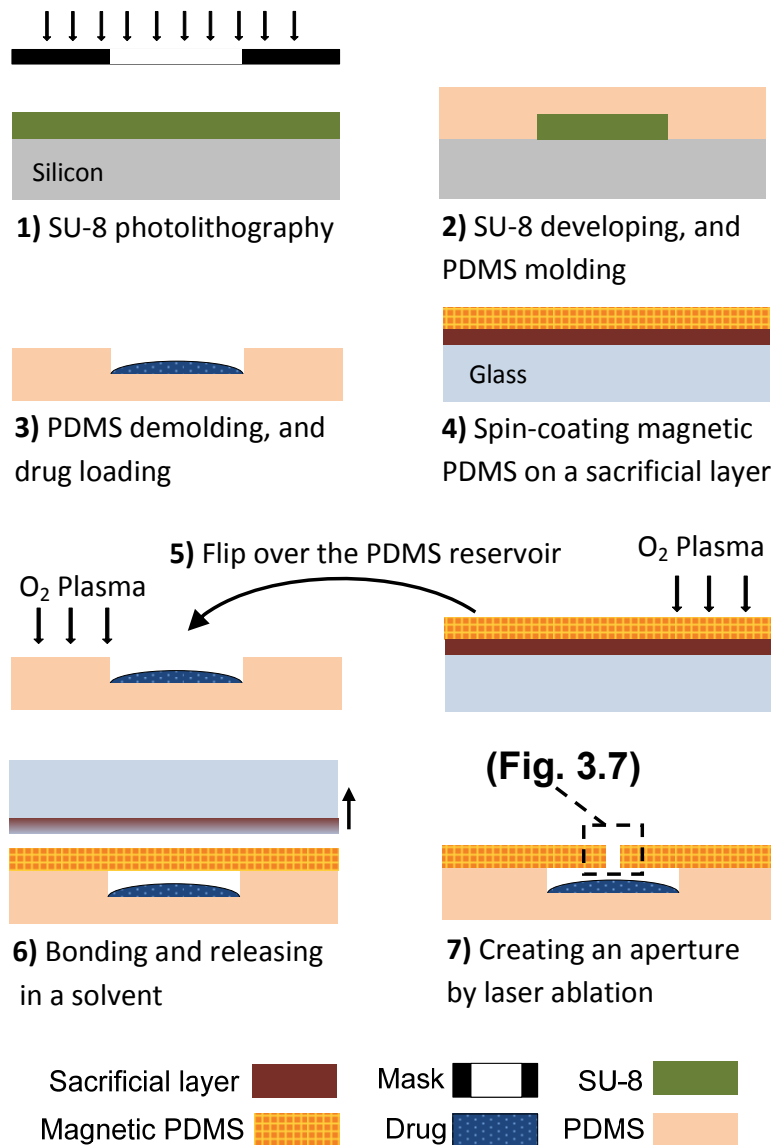
Figure 3.5 Major fabrication steps of a magnetically actuated drug delivery device.

Surface wettability of both pure and magnetic PDMS was characterized by contact angle measurements using the sessile drop method [84]. Bovine serum albumin (BSA) was purchased from Sigma-Aldrich Canada Ltd. (Ontario, Canada). Three concentrations of 1, 10, and 40 mg/ml (0.1%, 1%, and 4% w/v) BSA solutions in phosphate buffered saline (PBS) were studied for three incubation times: 2, 4, and 6 hours. Contact angle measurements were performed for both control (untreated) and BSA treated surfaces. Magnetic PDMS material was spin-coated on glass slides and cured at 80°C. The substrates were individually placed in petri dishes with different

concentrations of BSA in PBS. For various concentrations, separate pure (i.e. with no magnetic particles) and magnetic PDMS samples were prepared to study the effect of various incubation times on contact angle. Following incubation for an appropriate time at 37°C, the surfaces were gently washed three times with PBS and de-ionized water to remove non-adsorbed protein and dried with a clean air stream. For each measurement, a drop of 2 μl distilled water was deposited on the surface and an image was taken after 1 min for every reported data point. Untreated magnetic PDMS surfaces that served as control samples were also provided with a PBS wash step for consistency. On each sample, the contact angles were measured on at least three different locations and were averaged. Each data point was obtained by averaging a minimum of 6 samples and standard error bars represent one standard deviation from the measured values. To avoid operator dependency in the assignment of the tangent line, Drop Analysis (DropSnake) software based on a plugin for ImageJ was used [85].

Concentrations of MB in water were measured using a UV-Vis spectrophotometer (50 BIO, Varian Medical Systems Inc., Palo Alto, CA, USA). After the device surface was treated with BSA and the reservoir was filled with the fluid, the device was actuated inside a 20 ml vial filled with 4 ml of water. The field was provided with the rotating permanent magnet from below the vial. After each actuation and no-actuation period, water in the vial was replaced with fresh water and the MB concentration that had been released was measured.

3.4　Results and Discussions

SEM images of the cross-section of a device are shown in Figure 3.6. The device has a membrane of 41.8 ± 0.1 μm with largest agglomerated particle size measured as 5.75 μm and the reservoir height is 577.3 ± 1.5 μm. Figure 3.7 shows the top views of laser-drilled apertures in the magnetic membrane, using both IR and UV lasers. Figure 3.7-a shows an aperture ablated with CO_2 laser system using IR with settings of 3% power (~1.8 w), 5% speed (12.7 cm/s), and 500 pulses per inch (PPI). The resulting aperture measures as 131.7 ± 3.1 μm in diameter. A typical feature for the apertures created by this type of laser system is their tapered conical

shape with the error as large as +40 µm from the intended size. Figure 3.7-b shows an aperture ablated with Quicklaze system using UV light (355 nm wavelength) provided with laser pulses at 5 Hz with 0.11 mj (70% low) and a speed of 5 µm/sec. The aperture sizes fabricated using the Quicklaze systems are very close to intended size (less than 3 µm deviations). The UV laser-drilled aperture measures as 100×100 µm^2 with ± 2.5 µm deviation at each edge length.
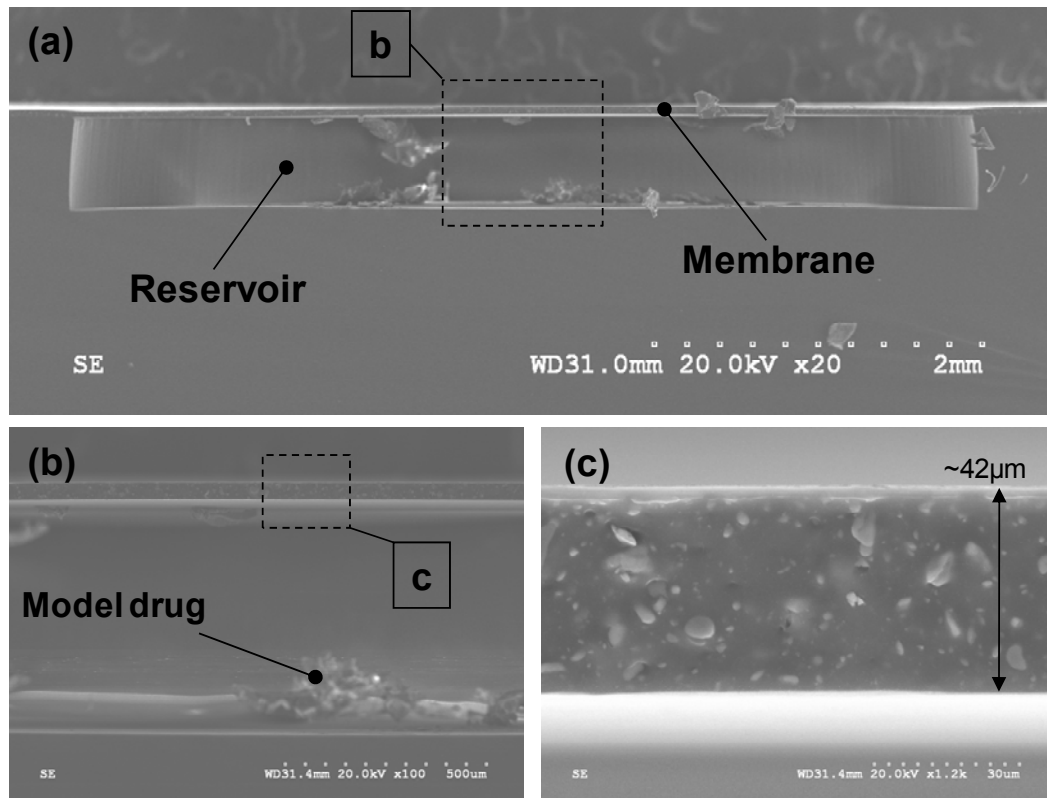
Figure 3.6 (a) cross-section of a fabricated device, (b) residues of a model drug and, (c) closer view of the magnetic PDMS membrane.
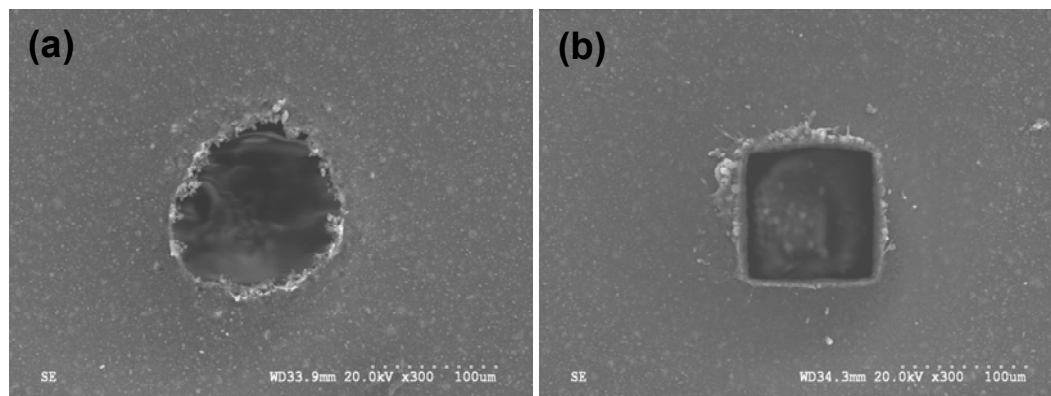
Figure 3.7 Laser-drilled apertures in the magnetic membranes ablated using (a) IR laser with 10.6 μm wavelength and (b) UV laser with 355 nm wavelength.

The short pulsed laser causes energy absorption and ablation only in the PDMS membrane layer. Upon inspection, no laser damage was observed on the bottom of reservoir using the current laser parameters. Therefore, it is unlikely that the laser ablation of the membrane would affect or decompose the drug that was uniformly dispersed and dried on the bottom of the reservoir. Furthermore, the narrowly focused laser beam might only impact a tiny percentage of the area of the base of the reservoir and hence only potentially interact with a tiny percentage of any drug in the reservoir.

3.4.1   Surface Modification of the Membrane

A necessary step to demonstrate a working device is to fill the reservoirs with water so that the dried drug in the reservoir may be dissolved and released from the device upon actuation of the membrane in a magnetic field.

Similar to pure PDMS, magnetic PDMS is also hydrophobic ($90° < \theta \leq 180°$) and exhibits a contact angle of $107.2°$, which is slightly smaller than that of pure PDMS ($110.7°$). As shown in Figure 3.8-a and b, due to the non-wetting property of the magnetic PDMS surface, the capillary forces oppose the flow through the aperture and a portion of surface tension ($\sigma \cos \theta$) acts on the wall boundary of the flow front. The required pressure to overcome the surface tension can be determined using Young-Laplace equation [86]

$$\Delta p = \sigma \left(\frac{1}{R_1} + \frac{1}{R_2} \right) \tag{3.6}$$

where σ is the surface tension of fluid and R_1 and R_2 are the principal radii of curvature of the flow front. For the rectangular laser-cut apertures the width and height of the aperture are equal, thus $R_1 = R_2 = R$. From the geometrical relations (Figure 3.8-b) the radius of curvature can be determined as

$$R = \frac{w}{2 \cos(\pi - \theta)} \tag{3.7}$$

where w is the width of the aperture. Substituting Eq. (3.7) in (3.6) results in

$$\Delta p = \frac{4 \sigma \cos(\pi - \theta)}{w} \tag{3.8}$$

For a circular aperture, w is replaced by the diameter of the aperture. Figure 3.8-c shows the required capillary break pressure versus aperture size in different contact angles while the surface tension, σ, for air-water interface is 0.072 N/m. It suggests that increasing aperture size is not an effective way to decrease the required pressure for larger aperture sizes. Moreover, increasing the aperture size is not desired since it will increase background diffusion, i.e. leaking of drug from the reservoir. Figure 3.8-c also shows that reducing surface hydrophobicity leads to requiring smaller pressures to overcome capillary forces. As shown in Figure 3.8-a, in order for the fluid to flow through the aperture, the force that is provided by application of a magnetic field on the membrane should overcome the capillary force. However, according to previous analysis, the permanent magnet setup can provide pressures of up to ~110 Pa on the magnetic membrane which is not enough pressure for the fluid to flow even at aperture size of 400 μm. Therefore, surface modification to achieve less hydrophobic or hydrophilic membrane material is a necessary step in filling process to obtain a functional device.
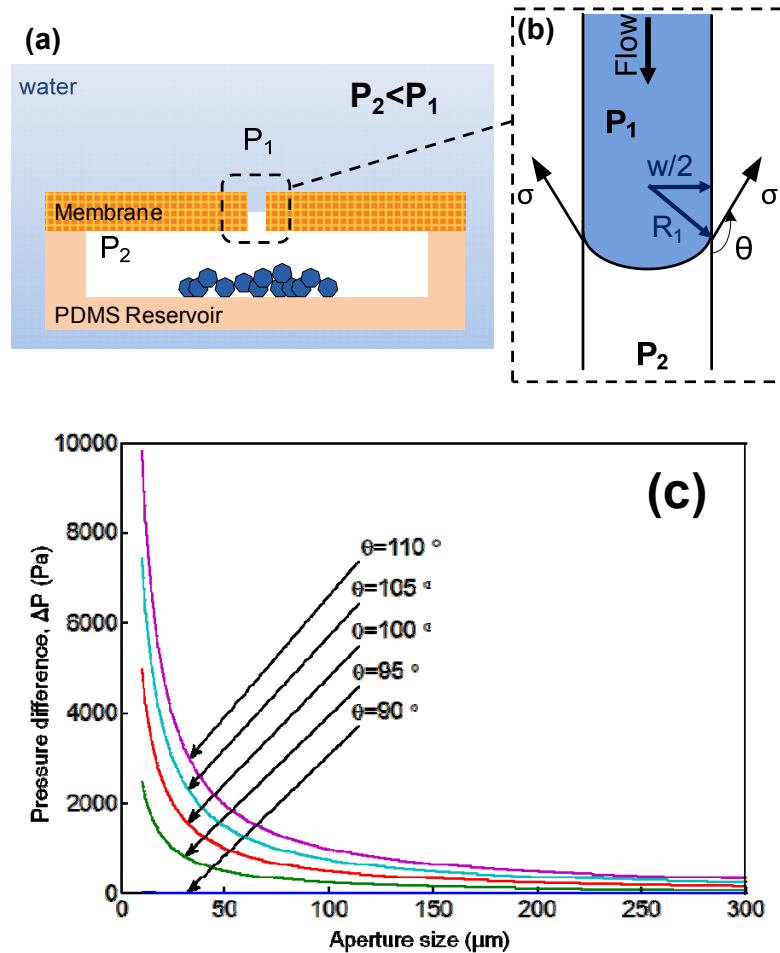
Figure 3.8 (a) solid drug in a device while immersed in water. An external pressure is needed to overcome capillary forces through the aperture to allow water get into the reservoir. (b) pressure-driven flow with surface tension opposing the fluid flow. (c) capillary break pressure as a function of aperture size and contact angle.

Previous studies have reported multiple techniques to improve the wettability of PDMS substrates [87] such as surface grafting [88, 89], oxygen plasma treatment [75], forming an interpenetrating polymer network with a more hydrophilic polymer [90], and protein modification [91]. Some of these methods do not prevent substrate hydrophobic recovery after a short time (e.g. plasma treatment), some involve extra steps and dedicated procedures that are not compatible with magnetic PDMS material (e.g. interpenetrating polymer network), and some require material bulk modification which may interfere with the magnetic property of PDMS composite (e.g. use of polymer blends).

BSA has been shown to increase the hydrophilicity of pure PDMS [92]; hence it is a promising candidate for the surface treatment of the magnetic membrane as the coating may reduce the water contact angle, decrease surface tension, and reduce restrictive capillary forces to enable water flow. Furthermore, albumin is a protein that is widely distributed in the body in blood and other fluids. We studied the effect of BSA non-specific adsorption on the magnetic PDMS membranes for various concentrations of BSA and incubation times to determine the optimal condition for membrane treatment.

The contact angle for untreated pure PDMS was measured to be 110.7 ± 0.9 degree consistent with literature reports [75]. One study showed that for a 1 mg/ml BSA solution, exposure for one hour resulted in a contact angle of 54° on a PDMS surface that has been pretreated with plasma [92]. Our measurements show the contact angle reaches 57.9 ± 5.4 degrees using a similar BSA concentration after 2 hours incubation time but without plasma pretreatment. Figure 3.9-a compares the effect of different BSA solution concentrations on contact angle for pure and magnetic PDMS substrates after two hours incubation at 37°C. The contact angle for the magnetic PDMS control samples was measured as 107.2 ± 4.4 degree (n=8), in agreement with the hydrophobic characteristic of the material. As shown in Figure 3.9, a two-hour exposure of the magnetic PDMS surface to three concentrations of BSA solution results in contact angles of 85 ± 5.6, 61.7 ± 15.5, and 47.2 ± 18.9 degrees (n>6) for 1, 10, and 40 mg/ml BSA concentrations, respectively. Both 10 mg/ml and 40 mg/ml concentrations resulted in 58% to 44% reductions of contact angles, respectively.

The effect of incubation time for various concentrations of BSA solution on the surface wettability of the magnetic PDMS substrates is shown in Figure 3.10. It shows that using a 40 mg/ml BSA solution maintains the contact angle at 47 degrees for longer incubation times. However, using other concentrations, the initial contact angles obtained after two hours increase up to 42% for 10 mg/ml solution (~88°) and 13% for 1 mg/ml solution (~96°) for longer incubation times and thus indicate the recovery of substrate hydrophobicity. Large error bars for each

condition may be associated with imperfect substrate coating with BSA for both magnetic and pure PDMS which was previously observed and studied [91] for PDMS substrate.
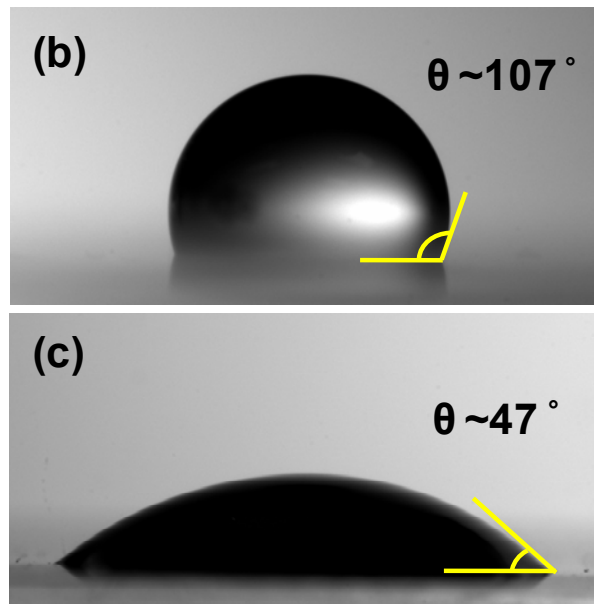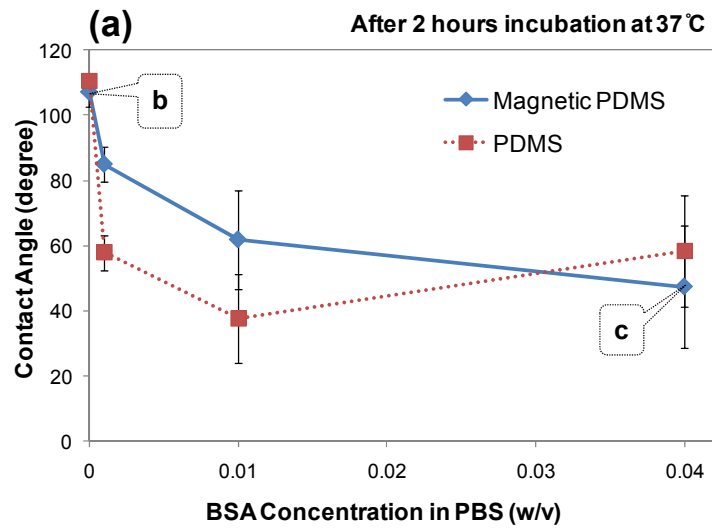
Figure 3.9 (a) effect of BSA concentration on the wettability of both magnetic and pure PDMS surfaces when they are incubated for 2 hours at 37°C. Image of a water drop on the magnetic PDMS surface and contact angles when the surface is (b) not treated (original surface) (c) incubated in 4% w/v BSA in PBS solution for two hours at 37°C.

It is anticipated that BSA will be deposited inside reservoir surfaces. However, MB is a freely water soluble compound (solubility of more than 40 mg/ml). Therefore, when the solution enters the reservoir, MB readily dissolves in the BSA solution (96% water). The BSA concentration in the reservoir stays at its original solution concentration as long as the device is kept in the same BSA concentration solution.

Consequently, to increase the wettability of the magnetic PDMS membrane and thus filling of the drug reservoir with water, a 40 mg/ml BSA concentration solution, which also corresponds to BSA physiologic concentration [93], is used for treatment of the membrane surface. Therefore, following step 7 in the fabrication process (Figure 3.5), the device was exposed to a 40 mg/ml BSA solution in PBS and incubated at 37°C. The change in the surface roughness of the aperture walls caused by laser drilling was ignored. The hydrophilic aperture walls results in surface-tension driven flow through the aperture. A reservoir with a volume of ~15.6 µl takes about 24-48 hours to completely fill with BSA solution at 37°C.
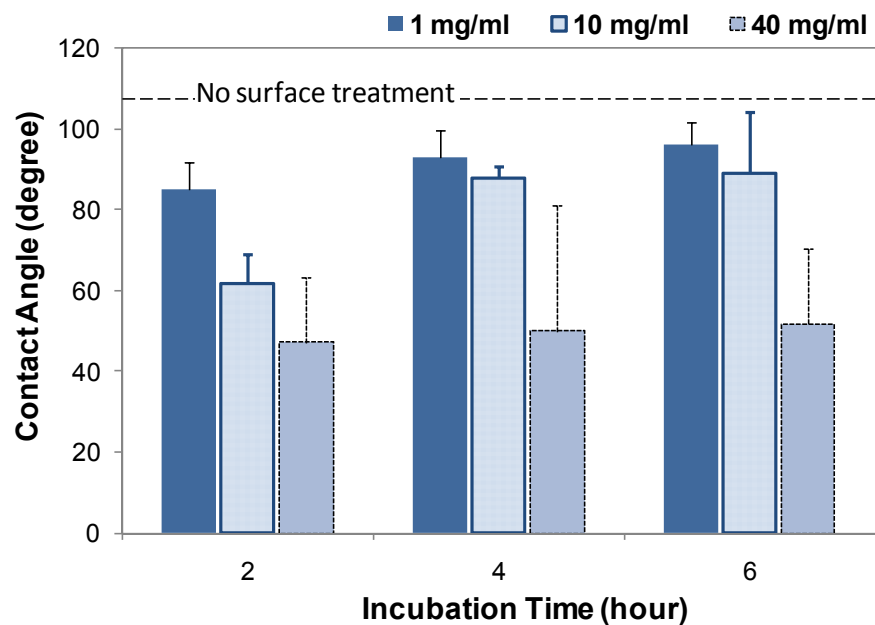
Figure 3.10 Effect of incubation time and BSA solution concentration on the surface wettability of the magnetic PDMS material

PDMS hydrophobicity has been found as one of the reasons for bubble formation inside PDMS microchannels. However, the presence of air bubbles within the reservoir of this device was rare. This absence may result from a reduced hydrophobicity of the surface following incubation with the BSA solution. Once the reservoir is filled with solution, surface tension would not play a role in the device operation.

3.4.2 Device Operation

A prototype device was actuated in water as shown in Figure 3.11. Each actuation is a combination of two intermediate events, discharge (with magnetic field) and mixing (without magnetic field where the membrane relaxes and the solution refills the reservoir). The model compound, MB, was deposited in powder form and dissolved in the water filling the reservoir after surface modification. Inside the reservoir, the pumped-in external solution mixes and equilibrates with the solution inside the reservoir through diffusion given a proper mixing time. To illustrate the operation of the device, it was actuated in water and the amount of released MB was measured after each actuation interval. Figure 3.12 shows representative data for three intermittent actuation and no-actuation intervals. The device was actuated under ~200 mT magnetic field with 25 actuations per minute. Each actuation interval was followed by an interval where the device was not actuated and therefore the release was associated with the diffusion of MB through the aperture.
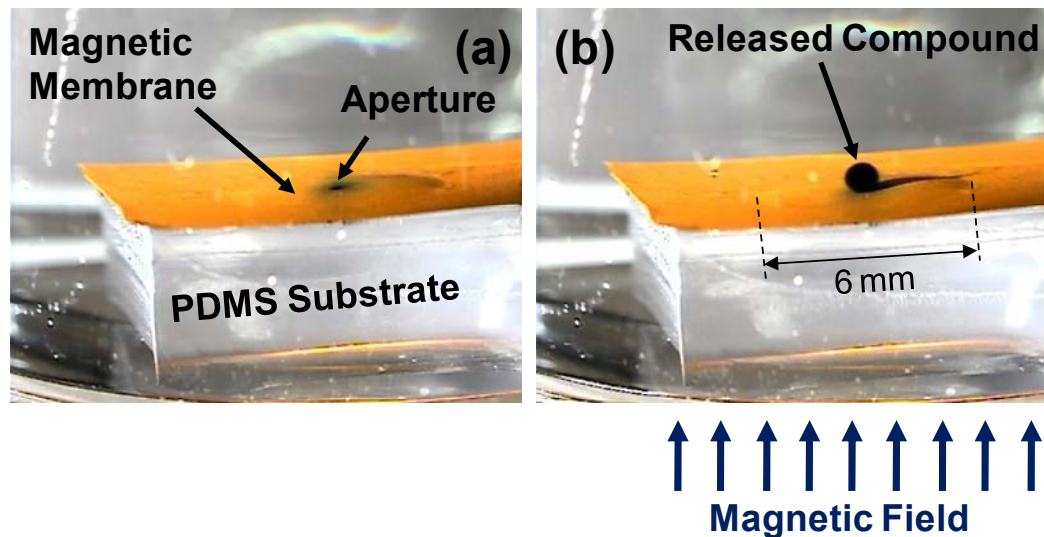
Figure 3.11 A prototype device in water, fabricated with 6-mm diameter membrane and ~210μm IR laser-cut aperture diameter. (a) no magnetic field is present. (b) after the application of a magnetic field of 200 mT from underneath the device. Magnetic actuation results in discharge of MB from the device.

Figure 3.12 shows that the amount of release in actuation mode is about ten times higher than that of no-actuation mode and thus provides an evidence for a device that could provide controlled on-demand dose sequencing. On average, 0.063 ± 0.048 μg/min MB was released in each actuation while the release in no-actuation mode was 0.0069 ± 0.0045 μg/min. The purpose of this drug delivery study was to measure MB release as a function of actuation and not to fully characterize the time dependency of release characteristics as one might do for a drug. Examination of a drug reservoir after it was emptied through successive actuations revealed no solid MB residue at the corners of a reservoir. The decreasing rate of MB release at 50 minutes and 100 minutes compared to 10 minutes probably arises from a decreased content of MB in the reservoir. Furthermore, the device was exposed to continuous actuations (i.e. 25 actuations/min) so that no time was allowed for mixing of fresh fluid inside the reservoir in each actuation which may also be one of the reasons for the decrease in release rates. These data were obtained in pilot experiments and serve to qualitatively illustrate a functioning device only.
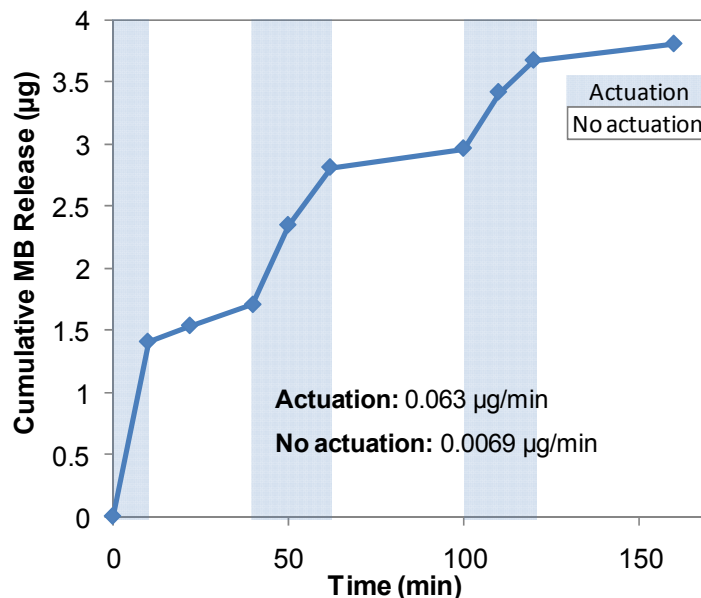
Figure 3.12 Intermittent release of MB from a device in water by application of ~200 mT magnetic field with 25 actuations per minute. After each actuation a period of release is followed with no actuation. Membrane diameter is 6 mm and the aperture diameter is ~210 µm.

3.5   Concluding Remarks

Magnetic actuation of the proposed MEMS drug delivery device was demonstrated in this chapter. The magnetic and mechanical design aspects of the device were discussed and fabrication steps were reported including drug loading and laser ablation processes. Furthermore, the need for increasing the surface wettability of the magnetic PDMS membrane was identified and necessary surface modification procedures and steps for reservoir filling were followed. Finally, the proposed device was demonstrated for on-demand releasing of a model drug compound.

CHAPTER 4

On-demand and Controlled Release of Docetaxel[3]

4.1 Introduction

In Chapter 3, the developed drug delivery device was shown to provide on-demand intermittent release of a water soluble model drug in a controlled manner. However, dosage control may be difficult to achieve for long term delivery as a result of decreasing concentrations of the water soluble drug in the reservoir. In this chapter, on-demand release of defined quantities of an antiproliferative and low aqueous solubility drug, docetaxel (DTX), from the drug delivery device is studied. Specifically, this chapter presents the long term drug release rates from the device, the effects of controlling parameters in drug release, and the background leakage of

---

[3] A version of this chapter has been published and presented at a conference.

- **F. N. Pirmoradi**, J. K. Jackson, H. M. Burt, M. Chiao, "On-demand Controlled Release of Docetaxel from a Battery-less MEMS Drug Delivery Device", *Lab on a Chip,* vol. 11, pp. 2744-2752, 2011 (DOI: 10.1039/c1lc20134d).

- **F. N. Pirmoradi**, J. K. Jackson, H. M. Burt, M. Chiao, "Delivery of an Anti-cancer Drug from a Magnetically Controlled MEMS Device Show Cytotoxicity in PC3 and HUVEC Cells", *Proceedings of the 16th International Conference on Solid-State Sensors, Actuators and Microsystems,* Beijing, China, June 5-9, 2011.

the device in "off" state. It is followed by studying the biological activity of the released drug after it is packaged in the device, using cell viability assay for two cell lines, HUVECs (human umbilical vein endothelial cells) and PC3 (prostate cancer) cells. The material in this chapter is organized as follows: Section 4.2 outlines the materials and experimental methods including the fabrication and drug loading processes and description of the actuation setup. Section 4.3 presents the results and further discusses the time constants required to ensure constant release rates.

4.2   Materials and Methods

4.2.1   Materials

All solvents were HPLC (high performance liquid chromatography) grade and obtained from Fisher Scientific (Ottawa, ON, Canada). Docetaxel powder was obtained from Phyton Biotech, Inc. (Delta, BC, Canada) and radioactive docetaxel (^{3}H-DTX) (specific activity 23 Ci/mM) was purchased from Moravek Biochemicals and Radiochemicals (Brea, CA). Trypan Blue (TB) (M_w=960.82 Da) was obtained from ICN Biomedicals, Inc. (Aurora, Ohio) and bovine serum albumin (BSA) was purchased from Sigma-Aldrich Canada Ltd. (Ontario, Canada). PC3 human prostate cancer cells were a kind gift of Dr. M. Gleave at the Prostate Centre, Vancouver General Hospital (Vancouver, BC, Canada). Human umbilical vein endothelial cells (HUVEC) and the associated culture media were obtained from Lonza Chemicals (Basel, Switzerland). PC3 cells were cultured in RPMI 1420 media supplemented with 5% FBS and 1% penicillin/streptomycin all from Invitrogen (Grand Island, NY, USA). DTX solubility was measured to be approximately 5 μg/ml after 45 min and stayed constant over time (see Appendix A for details).

4.2.2   Device Fabrication and Drug Encapsulation

The device fabrication steps were described in detail in Chapter 3. Briefly, the reservoir structure was fabricated using polydimethylsiloxane (PDMS). The magnetic membrane composite was prepared by incorporating coated iron oxide nanoparticles, EMG 1200 (Ferrotec, MA, USA), in a PDMS matrix. The membrane

was formed by spin-coating the composite onto a sacrificial layer. After loading of drug into the reservoirs, the membrane was permanently bonded to the reservoir layer using oxygen plasma. The devices were detached from the substrate by dissolving the sacrificial layer in a water bath. Finally, an aperture of 100×100 μm^2 was ablated with Quicklaze laser system (New Wave Research, Sunnyvale, CA) using UV light pulses at 5 Hz (355 nm wavelength) with 0.11 mj (70% low) and speed of 5 $\mu m/s$. The magnetic membrane had a nominal thickness of 40 μm and was fabricated with a diameter of 6 mm and the reservoir had a typical depth of 550 μm.

DTX loading was performed after treating the reservoir layer with oxygen plasma (100 mTorr pressure, 30 W power, and at 20°C) and before permanent bonding of the reservoir layer to the membrane layer. A mixture of ^{3}H-DTX and unlabeled DTX at the desired concentration of 20 mg/ml was prepared in a 50/50 solution of ethanol and dichloromethane (DCM). In each deposition cycle, 5 μl of the drug solution was deposited into a reservoir by a pipette and dried by evaporating the solvents. Deposition and drying process was repeated until the desired nominal drug content (e.g. 200 μg) was achieved. After the magnetic membrane was treated with oxygen plasma for 20 s [83], it was irreversibly bonded to the reservoir layer.

Similar steps were followed for the loading of TB solution in acetonitrile except that oxygen plasma treatment of both reservoir and membrane layers were performed after the desired amounts of TB had been deposited. There was no observed change in the UV-Vis absorbance spectrum of TB following O_2 plasma treatment, suggesting no plasma-induced changes in TB had occurred. Alternatively, TB exposure to plasma can be avoided if steps similar to DTX loading are followed.

4.2.3   Actuation Setup

The force on the membrane was induced by a mechanically moving cylindrical NdFeB permanent magnet (with a diameter of $\frac{1}{2}$"and a thickness of $\frac{3}{4}$", D8C, K&J Magnetics, Inc., PA, USA). The magnet was mounted on a computer controlled

motorized stage (an Atmega328 microcontroller on the Arduino Duemilanove board, by Arduino©, Italy). A 20-ml glass scintillation vial (Fisher Scientific, ON, Canada), with a prototype drug delivery device affixed to the bottom of it, was positioned in such a way that when the controller positions the moving permanent magnet below the vial, the magnetic field was applied from the bottom of the vial and perpendicular to the device membrane. The distance between the magnet and the device was adjustable. The change in magnetic flux density with respect to the distance of the membranes from the permanent magnet surface was characterized in Chapter 3 (see Appendix B). In this chapter, drug release was characterized based on magnetic flux density, however as shown in Chapter 3, Section 3.2, both field gradient and flux density are important for generating force on the membrane.

4.2.4   Controlled Release Studies

The MEMS devices were placed in 20-ml glass scintillation vials individually and were incubated with 4 ml of an aseptically filtered (0.2 micron filter) solution of 4% w/v BSA in phosphate buffered saline (PBS, pH 7.4) in a 37°C oven. This solution was considered to be a suitable model of physiological fluid. As discussed in Chapter 3, the hydrophobic magnetic PDMS membrane became more hydrophilic after the treatment of the surface with BSA solution so the reservoirs filled slowly over 24-48 hours. The solution-filled devices were individually kept in 4 ml of an aseptically filtered solution of 1% w/v BSA in PBS (referred to as BSA solution subsequently).

One *actuation cycle* is defined as a combination of two intermediate events, *discharge* (with magnetic field) and *mixing* (without magnetic field, membrane relaxes and solution refills the reservoir). Each actuation cycle is controlled by two time constants associated with these two events: (1) a *discharge time* (t_d) of 100 seconds which is required for complete release of the displaced volume in the reservoir when membrane deflects; and (2) a *mixing time* (t_w) of 200 seconds which is required for drug mixing with the pumped-in solution. Detailed experiments and simulations that lead to the selection of these two time constants are addressed in Section 3. At each measured data point (i.e. after actuation cycles and no-actuation

periods) the solution was removed and analyzed for DTX or TB content and replaced with a fresh 4 ml aseptically filtered BSA solution for the consecutive actuation and no-actuation periods.

Solutions for tritium-labeled DTX content measurement were subjected to drug extraction steps. One ml DCM, which is a water immiscible hydrophobic solvent, was added to the solution and vortex mixed in order to selectively dissolve and extract DTX in DCM. Interaction of the protein molecule with organic solvent (DCM) led to the protein's precipitation at the aqueous-organic interface. After allowing the organic and aqueous phases to separate for 10 min, the aqueous interface was aspirated out and the remaining organic phase (which contains the released drug from the device) was transferred into scintillation vials, filled with CytoScint liquid scintillation fluid (Fisher Scientific, Fair Lawn, NJ). Disintegrations per minute (DPM) were measured using a LS 6500 series, multi-purpose scintillation counter (Beckman Coulter, Inc., Brea, CA). A standard curve for converting DPM values to DTX content was created by introducing various volumes from drug stock solution (20 mg/ml) into 4 ml of 1% BSA solutions in PBS and following similar drug extraction steps. The measured DPM values for samples were always 100 times higher than the detection limit.

Concentrations of TB in BSA solution were measured using a UV-Vis spectrophotometer (50 BIO, Varian Medical Systems Inc., Palo Alto, CA, USA) by reading the absorbance at 600 nm. Calibration curves were created for conversion of absorbance values to TB concentration. The devices were actuated inside a 20 ml vial, filled with 4 ml of BSA solution. After each actuation and no-actuation period, the solution was replaced with a fresh solution and TB concentration was measured.

4.2.5   Cell Viability Study

A prototype device was actuated at the desired number of actuations in 1% BSA solution. The released DTX was extracted in 1 ml DCM, as described in Section 4.2.4. This mixture was dried down under nitrogen flow at 40°C and was then reconstituted in either HUVEC and PC3 cell media to the original volume of 4 ml.

Alternatively, fresh solutions of free DTX were prepared in various concentrations (2–250 nM) in acetonitrile, dried down under nitrogen flow at 40°C, and reconstituted in cell media.

PC3 and HUVEC cells were seeded in 96 well plates in their respective media at a concentration of 1500 cells per well. The cells were allowed to equilibrate for 2 days at which time they became approximately 50% confluent and were ready for drug incubation. Cells were incubated for 2 days at 37°C with 200 µl of either freshly prepared solutions of DTX at various concentrations or with the drug solution released from the device under various number of device actuations. Cell viability was determined using a CellTiter 96 AQ$_{ueous}$ Non-Radioactive Cell Proliferation Assay (MTS assay, Promega Corporation, Madison, WI) and quantified by reading the absorbance at 492 nm minus the absorbance at 610 nm using a spectrometric plate reader. In both experiments, the values presented are for the averages of six replicas for each condition.

4.3   Results and Discussions

4.3.1   Discharge Time

In each actuation event, it was desired to release a volume of drug solution that corresponded to the volume created by the membrane deflection when the membrane achieved a full deflection at the corresponding applied magnetic field. This volume was defined as V_d. To achieve complete release of V_d in each actuation, it was necessary to obtain the time required for continuous application of the magnetic field (t_d). This discharge time can be estimated using the following relation

$$t_d = \frac{V_d}{A_a\, v} \tag{4.1}$$

where A_a is the area of the aperture, v denotes the velocity of discharging fluid, and V_d is obtained using $V_d = \frac{\omega_0}{3} A_m$, where ω_0 is the estimated deflection of the membrane presented in Chapter 2 and A_m is the area of the circular membrane. Here, it is assumed that the fluid discharge velocity is constant during actuation and

is equal to the measured initial discharge velocity. However, the discharge velocity may vary during the actuation process and therefore this simplifying assumption may only be used for estimation purposes.

The viscosity of the BSA solution was unaffected by the addition of TB at a concentration of 1 mg/ml as measured by solution viscometry (data not shown). With nanomolar concentrations, it was assumed that the viscosities of DTX and TB solutions were not significantly different and therefore the velocity of the discharging fluid, v, was measured by actuating the devices that were filled with TB (see Appendix C for experiment details). The discharge of TB over time as a small visible bloom is illustrated in Figure 4.1-a when the device was actuated with a 176 mT magnetic field. The initial discharge velocity of TB solution from inside the reservoirs is shown in Figure 4.1-b when the devices were actuated in three magnetic fields. The horizontal error bars represent the variation in the thickness of the devices used and thus the variation in the associated applied magnetic fields. The experiment was repeated for a minimum of four times in each magnetic field strength and the vertical error bars represent one standard deviation from the measured values. Table 4.1 presents the maximum traveled distance of TB solution jet in these experiments. This is a distance after which the TB plume did not show any observable movement away from the membrane.

Table 4.1 Maximum travelled distance of TB solution during discharging (n=4).

Magnetic Field (mT)	Maximum Travelled Distance (μm)
162 ± 2	152.3 ± 21.7
176 ± 7	223.3 ± 23.2
204 ± 8	230.5 ± 11.5

Based on the data shown in Figure 4.1-b, the discharged velocity of TB solution, due to actuation under 210 mT magnetic field, is approximately 3.2 mm/s. From Eq. (4.1), for a device with a membrane of 6 mm in diameter and an aperture size of $100{\times}100$ μm^2 under the same magnetic field, (considering the membrane deflection

is 300 μm), the estimated time for a complete discharge of V_d (i.e. a portion of the reservoir volume that can be displaced due to full membrane deflection under a magnetic field) is approximately 100 s.

(a)

(b)
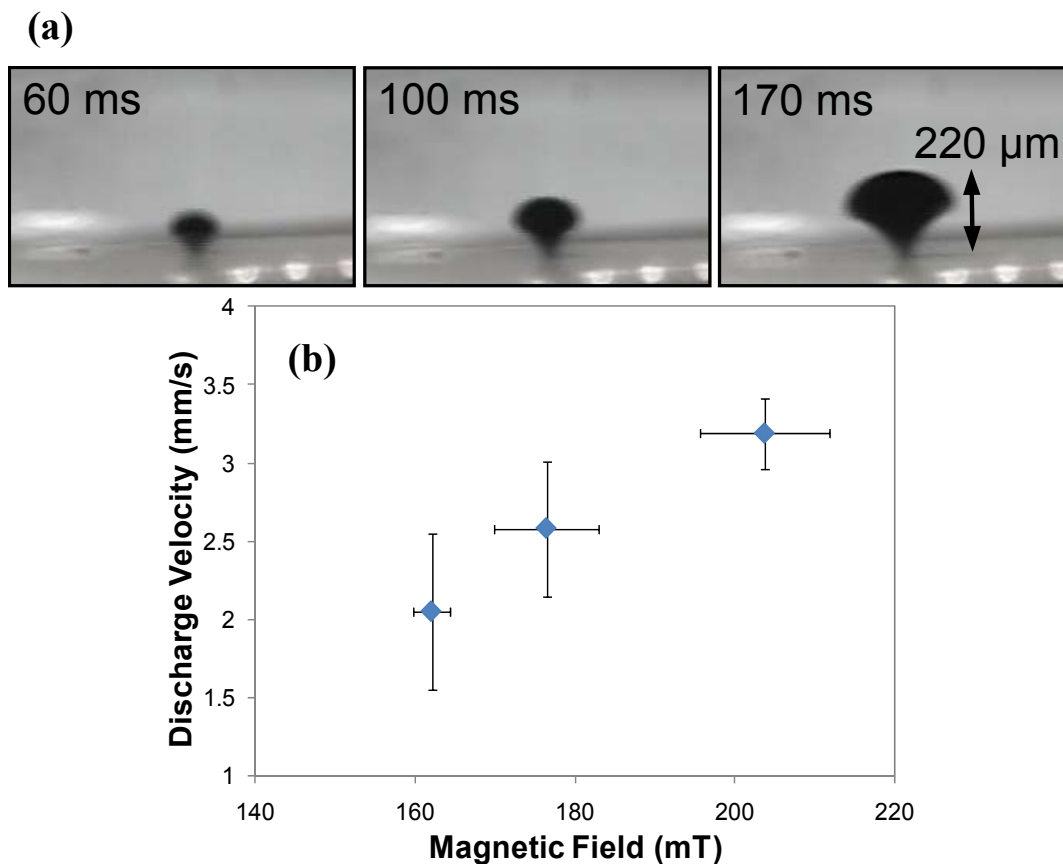
Figure 4.1 (a) sequence of TB solution discharge under ~176 mT magnetic field, (b) initial discharge velocity of TB solution from the devices into surrounding BSA solution.

4.3.2   Mixing Time in Reservoirs

Another important aspect in achieving constant and reproducible release of the drugs is to ensure thorough mixing of the entering solution with the drug inside the reservoir (i.e. concentration equilibration), in each actuation. To determine the mixing time, the mass balance equation for transport was solved using COMSOL Multiphysics software to estimate the required wait time before each actuation. This equation is defined as follows [94]:

$$\frac{\partial c}{\partial t} + \mathbf{u} \cdot \nabla c = \nabla \cdot (D \nabla c) \tag{4.2}$$

where c is the concentration of the solute (mol/m³), *D* denotes the diffusion coefficient (m²/s), and **u** is the velocity vector. The first term corresponds to the accumulation (or indeed consumption) of the solute, the second term accounts for the convective transport due to a velocity field **u**, and the third term describes the diffusion transport accounting for the interaction between the solute and the solvent.

In this system, the ratio of diffusion to convection time, given by the Péclet number (Pe=*vL/D*, with *D* the molecular diffusivity, *L* a typical length scale such as reservoir depth, and *v* the flow velocity), is 1<Pe<1000 for the duration of ~0.2 s while the velocity field exists. This is an indication of slower mixing time based on diffusion rather than convection during this period. Therefore, the mass balance equation is reduced to Fick's law for diffusive transport by ignoring transient velocity field, present inside the reservoir. Based on this assumption, the simulation results provide an upper limit of the required mixing time since the existence of such field will further facilitate mixing inside the reservoir and thus reduce the required mixing time before each actuation cycle. Furthermore, the velocity field only exists for 0.1% of the total mixing time, determined based on diffusion. Finite element simulation was performed for 200 s in 2D space considering isotropic diffusion and for both DTX and TB solutions with diffusion coefficients of 9×10^{-10} m²/s and 4.35×10^{-11} m²/s, respectively (see Appendix D for details). Figure 4.2 shows that for a mixing time of 200 s, the concentration of DTX in the pumped-in fluid reaches 95% of the reservoir concentration. Therefore, in all drug release experiments, 200 s was chosen as the *mixing time*.
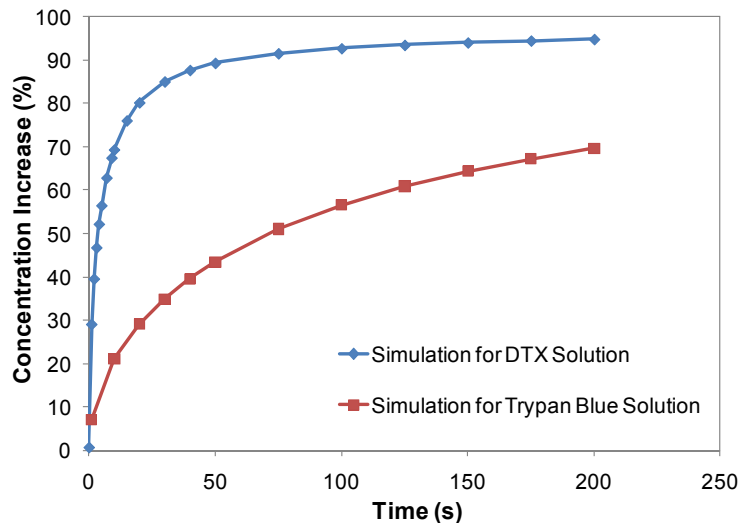
Figure 4.2 Average concentration of the pumped-in solution compared to the average concentration of the entire reservoir.

4.3.3   Docetaxel Controlled Release

All devices used in the experiments had a membrane diameter of 6 mm, a nominal thickness of 40 μm, and a nominal reservoir depth of 550 μm. Due to the low aqueous solubility of DTX, only a predefined amount of solid DTX may be dissolved (up to its saturation solubility) in the reservoir in each actuation cycle. This would have two impacts on the device operation: (1) Constant concentration of DTX solution will be available for delivery in the reservoir. The concentration of DTX solution will not decrease with time as other water soluble drugs; and (2) Solid form DTX (undegraded) will be maintained in the reservoir for extended periods of time.

4.3.3.1   Effects of Number of Actuation Cycles and Magnetic Field

The amount of released drug was demonstrated to be controllable by adjusting two parameters: (1) number of actuation cycles; and (2) the distance of the permanent magnet from the device and thus the size of the magnetic field strength and gradient. The amount of released DTX from a device under 255 mT magnetic field was found to follow a linear relationship with the number of actuation cycles so that as the actuation cycle number increased the amount of released drug increased

61

in a proportional amount as shown in Figure 4.3-a. A similar relationship was observed for the amount of released drug as a function of magnetic field strength (Figure 4.3-b). The amount of released DTX reported at a specific magnetic field represents the release after ten consecutive actuation cycles for all points. The magnetic field values were experimentally obtained with respect to distance as described in Chapter 3. Linear DTX release profiles with respect to magnetic field and the number of actuation cycles allows for highly controlled on demand dosing.

Furthermore, if it is assumed that: (1) the membrane reaches its full deformation at a corresponding magnetic field; and (2) the DTX concentration remains at 5 µg/ml at all times in the reservoir, membrane deflection can be theoretically calculated based on the amount of released DTX shown in Figure 4.3-b, with respect to magnetic field. This calculation showed a linear relationship between membrane deflection and magnetic field and gave a deflection of ~300 µm at 210 mT.
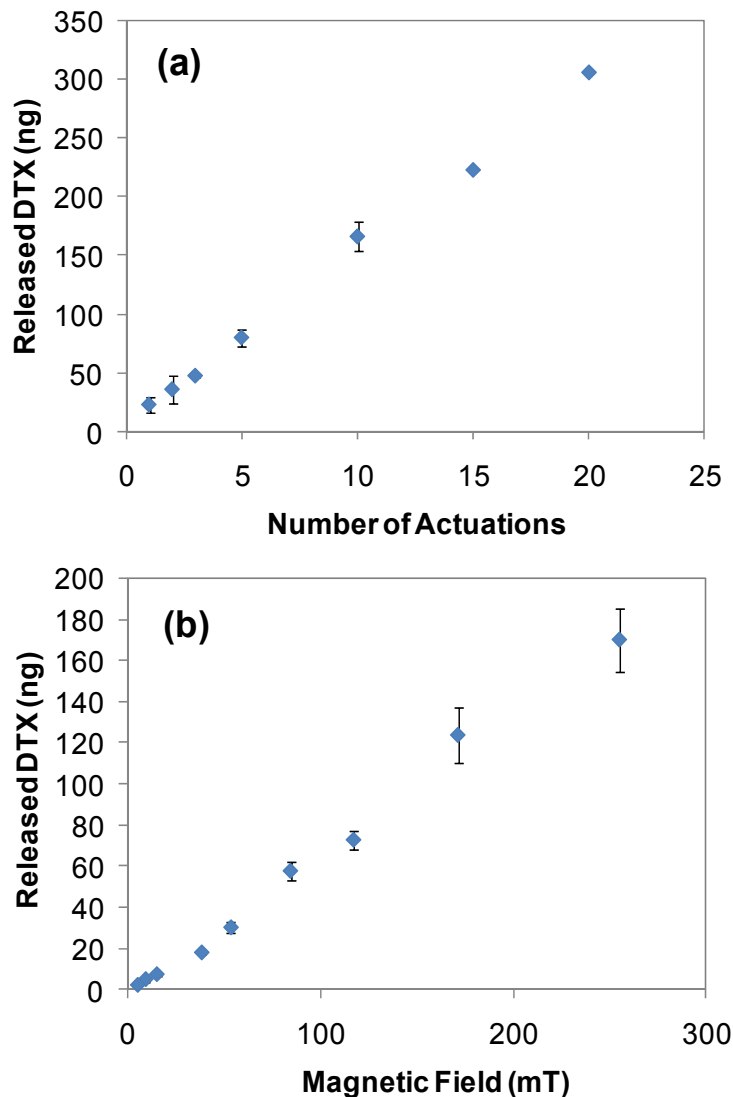
Figure 4.3 (a) amount of released DTX from a device operated with various number of actuation cycles under 255 mT magnetic field. (b) amount of released DTX in various magnetic fields. Each data point corresponds to 10 actuation cycles for all the points in (b). Error bars represent one standard deviation from the measured values for a single device.

4.3.3.2   Long-term, On-demand Release Profiles

In all controlled release experiments, each *actuation mode* consists of three *actuation intervals* and each actuation interval includes ten consecutive *actuation cycles* (Figure 4.4). Therefore each *actuation interval* takes 50 minutes[4] to

---

[4] One actuation interval includes ten actuation cycles, as such it equals to ten times 300 s (50 min).

complete. In the no-actuation periods, the device was left in BSA solution and thus drug release is uncontrolled and is expected to occur via background diffusion through the 100×100 µm^2 laser-drilled aperture.

Constant DTX release from a device using a 255 mT magnetic field is demonstrated in each actuation cycle. Serial cumulative release of DTX with and without magnetic actuation is shown in Figure 4.4-a. The slope of the cumulative release curve is a quantitative measure of the release rate. A constant release rate of 171.7 ± 16.7 ng per actuation interval (3.4 ng/min release rate) was achieved by magnetic actuation for 13 intermittent releases over 13 days. These release rates are shown in Figure 4.4-b for the device used in Figure 4.4-a. Each data point is the average of the release rates for three consecutive actuation intervals. Drug release during no-actuation period was measured to be 0.053 ± 0.014 ng/min at the end of each period. A 64-fold increase in DTX release has been achieved by magnetic actuations compared to no-actuations.
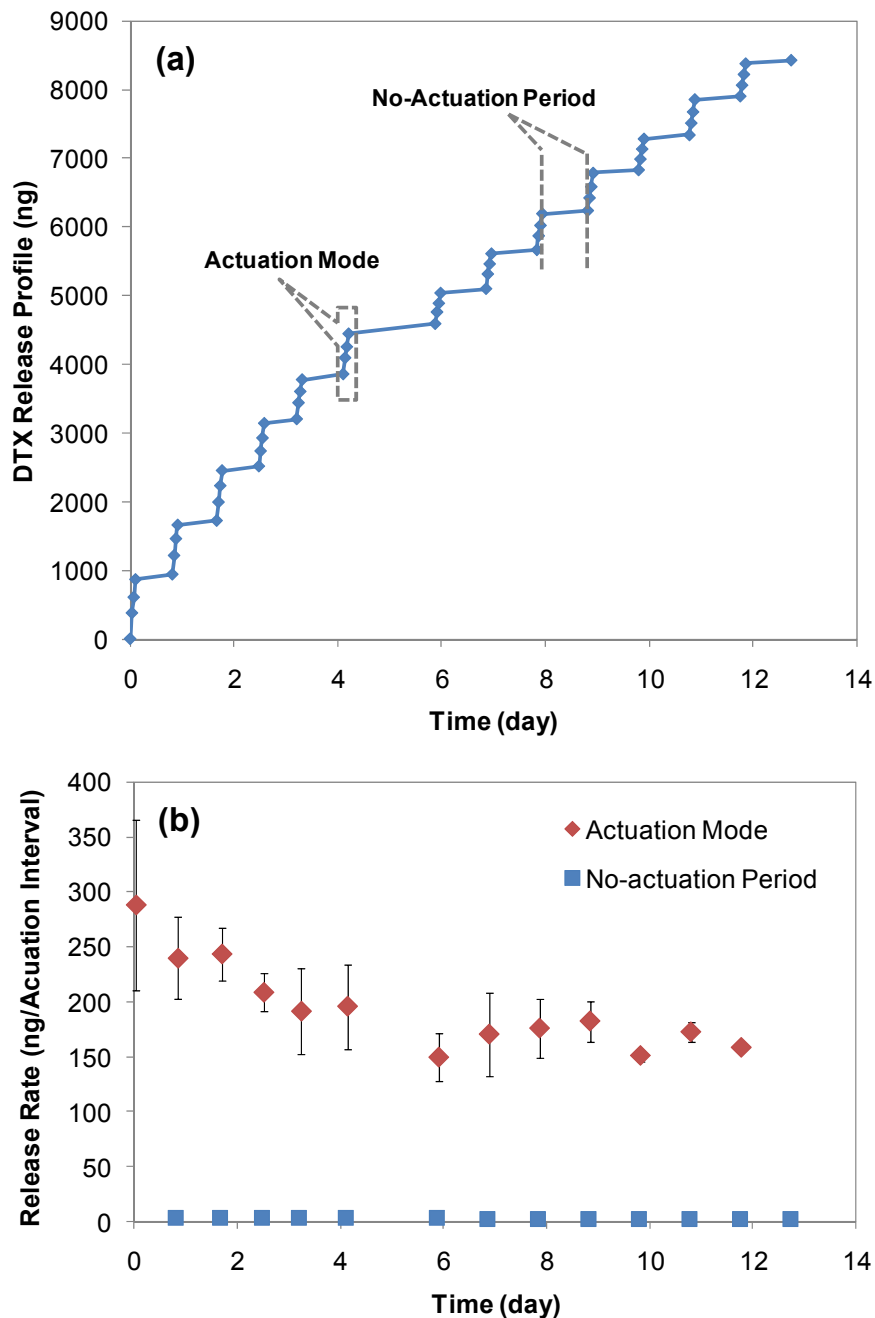
Figure 4.4 Release profile of tritium-labelled DTX from a device (membrane: $\varnothing$6 mm $\times$ t=40 µm, aperture: 100 $\times$ 100 µm^2, reservoir depth: ~550 µm) operated in a 255 mT magnetic field (a) cumulative DTX release includes a series of *actuation modes* followed by *no-actuation periods*. Each data point represents ten consecutive *actuation cycles*, (b) average DTX release rates from the device. Diamonds represent the average of the release rates for three consecutive *actuation intervals* with the error bars representing one standard deviation from measured values. Squares represent the release rate in *no-actuation* periods.

The long-term operation of the drug delivery device was investigated and the device used to collect the data shown in Figure 4.4 was left in BSA solution for 22 more days and actuated once more with the same conditions. The results showed that the release rate remained constant at 160 ± 10.2 ng per actuation interval which illustrates the consistency of the release rate over 35 days of device operation. Furthermore, similar experiments for three other devices were performed using a 213 mT magnetic field over 6 days and found that 129 ± 32.3 ng of DTX was released per actuation interval (Appendix E). This amount is in agreement with the prediction provided from data shown in Figure 4.3-b.

The drug release experiments further suggest the following: (1) the process of drug release can be "switched off" by removing the magnetic field and re-activated by re-applying the magnetic field, and (2) the resulting constant release rates are in line with the predicted values from simulation determinations for the required mixing time and the calculations for complete discharge of displaced volume after membrane actuation. The on-off switchable controlled drug release, may allow fine-tuned control of drug doses administered from implanted devices.

4.3.4 Trypan Blue Controlled Release

For comparison purposes, TB, a compound with a much higher aqueous solubility (between 1 and 10 mg/ml) than DTX (5-7 µg/ml), was studied in drug release experiments (Appendix F). The release profile of TB shows that on-demand release of TB could also be achieved using this device (Figure 4.5). The release of TB using a 191 ± 8 mT applied magnetic field was measured for five intermittent actuations and for three devices. Each point represents the average release rates for three consecutive actuations in the corresponding actuation intervals. The large error bars may result from a decreasing concentration of TB inside the reservoir after each actuation. The release rates decreased from ~13 µg to ~4.5 µg per actuation interval after five actuation modes. These release rates were approximately 100 fold greater than for DTX in agreement with the water solubility differences of the two compounds. The decrease in release rate with actuation number may relate to the decrease in TB concentration inside the reservoir after

successive releases. A release rate of 3.8 ± 2 ng/min was observed during no-actuation periods for 10 days while the devices were left in PBS solution.

Based on the release data obtained for both DTX (a low solubility compound) and TB (a higher solubility compound), it was observed that the drug delivery device offers a better dose control for DTX delivery than TB. It was hypothesized that the concentration of DTX inside the reservoir remained constant at 5 μg/ml as long as undissolved (solid) DTX is available inside the reservoirs and therefore constant doses could be delivered at each actuation. The release studies and the differences in DTX and TB release profiles (constant compared to decreasing release rates) establish the validity of this hypothesis. In each delivery cycle, the amount of drug, available in the reservoir before membrane actuation (i.e. DTX concentration), remains constant at the limit of DTX solubility (5 μg/ml). Therefore constant doses could be delivered under the same magnetic field. Adjusting the control parameters may provide required doses for different situations.

Since loadings of more than 200 μg DTX in the reservoirs were possible, the amount of DTX inside the reservoir could theoretically last for approximately one year (based on the release amount in Figure 4.4, ~10 μg in 13 days). Furthermore, no clogging of the aperture was observed throughout the experiments following examination of the devices using an optical microscope.
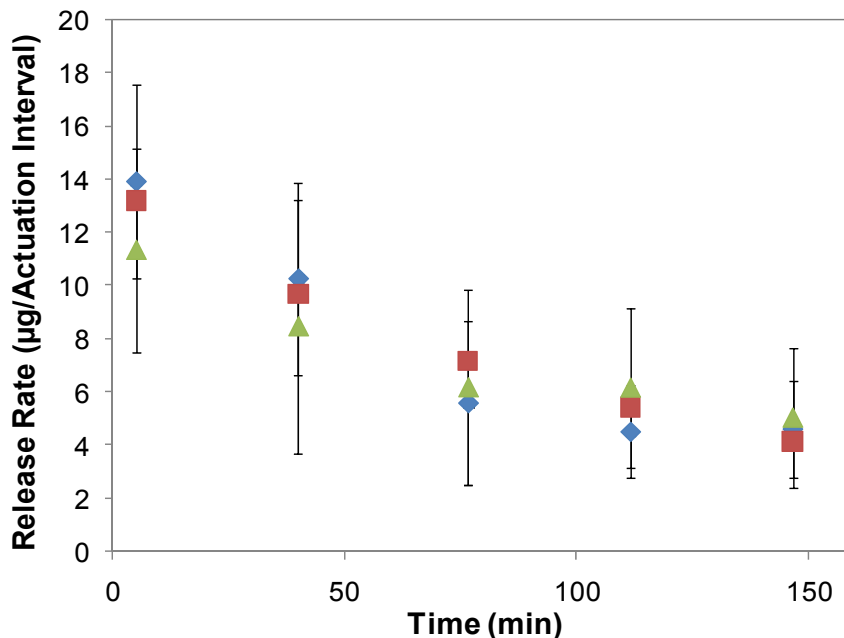
Figure 4.5 Average release rates of TB per actuation interval for three devices (membrane: Ø6 mm × *t*=40 μm, aperture: 100 × 100 μm², reservoir depth: ~550 μm) operated under ~191 mT magnetic field. The no-actuation period is 30 min in all cases. Each data point represents the average of the release in three consecutive *actuation cycles* in each *actuation interval*. The error bars represent one standard deviation from measured values.

4.3.5   Cell Viability Following DTX Delivery

The biological activity of the DTX released from a device was investigated. This was achieved by incubating cells with the released drug in cell culture media and measuring the drug induced inhibition of proliferation in comparison to the inhibition caused by freshly made drug solutions. The device used for this study had been fabricated and left in BSA solution for two months (with an open aperture) prior to the experiment. The amount of DTX release during this period was estimated to be ~4.5 μg based on measured DTX diffusion rate. It was then actuated under a 255 mT magnetic field for different numbers of actuation cycles. The amounts of released drug were then experimentally interpolated from "number of actuations" to "drug concentrations", using Figure 4.3-a.

Taxanes are antiproliferative drugs mainly used for their anticancer and antiangiogenic effects. Unwanted proliferation of capillary cells in the retina

(angiogenesis) is responsible for compromising retinal function resulting in vision loss. Therefore, endothelial cells (HUVEC-capillary cells) were used in these proliferation studies, as these cells would be the target cells in the retina for treatment with docetaxel and therefore directly related to any clinical application of this system. PC3 prostate cancer cells were used as another representative example of a diseased cell line that might be treated using a docetaxel controlled release system such as described in this chapter. Therefore, DTX released from the device, with and without actuation, was incubated with these two cell lines, HUVEC and PC3 cells, to investigate cell viability. The no-actuation period corresponds to the period that the device was left in the solution for 10 min. The amount of released DTX during this time corresponds to the diffusion of approximately 0.5 ng (0.053 ng/min diffusion rate times 10 min experiment time) through the aperture and results in no change in cell viability in PC3 cells. However, HUVECs are more sensitive to DTX and this amount of released DTX inhibited HUVEC proliferation by approximately 60% over control (no drug). These data are shown in Figure 4.6. The drug released after one and ten actuations of the device resulted in a decrease in cell viability in both cell lines as shown in Figure 4.6. Cell viability in HUVECs and PC3 cells decreased to 24% and 58% after one actuation and to 21% and 34% after ten actuations, respectively. The results indicate a functioning actuation process of the device in the magnetic field with associated on-demand release of sufficient drug to significantly inhibit cell proliferations.
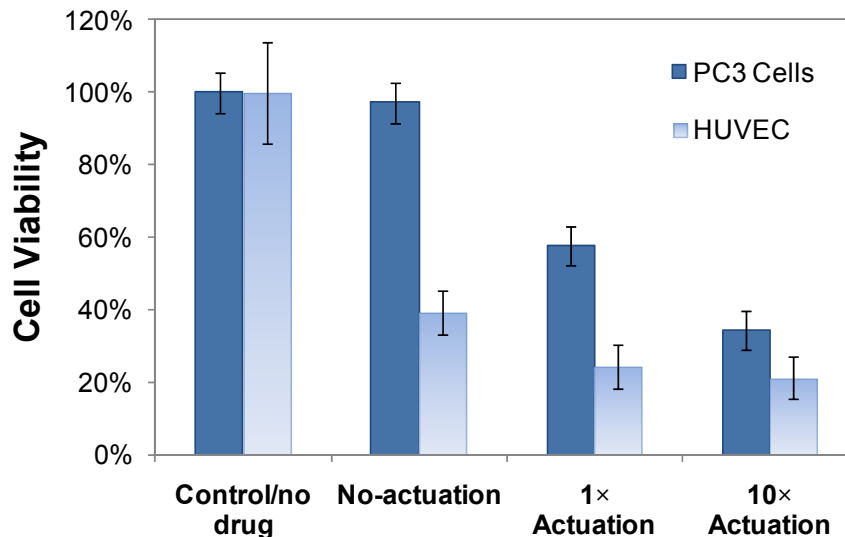
Figure 4.6 Viability of PC3 cells and HUVECs in the presence of released DTX from a device in two modes of operation: no-actuation and actuation ("×" refers to the number of actuation cycles). Actuations were performed in a 255 mT magnetic field. Error bars represent one standard deviation in measured values.

The cell viability for both cell lines were studied when the cells were incubated with either the freshly prepared DTX at various concentrations or the DTX released from the device under various number of actuations. In both cases, the cell viability in the presence of released drug closely follows that of fresh free drugs as shown in Figure 4.7-a and b. The cell viability equilibrated at ~34% for PC3 cells and ~ 24% for HUVECs, for both cell lines when they were either incubated with fresh free drug or incubated with the drug released from the device. The results confirmed that the antiproliferative effect of DTX was maintained over two months and the released drug from the device had approximately the same effect on cells as the freshly made drug solutions, establishing that DTX does not degrade inside the PDMS MEMS device after two months.
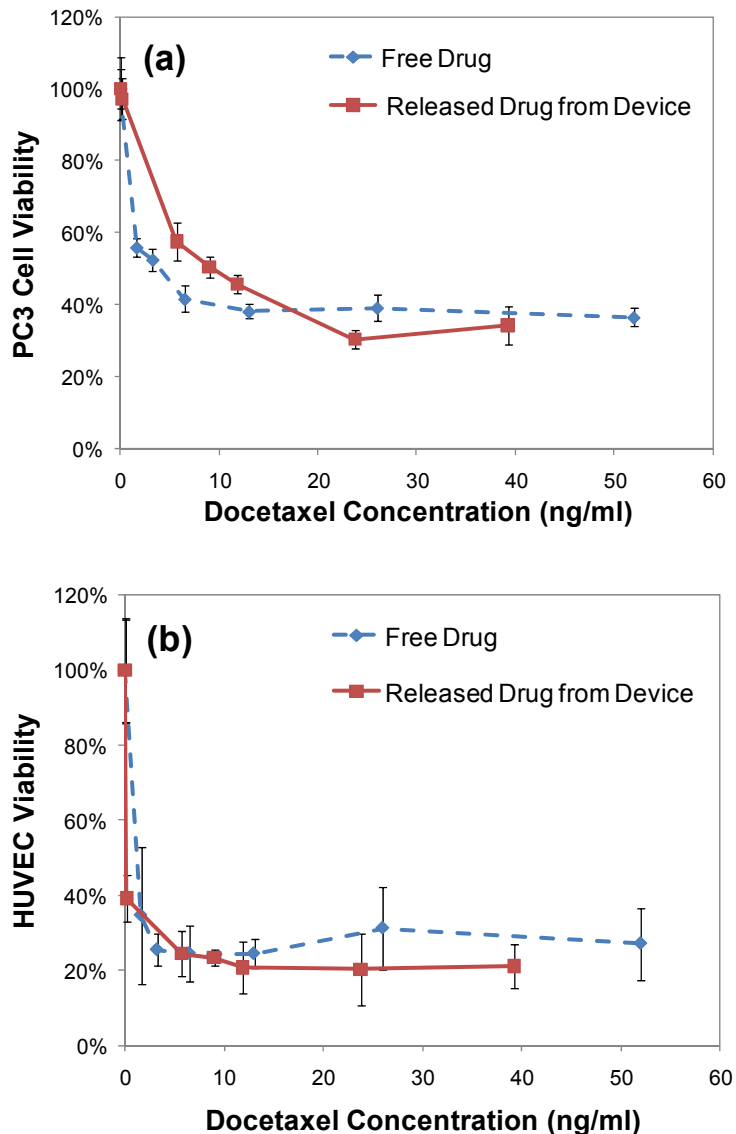
Figure 4.7 (a) PC3 cells viability and (b) HUVECs viability following exposure to DTX both in the form of fresh free drug and DTX released from a device, in various concentrations. The device was actuated under 255 mT magnetic field. Error bars represent one standard deviation from the measured values (6 repeats for each condition).

4.4 Concluding Remarks

In this chapter, DTX delivery using the proposed drug delivery device was demonstrated. On-demand and reproducible controlled release profiles were obtained. Constant DTX release rates for 35 days with nanomolar drug

71

concentrations were achieved. The release rates and drug dosing were controlled by magnetic field strength and cycles of actuation, respectively. Two time constants were identified to ensure constant release rates. The biological activity of the released drug was investigated using a cytotoxicity assay for two cell lines, HUVEC and PC3 cells. DTX showed no degradation two months after it was packaged inside a drug delivery device.

CHAPTER 5

Conclusions and Future Work

The effectiveness of drug therapy is dependent on the therapeutic concentrations of drugs at the disease site. This thesis described the concept, theory, fabrication process, and proof-of-principle release studies for a controlled release drug delivery device. Controlled and localized drug delivery systems provide temporal and spatial control of drug release and offer significant advantages over conventional immediate-release delivery systems. The device proposed in this thesis consisted of a drug-loaded microreservoir that is sealed by an elastic magnetic PDMS membrane with a laser-drilled aperture. Drug release was triggered in the presence of an external magnetic field by deforming the magnetic membrane and therefore discharging the drug solution from the device. The use of magnetic actuation for on-demand and controlled dose sequencing eliminated the need for an on-board power source. This controlled and on-demand release of antiproliferative drugs from the device is indicative of the great potential the proposed device has for application in the treatment of proliferative retinopathy, which requires accurate delivery of nanomolar drug concentrations.

The work in this thesis included chapters on magnetic material development (Chapter 2), device design and fabrication (Chapter 3), and proof-of-principle drug release studies (Chapter 4) and is summarized in the following section.

5.1   Summary

In Chapter 2, the development of new magnetic PDMS composites for use in fabrication of the proposed drug delivery device was described. The composites were developed by incorporating coated iron oxide nanoparticles with PDMS matrix. Existing magnetic polymeric materials have particle agglomeration problems, which result in rough surfaces and uneven mechanical and optical properties. The contribution made in Chapter 2 was the demonstration of a new magnetic material with much improvement in reducing particle agglomeration compared to existing polymer magnetic materials. It was shown that the use of iron oxide nanoparticles (10 nm in diameter) with fatty acid and hydrophobic coatings inhibited aggregation of particles in the PDMS polymer matrix. Agglomerated particle size in thin-film PDMS composites incorporated with uncoated and coated particles were 51±24 μm and 1.6±0.25 μm, respectively. As a result, the composite could be spin-coated to form a very thin (~ 35 μm or less) magnetic membrane, which could easily be incorporated into MEMS structures. Furthermore, the new membranes showed a minimum of four times decrease in surface roughness compared to the composites fabricated with non-coated iron oxide particles. Reduced surface roughness provided the membrane with excellent sealing property when used as the actuating membrane component of the proposed controlled release drug delivery device, sealing the drug reservoirs. The fabrication process of these PDMS composites was presented in detail and their mechanical and magnetic properties were characterized. They exhibited a saturation magnetization ranged from 22.8 to 23.94 emu/g. According to the stress-strain curves of the composites their Young's Moduli were derived, ranging from 0.6 MPa to 1.1 MPa. Their favorable elastic property became valuable when they were employed in the fabrication of the proposed drug delivery device. Finally, free-standing magnetic membranes were fabricated in different sizes and actuated in magnetic fields. Large deflections of these magnetic membranes make them attractive candidates for actuation in microdevices.

In Chapter 3, the development of the proposed MEMS drug delivery device that could be remotely actuated by a magnetic field to trigger drug release was presented. The concept of the magnetic actuation of the device was demonstrated. A detailed analysis of the magnetic actuation forces as well as estimations of the resulting membrane deflections were provided. Magnetic analysis estimated that a force of 1.3 mN can be exerted on a magnetic PDMS membrane under a 200 mT magnetic field which could result in approximately 290 μm membrane deflections for a membrane with 6 mm diameter and 40 μm thickness. Fabrication steps were reported including drug loading using solvent evaporation methods and laser ablation using UV and IR laser systems. Post-processing procedures using bovine serum albumin (BSA) adsorption on magnetic PDMS surfaces were carried out. These procedures were to modify the surface wettability of the magnetic membrane and to allow drug reservoir to fill with water and the drug in the reservoirs to dissolve. Detailed surface modification processes were described and characterized. Finally, the on-demand delivery of methylene blue as a model drug was demonstrated by actuating a device in water. Intermittent magnetic actuations of the device in a ~ 200 mT magnetic field showed a 10-fold increase in MB release compared to background release when the device was not actuated.

In Chapter 4, the use of the proposed controlled release drug delivery device to deliver an antiproliferative drug, DTX, was studied. It was demonstrated that the release profile may be controlled via magnetic field strength and a desired dosing may be achieved through repeating cycles of actuation. Two time constants were identified to ensure constant release rates: discharge time and mixing time. Simulation studies established that the concentration of DTX in the pumped-in fluid reaches 95% of that for the reservoir in 200 s. This was confirmed in drug release experiments by achieving constant release rates during three consecutive actuation events.

Controlled, intermittent DTX release rates of 171 ± 16.7 ng per actuation interval were achieved for 13 days using a 255 mT magnetic field. Similar release rates were observed when the device was actuated after 35 days. The background leakage

of the drug solution through the aperture (i.e. "off" state) was 64-fold smaller than the amount released in the actuation mode (i.e. "on" state). The cumulative release of DTX from three prototype devices was further demonstrated under a 213 mT magnetic field over a period of 6 days. The release of a model drug, TB, having higher aqueous solubility compared to that for DTX, was carried out for five intermittent actuation modes. The results showed a decrease in release rates suggesting a decreasing concentration of TB inside the reservoir following actuation. The constant release rate for DTX was the indication of a constant concentration of DTX inside the reservoir and therefore confirmed our hypothesis that the DTX concentration may be held constant at the saturation solubility, assuming the availability of solid (undissolved) DTX in the reservoir.

The biological activity of the DTX released from a device was investigated two months after the drug was packaged in the MEMS device and left in water with an open aperture. This was achieved by incubating cells (HUVEC and PC3) with the released drug in cell culture media and measuring the drug-induced inhibition of proliferation in comparison to the inhibition found in cells incubated with freshly made drug solutions. These studies confirmed that the antiproliferative effect of DTX was maintained over this period, establishing that the drug does not degrade within the PDMS MEMS device over this time. The results demonstrated the capability of the MEMS drug delivery device to achieve controlled delivery of low aqueous solubility compounds with well defined temporal control.

5.2 Future Work

One research direction would be to investigate the biocompatibility of the device. PDMS is one of the most commonly used polymers in MEMS [95]. Microfluidic devices fabricated with PDMS have been increasingly used for studies involving biological material [96], such as in bioreactors for perfusion culturing of cells [97, 98]. PDMS microdevices fabricated in three dimensions have been used in bone tissue engineering [99] and in various applications for monitoring and studying cell proliferation [100]. Belanger et al. [101] summarized PDMS biocompatibility and inflammatory response studies for both *in vitro* and *in vivo* applications and

concluded that PDMS appears to be a suitable reference material for the evaluation of biocompatibility of materials. Whilst most studies confirm the biocompatibility of PDMS, one study reported a mild to moderate inflammatory response fourteen days after implantation of a PDMS implant [102]. Furthermore, ocular implants made of PDMS have been successfully deployed [31, 103]. These studies largely confirm the biocompatibility of PDMS. However, further investigation to evaluate the biocompatibility of the drug delivery device described in this thesis following implantation *in vivo* is required.

The packaging of the proposed control released drug delivery device is important for its use in real applications, particularly for ocular drug delivery. The out-of-plane moving membrane within the device necessitates the need for suitable packaging to ensure proper functionality after implantation. In the design of the device packaging, the elevated pressure exertion on the implants generated by tissues and eye movement needs to be estimated and overcome. Using microfabrication technology to construct a perforated protective structure to cage the moving membrane, by employing a variety of polymers currently in use for medical devices, is an interesting area for future research.

One important addition to the current design of the controlled release drug delivery device is the addition of a valve system. Although the background leakage from the device is minimal and can also be improved by optimizing the aperture size, the integration of a valve system could theoretically reduce the background leakage further. Furthermore, unexpected release due to environmental conditions may be reduced by a valve system. Also, integrating a valve system could be beneficial in restricting the fluid flow in one direction, which will eliminate the waiting time for proper mixing inside the reservoir. Among the methods for developing a valve system, the use of the new materials that are responsive to a range of stimuli such as magnetic and ultrasound or are responsive to the physiological environment is promising and requires further investigation.

The work presented in this thesis was a proof-of-principle demonstration *in vitro*. A further development of the device would be to test the drug release in animal

models. For this purpose, it is necessary to study and identify the best location for the implantation of the device, the necessary geometrical requirements, and quantifiable measures for evaluation of the drug release. The primary goal of initial *in vivo* studies would be a qualitative demonstration of drug release to investigate how the release is affected by a living system. Later *in vivo* studies could investigate the release rate, total mass released, and the concentration vs. time profile for understanding the type of mass transport mechanisms at the implant site.

Finally, the study of the longer-term therapeutic effectiveness of drugs within MEMS devices is required for different applications based on the required period of treatment. It would also be relevant to investigate the long-term functionality of magnetic membranes in an aqueous environment.

BIBLIOGRAPHY

[1]   D. Paolino, P. Sinha, M. Fresta, and M. Ferrari, "Drug delivery systems," in *Encyclopedia of Medical Devices and Instrumentation*, J. G. Webster, Ed., 2nd ed., John Wiley & Sons, Inc., 2006, pp. 437-495.

[2]   S. L. Tao and T. A. Desai, "Microfabricated drug delivery systems: from particles to pores," *Advanced Drug Delivery Reviews,* vol. 55, pp. 315-328, 2003.

[3]   G. Gaucher, R. H. Marchessault, and J.-C. Leroux, "Polyester-based micelles and nanoparticles for the parenteral delivery of taxanes," *Journal of Controlled Release,* vol. 143, pp. 2-12, 2010.

[4]   P. S. Silva, J. D. Cavallerano, J. K. Sun, L. M. Aiello, and L. P. Aiello, "Effect of systemic medications on onset and progression of diabetic retinopathy," *Nature Reviews Endocrinology,* vol. 6, pp. 494-508, 2010.

[5]   E. S. Katharina, V. K. Gabriela, S. Werner, and B. Susanne, "Update on ocular complications of systemic cancer chemotherapy," *Survey of ophthalmology,* vol. 51, pp. 19-40, 2006.

[6]   J. Siepmann and F. Siepmann, "Time-controlled drug delivery systems," in *Modern Pharmaceutics, volume 2: Applications and Advances.*, A. T. Florence and J. Siepmann, Eds., 5th ed., New York: Informa Healthcare, Inc., 2009, pp. 1-22.

[7]   K. E. Uhrich, S. M. Cannizzaro, R. S. Langer, and K. M. Shakesheff, "Polymeric systems for controlled drug release," *Chemical Reviews,* vol. 99, pp. 3181-3198, 1999.

[8]   A. Göpferich, "Mechanisms of polymer degradation and erosion," *Biomaterials,* vol. 17, pp. 103-114, 1996.

[9]   R. Yoshida, "Design of functional polymer gels and their application to biomimetic materials," *Current Organic Chemistry,* vol. 9, pp. 1617-1641, 2005.

[10]   B. Narasimhan and R. Langer, "Zero-order release of micro- and macromolecules from polymeric devices: the role of the burst effect," *Journal of Controlled Release,* vol. 47, pp. 13-20, 1997.

[11]   S. Sharma, A. J. Nijdam, P. M. Sinha, R. J. Walczak, X. Liu, M. M. C. Cheng, and M. Ferrari, "Controlled-release microchips," *Expert Opinion on Drug Delivery,* vol. 3, pp. 379-394, 2006.

[12]   B. P. Timko, T. Dvir, and D. S. Kohane, "Remotely triggerable drug delivery systems," *Advanced Materials,* vol. 22, pp. 4925-4943, 2010.

[13]   K. C. Wood, N. S. Zacharia, D. J. Schmidt, S. N. Wrightman, B. J. Andaya, and P. T. Hammond, "Electroactive controlled release thin films," *Proceedings of the National Academy of Sciences,* vol. 105, pp. 2280-2285, 2008.

[14]   T.-Y. Liu, S.-H. Hu, K.-H. Liu, D.-M. Liu, and S.-Y. Chen, "Study on controlled drug permeation of magnetic-sensitive ferrogels: Effect of Fe_3O_4 and PVA," *Journal of Controlled Release,* vol. 126, pp. 228-236, 2008.

[15]   J. Kost and R. Langer, "Responsive polymeric delivery systems," *Advanced Drug Delivery Reviews,* vol. 46, pp. 125-148, 2001.

[16]   N. A. Peppas, J. Z. Hilt, A. Khademhosseini, and R. Langer, "Hydrogels in biology and medicine: from molecular principles to bionanotechnology," *Advanced Materials,* vol. 18, pp. 1345-1360, 2006.

[17]   M. Staples, "Microchips and controlled-release drug reservoirs," *Wiley Interdisciplinary Reviews: Nanomedicine and Nanobiotechnology,* vol. 2, pp. 400-417, 2010.

[18] B. Ziaie, A. Baldi, M. Lei, Y. Gu, and R. A. Siegel, "Hard and soft micromachining for BioMEMS: review of techniques and examples of applications in microfluidics and drug delivery," *Advanced Drug Delivery Reviews,* vol. 56, pp. 145-172, 2004.

[19] N.-T. Nguyen, X. Huang, and T. K. Chuan, "MEMS-Micropumps: a review," *Journal of Fluids Engineering,* vol. 124, pp. 384-392, 2002.

[20] J. T. Santini, M. J. Cima, and R. Langer, "A controlled-release microchip," *Nature,* vol. 397, pp. 335-338, 1999.

[21] J. M. Maloney, S. A. Uhland, B. F. Polito, J. N. F. Sheppard, C. M. Pelta, and J. J. T. Santini, "Electrothermally activated microchips for implantable drug delivery and biosensing," *Journal of Controlled Release,* vol. 109, pp. 244-255, 2005.

[22] J. H. Prescott, S. Lipka, S. Baldwin, N. F. Sheppard, J. M. Maloney, J. Coppeta, B. Yomtov, M. A. Staples, and J. T. Santini, "Chronic, programmed polypeptide delivery from an implanted, multireservoir microchip device," *Nature Biotechnology,* vol. 24, pp. 437-438, 2006.

[23] Y. Li, R. S. Shawgo, B. Tyler, P. T. Henderson, J. S. Vogel, A. Rosenberg, P. B. Storm, R. Langer, H. Brem, and M. J. Cima, "In vivo release from a drug delivery MEMS device," *Journal of Controlled Release,* vol. 100, pp. 211-219, 2004.

[24] Y. Li, D. Hong Linh Ho, B. Tyler, T. Williams, M. Tupper, R. Langer, H. Brem, and M. J. Cima, "In vivo delivery of BCNU from a MEMS device to a tumor model," *Journal of Controlled Release,* vol. 106, pp. 138-145, 2005.

[25] N. Elman, H. Ho Duc, and M. Cima, "An implantable MEMS drug delivery device for rapid delivery in ambulatory emergency care," *Biomedical Microdevices,* vol. 11, pp. 625-631, 2009.

[26]   A. Nisar, N. Afzulpurkar, B. Mahaisavariya, and A. Tuantranont, "MEMS-based micropumps in drug delivery and biomedical applications," *Sensors and Actuators B: Chemical,* vol. 130, pp. 917-942, 2008.

[27]   T. B. Tang, S. Smith, B. W. Flynn, J. T. M. Stevenson, A. M. Gundlach, H. M. Reekie, A. F. Murray, D. Renshaw, B. Dhillon, A. Ohtori, Y. Inoue, J. G. Terry, and A. J. Walton, "Implementation of wireless power transfer and communications for an implantable ocular drug delivery system," *IET Nanobiotechnology,* vol. 2, pp. 72-79, 2008.

[28]   W. Ryu, Z. Huang, F. B. Prinz, S. B. Goodman, and R. Fasching, "Biodegradable micro-osmotic pump for long-term and controlled release of basic fibroblast growth factor," *Journal of Controlled Release,* vol. 124, pp. 98-105, 2007.

[29]   W.-C. Huang, S.-H. Hu, K.-H. Liu, S.-Y. Chen, and D.-M. Liu, "A flexible drug delivery chip for the magnetically-controlled release of anti-epileptic drugs," *Journal of Controlled Release,* vol. 139, pp. 221-228, 2009.

[30]   K. Cai, Z. Luo, Y. Hu, X. Chen, Y. Liao, L. Yang, and L. Deng, "Magnetically triggered reversible controlled drug delivery from microfabricated polymeric multireservoir devices," *Advanced Materials,* vol. 21, pp. 4045-4049, 2009.

[31]   R. Lo, P.-Y. Li, S. Saati, R. Agrawal, M. Humayun, and E. Meng, "A passive MEMS drug delivery pump for treatment of ocular diseases," *Biomedical Microdevices,* vol. 11, pp. 959-970, 2009.

[32]   M. Rajappa, P. Saxena, J. Kaur, and S. M. Gregory, "Ocular angiogenesis: mechanisms and recent advances in therapy," in *Advances in Clinical Chemistry*. vol. 50, G. S. Makowski, Ed., Elsevier, 2010, pp. 103-121.

[33]   L. P. Aiello, "Angiogenic pathways in diabetic retinopathy," *New England Journal of Medicine,* vol. 353, pp. 839-841, 2005.

[34] Q. Mohamed, M. C. Gillies, and T. Y. Wong, "Management of diabetic retinopathy," *JAMA: The Journal of the American Medical Association,* vol. 298, pp. 902-916, 2007.

[35] L. M. Aiello, "Perspectives on diabetic retinopathy," *American Journal of Ophthalmology,* vol. 136, pp. 122-135, 2003.

[36] S. S. Lee and M. R. Robinson, "Novel drug delivery systems for retinal diseases," *Ophthalmic Research,* vol. 41, pp. 124-135, 2009.

[37] D. H. Geroski and H. F. Edelhauser, "Drug delivery for posterior segment eye disease," *Investigative Ophthalmology & Visual Science,* vol. 41, pp. 961-964, 2000.

[38] T. R. Thrimawithana, S. Young, C. R. Bunt, C. Green, and R. G. Alany, "Drug delivery to the posterior segment of the eye," *Drug Discovery Today,* 2010 (In Press).

[39] J. Jackson, M. Gleave, J. Gleave, and H. Burt, "The inhibition of angiogenesis by antisense oligonucleotides to clusterin," *Angiogenesis,* vol. 8, pp. 229-238, 2005.

[40] E. Barbu, L. Verestiuc, T. G. Nevell, and J. Tsibouklis, "Polymeric materials for ophthalmic drug delivery: trends and perspectives," *Journal of Materials Chemistry,* vol. 16, pp. 3439-3443, 2006.

[41] H. F. Edelhauser, C. L. Rowe-Rendleman, M. R. Robinson, D. G. Dawson, G. J. Chader, H. E. Grossniklaus, K. D. Rittenhouse, C. G. Wilson, D. A. Weber, B. D. Kuppermann, K. G. Csaky, T. W. Olsen, U. B. Kompella, V. M. Holers, G. S. Hageman, B. C. Gilger, P. A. Campochiaro, S. M. Whitcup, and W. T. Wong, "Ophthalmic drug delivery systems for the treatment of retinal diseases: basic research to clinical applications," *Investigative Ophthalmology & Visual Science,* vol. 51, pp. 5403-5420, 2010.

[42] J. R. Gebhard and D. Patel, "Taxane compounds for treating eye disease," United States Patent, US 0 016 256 A1, Jan. 2010.

[43] R. T. Liggins, S. D'Amours, J. S. Demetrick, L. S. Machan, and H. M. Burt, "Paclitaxel loaded poly(-lactic acid) microspheres for the prevention of intraperitoneal carcinomatosis after a surgical repair and tumor cell spill," *Biomaterials,* vol. 21, pp. 1959-1969, 2000.

[44] J. K. Jackson, M. E. Gleave, V. Yago, E. Beraldi, W. L. Hunter, and H. M. Burt, "The suppression of human prostate tumor growth in mice by the intratumoral injection of a slow-release polymeric paste formulation of paclitaxel," *Cancer Research,* vol. 60, pp. 4146-4151, 2000.

[45] H. M. Burt and W. L. Hunter, "Drug-eluting stents: a multidisciplinary success story," *Advanced Drug Delivery Reviews,* vol. 58, pp. 350-357, 2006.

[46] M. R. J. Gibbs, E. W. Hill, and P. J. Wright, "Magnetic materials for MEMS applications," *Journal of Physics D: Applied Physics,* vol. 37, pp. R237–R244, 2004.

[47] J. Y. Park and M. G. Allen, "Development of magnetic materials and processing techniques applicable to integrated micromagnetic devices," *Journal of Micromechanics and Microengineering,* vol. 8, pp. 307-316, 1998.

[48] Y.-f. Su, W.-y. Chen, F. Cui, and W.-p. Zhang, "Design and fabrication process of electromagnetically actuated valveless micropump with two parallel flexible diaphragms," *Journal of Shanghai University (English Edition),* vol. 11, pp. 79-83, 2007.

[49] C. P. B. Siu, H. Zeng, and M. Chiao, "Magnetically actuated MEMS microlens scanner for in vivo medical imaging," *Optical Express,* vol. 15, pp. 11154-11166, 2007.

[50] S. Santra, P. Holloway, and C. D. Batich, "Fabrication and testing of a magnetically actuated micropump," *Sensors and Actuators B: Chemical,* vol. 87, pp. 358-358, 2002.

[51] M. Khoo and C. Liu, "Micro magnetic silicone elastomer membrane actuator," *Sensors and Actuators A: Physical,* vol. 89, pp. 259-266, 2001.

[52] H. Ren and E. Gerhard, "Design and fabrication of a current-pulse-excited bistable magnetic microactuator," *Sensors and Actuators A: Physical,* vol. 58, pp. 259-264, 1997.

[53] T.-S. Chin, "Permanent magnet films for applications in microelectromechanical systems," *Journal of Magnetism and Magnetic Materials,* vol. 209, pp. 75-79, 2000.

[54] D. Niarchos, "Magnetic MEMS: key issues and some applications," *Sensors and Actuators A: Physical,* vol. 109, pp. 166-173, 2003.

[55] H. A. Jehn and B. Rother, "Homogeneity of multi-component PVD hard coatings deposited by multi-source arrangements," *Surface and Coatings Technology,* vol. 112, pp. 103-107, 1999.

[56] S. Guan, B. J. Nelson, and K. Vollmers, "Electrochemical codeposition of magnetic particle-ferromagnetic matrix composites for magnetic MEMS actuator applications," *Journal of The Electrochemical Society,* vol. 151, pp. C545-C549, 2004.

[57] N. V. Myung, D. Y. Park, B. Y. Yoo, and P. T. A. Sumodjo, "Development of electroplated magnetic materials for MEMS," *Journal of Magnetism and Magnetic Materials,* vol. 265, pp. 189-198, 2003.

[58] J. W. Judy, R. S. Muller, and H. H. Zappe, "Magnetic microactuation of polysilicon flexure structures," *Journal of Microelectromechanical Systems,* vol. 4, pp. 162-169, 1995.

[59]   J. W. Judy and R. S. Muller, "Magnetically actuated, addressable microstructures," *Journal of Microelectromechanical System,* vol. 6, pp. 249-256, 1997.

[60]   C. Liu, T. Tsao, G.-B. Lee, J. T. S. Leu, Y. W. Yi, Y.-C. Tai, and C.-M. Ho, "Out-of-plane magnetic actuators with electroplated permalloy for fluid dynamics control," *Sensors and Actuators A: Physical,* vol. 78, pp. 190-197, 1999.

[61]   T. M. Liakopoulos, Z. Wenjin, and C. H. Ahn, "Micromachined thick permanent magnet arrays on silicon wafers," *IEEE Transactions on Magnetics,* vol. 32, pp. 5154-5156, 1996.

[62]   H. J. Cho, S. Bhansali, and C. H. Ahn, "Electroplated thick permanent magnet arrays with controlled direction of magnetization for MEMS application," *Journal of Applied Physics,* vol. 87, pp. 6340-6342, 2000.

[63]   L. K. Lagorce and M. G. Allen, "Magnetic and mechanical properties of micromachined Strontium Ferrite/Polyimide composites," *Journal of microelectromechanical systems,* vol. 6, pp. 307-312, 1997.

[64]   L. K. Lagorce, O. Brand, and M. G. Allen, "Magnetic microactuators based on polymer magnets," *Journal of microelectromechanical systems,* vol. 8, pp. 2-9, 1999.

[65]   B. Pawlowski and J. Töpfer, "Permanent magnetic NdFeB thick films," *Journal of Materials Science,* vol. 39, pp. 1321-1324, 2004.

[66]   C. Yamahata, C. Lotto, E. Al-Assaf, and M. A. M. Gijs, "A PMMA valveless micropump using electromagnetic actuation," *Microfluidics and Nanofluidics,* vol. 1, pp. 197-207, 2005.

[67]   W. Wang, Z. Yao, J. C. Chen, and J. Fang, "Composite elastic magnet films with hard magnetic feature," *Journal of Micromechanics and microengineering,* vol. 14, pp. 1321-1327, 2004.

[68] F. Fahrni, M. W. J. Prins, and L. J. van Ijzendoorn, "Magnetization and actuation of polymeric microstructures with magnetic nanoparticles for application in microfluidics," *Journal of Magnetism and Magnetic Materials,* vol. 321, pp. 1843-1850, 2009.

[69] N. Sundararajan, D. Kim, and A. A. Berlin, "Microfluidic operations using deformable polymer membranes fabricated by single layer soft lithography," *Lab on a Chip,* vol. 5, pp. 350-354, 2005.

[70] C. Yamahata, C. Vandevyver, F. Lacharme, P. Izewska, H. Vogel, R. Freitag, and M. A. M. Gijs, "Pumping of mammalian cells with a nozzle-diffuser micropump," *Lab on a Chip,* vol. 5, pp. 1083-1088, 2005.

[71] F. Caruso, "Nanoengineering of particle surfaces," *Advanced Materials,* vol. 13, pp. 11-22, 2001.

[72] W.-J. Chang, D. Akin, M. Sedlak, M. R. Ladisch, and R. Bashir, "Poly(dimethylsiloxane) (PDMS) and Silicon hybrid biochip for bacterial culture," *Biomedical Microdevices,* vol. 5, pp. 281-290, 2003.

[73] J. C. Lotters, W. Olthuis, P. H. Veltink, and P. Bergveld, "The mechanical properties of the rubber elastic polymer polydimethylsiloxane for sensor applications," *Journal of Micromechanics and Microengineering,* vol. 7, pp. 145-147, 1997.

[74] A. Thangawng, R. Ruoff, M. Swartz, and M. Glucksberg, "An ultra-thin PDMS membrane as a bio/micro–nano interface: fabrication and characterization," *Biomedical Microdevices,* vol. 9, pp. 587-595, 2007.

[75] S. Bhattacharya, A. Datta, J. M. Berg, and S. A. G. S. Gangopadhyay, "Studies on surface wettability of poly(dimethyl) siloxane (PDMS) and glass under oxygen-plasma treatment and correlation with bond strength," *Journal of Microelectromechanical Systems,* vol. 14, pp. 590-597, 2005.

[76] M. A. M. Gijs, "Magnetic bead handling on-chip: new opportunities for analytical applications," *Microfluidics and Nanofluidics,* vol. 1, pp. 22-40, 2004.

[77] C. D. Han, C. Sandford, and H. J. Yoo, "Effects of titanate coupling agents on the rheological and mechanical properties of filled polyolefins," *Polymer Engineering & Science,* vol. 18, pp. 849-854, 1978.

[78] L. Bokobza and O. Rapoport, "Reinforcement of natural rubber," *Journal of Applied Polymer Science,* vol. 85, pp. 2301-2316, 2002.

[79] D. R. Saini, A. V. Shenoy, and V. M. Nadkarni, "Effect of surface treatments on rheological, mechanical and magnetic properties of ferrite-filled polymeric systems," *Polymer Engineering & Science,* vol. 25, pp. 807-811, 1985.

[80] S. P. Timoshenko and S. Woinowsky-Krieger, *Theory of Plates and Shells*, 2nd ed., McGraw-Hill, 1959.

[81] D. X. Chen, J. A. Brug, and R. B. Goldfarb, "Demagnetizing factors for cylinders," *IEEE Transactions on Magnetics,* vol. 27, pp. 3601-3619, 1991.

[82] J. J. Abbott, O. Ergeneman, M. P. Kummer, A. M. Hirt, and B. J. Nelson, "Modeling magnetic torque and force for controlled manipulation of soft-magnetic bodies," *IEEE Transactions on Robotics,* vol. 23, pp. 1247-1252, 2007.

[83] F. N. Pirmoradi, L. Cheng, and M. Chiao, "A magnetic poly(dimethylesiloxane) composite membrane incorporated with uniformly dispersed, coated iron oxide nanoparticles," *Journal of Micromechanics and Microengineering,* vol. 20, p. 015032, 2010.

[84] A. F. Stalder, G. Kulik, D. Sage, L. Barbieri, and P. Hoffmann, "A snake-based approach to accurate determination of both contact points and contact angles," *Colloids and Surfaces A: Physicochemical and Engineering Aspects,* vol. 286, pp. 92-103, 2006.

[85] A. F. Stalder, G. Kulik, D. Sage, L. Barbieri, and P. Hoffmann. (2006, accessed: 10 December 2010). *Drop Analysis Software*. Available: http://bigwww.epfl.ch/demo/dropanalysis/

[86] G. Frank, M. Rabold, and P. Woias, "Strategies for void-free liquid filling of micro cavities," *Journal of Micromechanics and Microengineering,* vol. 16, pp. 1321-1330, 2006.

[87] H. Makamba, J. H. Kim, K. Lim, N. Park, and J. H. Hahn, "Surface modification of poly(dimethylsiloxane) microchannels," *ELECTROPHORESIS,* vol. 24, pp. 3607-3619, 2003.

[88] S. Sugiura, J.-i. Edahiro, K. Sumaru, and T. Kanamori, "Surface modification of polydimethylsiloxane with photo-grafted poly(ethylene glycol) for micropatterned protein adsorption and cell adhesion," *Colloids and Surfaces B: Biointerfaces,* vol. 63, pp. 301-305, 2008.

[89] C. Donzel, M. Geissler, A. Bernard, H. Wolf, B. Michel, J. Hilborn, and E. Delamarche, "Hydrophilic Poly(dimethylsiloxane) stamps for microcontact printing," *Advanced Materials,* vol. 13, pp. 1164-1167, 2001.

[90] A. Hillerström and B. Kronberg, "A two-step method for the synthesis of a hydrophilic PDMS interpenetrating polymer network," *Journal of Applied Polymer Science,* vol. 110, pp. 3059-3067, 2008.

[91] W. Schrott, Z. Slouka, P. Cervenka, J. Ston, M. Nebyla, M. Pribyl, and D. Snita, "Study on surface properties of PDMS microfluidic chips treated with albumin," *Biomicrofluidics,* vol. 3, pp. 044101-15, 2009.

[92] K. S. Phillips and Q. Cheng, "Microfluidic immunoassay for bacterial toxins with supported phospholipid bilayer membranes on Poly(dimethylsiloxane)," *Analytical Chemistry,* vol. 77, pp. 327-334, 2004.

[93] A. Krishnan, Y.-H. Liu, P. Cha, D. Allara, and E. A. Vogler, "Interfacial energetics of globular-blood protein adsorption to a hydrophobic interface from aqueous-buffer solution," *Journa l of the Royal Society Interface,* vol. 3, pp. 283-301, 2006.

[94] R. B. Bird, W. E. Stewart, and E. N. Lightfoot, *Transport phenomena*, 2nd ed., New York: John Wiley & Sons, Inc., 2007.

[95] G. M. Whitesides, E. Ostuni, S. Takayama, X. Jiang, and D. E. Ingber, "Soft lithography in biology and biochemistry," *Annual Review of Biomedical Engineering,* vol. 3, pp. 335-373, 2001.

[96] S. K. Sia and G. M. Whitesides, "Microfluidic devices fabricated in Poly(dimethylsiloxane) for biological studies," *ELECTROPHORESIS,* vol. 24, pp. 3563-3576, 2003.

[97] N. Ming, T. Wen Hao, C. Deepak, R. Nur Aida Abdul, I. Ciprian, and Y. Hanry, "Cell culture on MEMS platforms: a review," *International Journal of Molecular Sciences,* vol. 10, pp. 5411–5441, 2009.

[98] S. Ostrovidov, J. Jiang, Y. Sakai, and T. Fujii, "Membrane-based PDMS microbioreactor for perfused 3D primary rat hepatocyte cultures," *Biomedical Microdevices,* vol. 6, pp. 279-287, 2004.

[99] E. Leclerc, B. David, L. Griscom, B. Lepioufle, T. Fujii, P. Layrolle, and C. Legallaisa, "Study of osteoblastic cells in a microfluidic environment," *Biomaterials,* vol. 27, pp. 586-595, 2006.

[100] M. W. Li, D. M. Spence, and R. S. Martin, "A Microchip-based system for immobilizing PC 12 cells and amperometrically detecting catecholamines released after stimulation with Calcium," *Electroanalysis,* vol. 17, pp. 1171-1180, 2005.

[101] M. C. Bélanger and Y. Marois, "Hemocompatibility, biocompatibility, inflammatory and in vivo studies of primary reference materials low-density polyethylene and polydimethylsiloxane: A review," *Journal of Biomedical Materials Research,* vol. 58, pp. 467-477, 2001.

[102] A. Dalu, B. S. Blaydes, L. G. Lomax, and K. B. Delclos, "A comparison of the inflammatory response to a polydimethylsiloxane implant in male and female Balb/c mice," *Biomaterials,* vol. 21, pp. 1947-1957, 2000.

[103] M. Tunc, M. Humayun, X. Cheng, and B. D. Ratner, "A reversible thermosensitive adhesive for retinal implants: in vivo experience with plasma-deposited poly(N-Isopropyl Acrylamide)," *RETINA,* vol. 28, pp. 1338-1343 2008.

[104] Lawrence K. Fung, Matthew G. Ewend, Allen Sills, Eric P. Sipos, Reid Thompson, Mark Watts, O. Michael Colvin, Henry Brern, and W. M. Saltzman, "Pharmacokinetics of interstitial delivery of Carmustine, 4-Hydroperoxycyclophosphamide, and Paclitaxel from a biodegradable polymer implant in the monkey brain," *Cancer Research,* vol. 58, pp. 672-684, 1998.

[105] M. K. Inglesby and S. H. Zeronian, "Diffusion coefficients for direct dyes in aqueous and polar aprotic solvents by the NMR pulsed-field gradient technique," *Dyes and Pigments,* vol. 50, pp. 3-11, 2001.

APPENDICES

Appendix A : DTX Solubility

A.1   Experiment

Solid DTX (2 mg) was mixed in 20 ml PBS and samples of solutions were taken at specific time points. The concentration of DTX in the samples was measured using reversed phase high pressure liquid chromatography (HPLC) (Waters HPLC system with millennium software) with a symmetry C18 column (4 mm × 150 mm , Waters Nova-Pak, Milford, MA) at a flow rate of 1 ml/min. The mobile phase was composed of 58% acetonitrile, 37% distilled water, and 5% methanol. Sample injection volumes were 20 µl and detection was performed using UV at a wavelength of 232 nm. Before DTX analysis by HPLC, the samples were centrifuged at 14000 rpm for 4 minutes (microfuge® 18 centrifuge Beckman Coulter, Inc., Brea, CA).

A.2   Results

The concentration of DTX in PBS was measured at different time points (Figure A.1). DTX concentration increased to 11.5 µg/ml in the first 6 min, decreasing to approximately 5 µg/ml after about 45 min, and remaining constant at that concentration after that time. Therefore, once the filling process of the reservoir is complete (over 24 h) the DTX concentration inside the reservoir may reach an equilibrium state so it is expected that the concentration in the reservoir stays constant at equilibrium as long as there is DTX solid available in the reservoir.
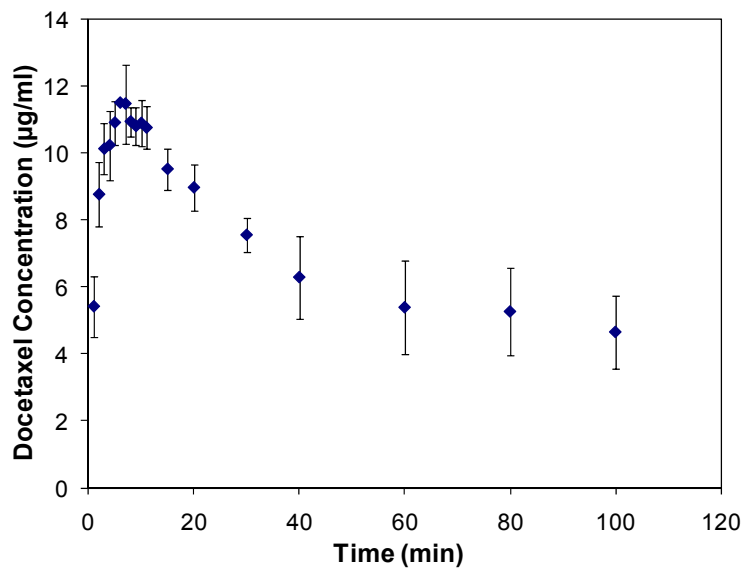
Figure A.1 Docetaxel solubility as a function of time, in PBS. Error bars represent one standard deviation in measured values. The experiment was repeated three times (n=3).

Appendix B : Actuation Setup
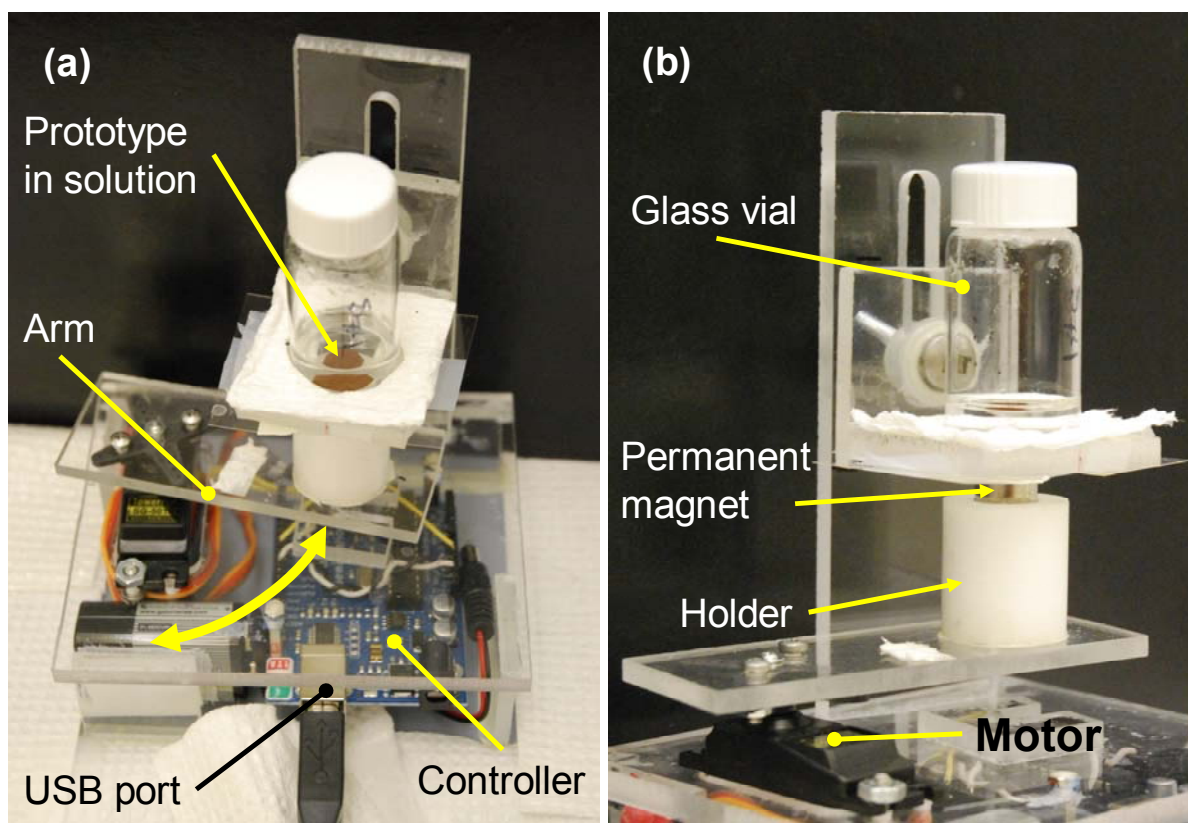
Figure A.2 Actuation setup.

Appendix C : Discharge Time Measurement

TB loaded devices were actuated inside 20 ml glass scintillation vials filled with 4 ml BSA solution while a stereo microscope (Olympus SZ61, Olympus Imaging America, Inc. ,PA, USA) with a CCD camera was used to take videos (33 frames/second) of TB solution discharge. Video frames were then extracted and the initial discharge velocity was obtained by measuring the TB solution travel distance in the first frame divided by the time taken for its travel (0.03 s). The distance was measured from the membrane surface in the direction perpendicular to the membrane surface using Image J, a general purpose open source image-processing package, and converted to magnetic field values using a characterization curve obtained in Chapter 3.

Appendix D : Mixing Time

Simulation was performed by considering isotropic diffusion in 2D with the reservoir size of 6×0.4 mm^2. The pumped-in fluid represented by a sphere has a radius of 0.1 mm, based on the maximum traveled distance presented in Table 4.1. The diffusion coefficient value for DTX was assumed to be equal to that of Paclitaxel (D = 9×10^{-10} m^2/s [104]) due to the similar molecular structures of the drugs. The initial concentration of DTX in the reservoir was set to 5 μg/ml or 0.0068 mol/m^3 (considering DTX molar mass of 807.88 g/mol) based on the DTX equilibrated aqueous solubility (Figure A.1). The diffusion coefficient of TB was obtained based on extrapolation of the data reported by Inglesby and colleague [105] and set to 4.35×10^{-11} m^2/s at 23°C. We set the initial concentration of TB solution in the reservoir to 1 mg/ml or ~1 mol/m^3 as a conservative measure.

Figure A.3 shows the simulation results after 200 s from the time fluid was pumped into the reservoirs for both DTX and TB solutions. The average concentration of the pumped-in fluid over time can serve as a measure for determining the required *mixing time* (t_w) before each actuation cycle. This measure is presented in Figure 4.2 as the average concentration in the sphere domain over the average concentration in the entire reservoir for both DTX and TB solutions in the reservoirs. According to the data in Figure 4.2, if 200 s is allowed before each actuation, the average concentration of DTX and TB in the pumped-in fluid reaches 95% and 70% of that of the reservoir. Based on the simulation results, in all the experiments with DTX and TB, t_w was set to 200 s. Although, due to the lower diffusion coefficient of TB compared to DTX, a longer equilibration time is required for TB solution, similar wait times for both solutions were used for comparison purposes.
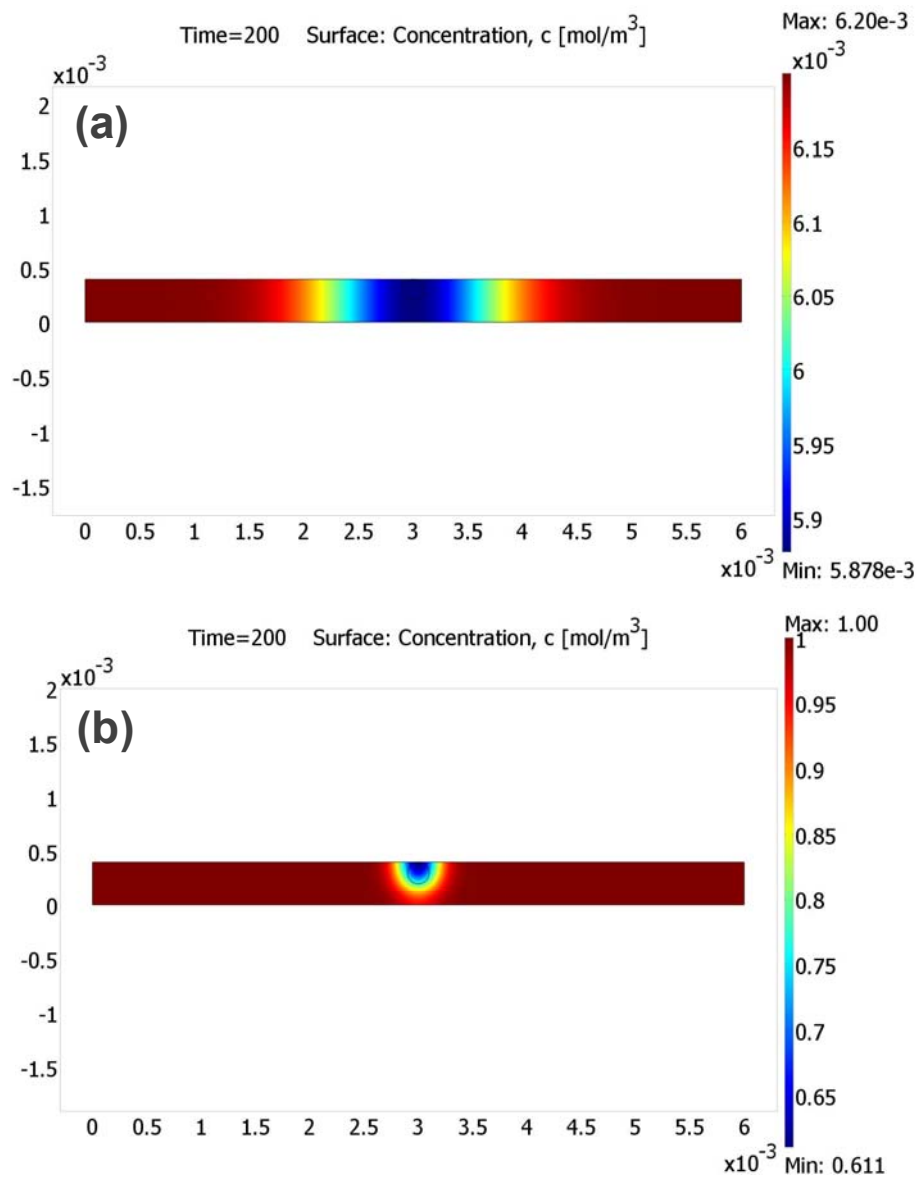
Figure A.3 Diffusion transport of pumped-in fluid inside the reservoir filled with (a) DTX, and (b) TB, after 200 s.

Appendix E : Cumulative DTX Release
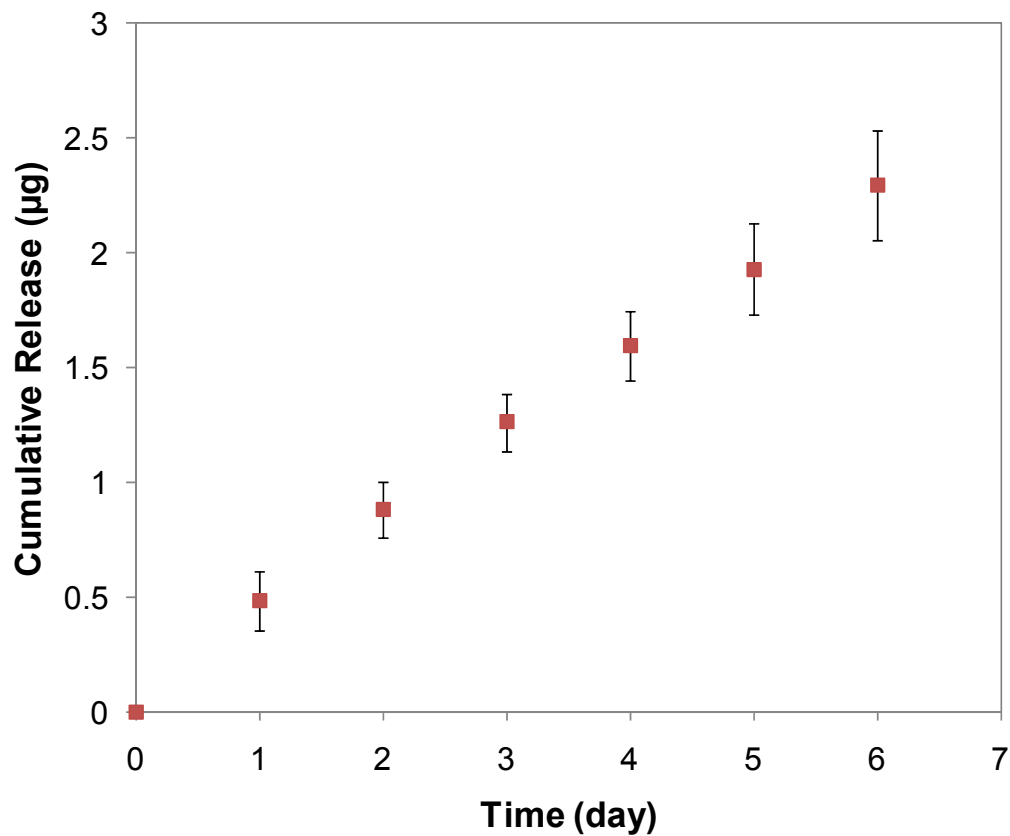
Figure A.4 Cumulative ^{3}H-DTX released from devices operated in a 213 mT magnetic field over six days (n=3). Each point includes thirty actuation cycles for each device which were then averaged between devices. Error bars represent the cumulative error in the measurement period.

Appendix F : TB Release Profile
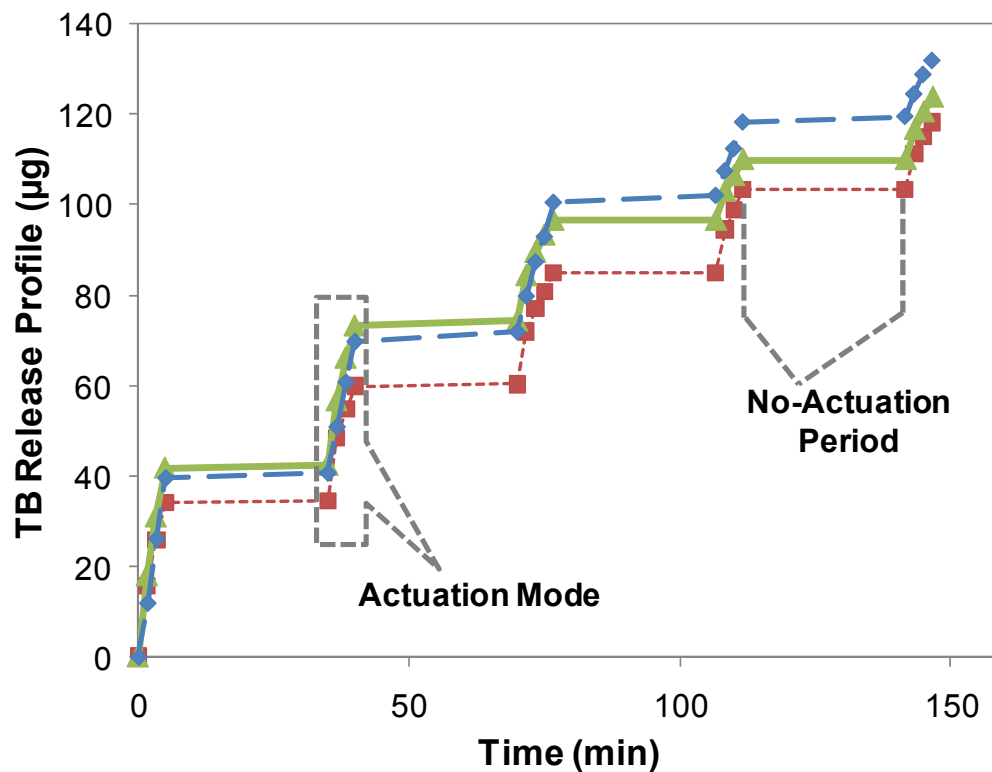
Figure A.5 Intermittent release of TB in actuation and no-actuation periods from three devices (membrane: ∅6 mm × *t*=40 μm, aperture: 100 × 100 μm², reservoir depth: ~550 μm) operated in ~191 mT applied magnetic field. The no-actuation period is 30 min in all cases. Each data point represents one actuation cycle.